Sabrina Julia Kogler, BSc

Engineering geological aspects of parts of the landslide Perfuchsberg near Landeck (Tyrol, Austria)

MASTER'S THESIS

to achieve the university degree of

Master of Science

Master's degree programme: Earth Sciences

submitted to

Graz University of Technology

Supervisor

Univ.-Prof. B.A. M.Sc. Ph.D. Daniel Scott Kieffer

Institute of Applied Geosciences

Mag.rer.nat. Dr.rer.nat Daniela Anna Engl

Graz, October 2015

AFFIDAVIT

EIDESSTATTLICHE ERKLÄRUNG

I declare that I have authored this thesis independently, that I have not used other than the declared sources/resources, and that I have explicitly indicated all material which has been quoted either literally or by content from the sources used. The text document uploaded to TUGRAZonline is identical to the present master‘s thesis.

Ich erkläre an Eides statt, dass ich die vorliegende Arbeit selbstständig verfasst, andere als die angegebenen Quellen/Hilfsmittel nicht benutzt, und die den benutzten Quellen wörtlich und inhaltlich entnommenen Stellen als solche kenntlich gemacht habe. Das in TUGRAZonline hochgeladene Textdokument ist mit der vorliegenden Masterarbeit identisch.

Date / Datum

Signature / Unterschrift

Acknowledgements

I am thankful to many people for their support and encouragement which was so important and unaffordable during writing this master thesis and the years of study. Without your help this completion would not have been possible. I want to thank:

- my advisors Scott Kieffer and Daniela Engel for their help and support;
- Gerhard Poscher and his team from geo.zt in Hall in Tirol;
- the members of the Institute of Applied Geosciences for their support especially during the laboratory investigations and analysis;
- my friends and colleagues for the great time, interesting dialogues and help during the last years;
- my family, especially my parents for their confidence and unconditional support in all issues. Thank you so much!!!

Abstract

The area around Landeck in the Tyrol Upland, Austria, features a significant density of deep-seated landslides. In the course of the present thesis the failure mechanisms and kinematics of the slope instability at the area of Perfuchsberg, in the west of Landeck, get investigated and determined. To support these analyses, detailed geological and geomorphological field mapping, rock sampling, laboratory investigations and engineering geological analysis are performed.

The intense sheared rock mass and the geologic structure have favoured a complex landsliding process: On the basis of engineering geologic investigations performed, it is suggested that the landslide initiation was controlled by joint set 4 (53/62°) and 5 (336/21°). A basal shear zone is then suggest to have developed in close connection with joint set 5 (336/21°). Kinematic, stability and sensitivity analyses compute a friction angle for the shear zone material for the limit equilibrium state of at least 21° depending on the hydraulic conditions within the slope. The depth of the landslide get interpret of approx. 60 m based on cross section analysis, borings and the reconstruction of the pre-failure topography. The separated landslide from the entire Perfuchsberg landslide, get best classified as a rockslide initiated by two joint panes with active secondary shallow slides at the toe of the slope. The breaks and cracks at the upper area, behind the headscarp, could be caused by (large scale) toppling referring to kinematic analysis. Furthermore at the steep headscarp area secondary failures like rock fall events are detected.

At a second area of the study area large open breaks, cracks and steep rock faces get observed during field investigations, cross section analysis and laserscan data interpretation. Based on engineering geological analysis joint set 3 (337/81°) and joint set 4 (53/62°) are supposed to be involved in this failure mechanism. Kinematic and sensitivity analysis calculate a friction angle for the shear zone material for the limit equilibrium state of 15-20° depending on the cohesion of the joint planes and the hydraulic conditions within the slope. It could be suggest that the failure mechanism is (large scale) toppling on the steep rock faces with secondary failures like rock falling events on the steep rock faces. The size of the rocks vary from large boulders to small stones and debris referred to detailed field observations.

It is most likely that Quaternary processes, such as the oversteepening of the slope, or large amount of water after melting of the glacier, caused and triggered this complex landslide process. The present day movement is assumed to be significantly influenced by the erosion of the Sanna River at the toe of the study area and heavy rainfalls or snowmelts.

Kurzfassung

Das Gebiet um Landeck, im Tiroler Oberland, Österreich, zeigt ein erhebliches Vorkommen von tiefgründigen Hangbewegungen. Diese Masterarbeit soll die Versagensmechanismen und die Kinematik der Hanginstabilitäten im Bereich Perfuchsberg, westlich von Landeck, untersuchen und bestimmen. Auf Basis einer vorrangegangenen geologischen und geomorphologischen Kartierung, werden detaillierte geologische und geomorphologische Geländekarten erstellt, Gesteinsproben entnommen, Laboruntersuchungen und ingenieurgeologische Analysen durchgeführt.

Das intensiv gescherte und tektonisch beanspruchte Gebirge begünstigte das Auftreten eines komplexen Hangversagensprozesses: Aufgrund der durchgeführten ingenieurgeologischen Untersuchungen wird angenommen, dass das Hangversagen durch das Vorkommen der Trennflächen 4 (53/62°) und 5 (336/21°) verursacht wurde. Eine basale Scherzone sollte sich anschließend im Zusammenhang mit Trennfläche 5 (336/21°) gebildet haben. Kinematik, Stabilitäts- und Sensitivitätsanalysen berechneten für den Gleichgewichtszustand, abhängig von den hydraulischen Bedingungen, einen Reibungswinkel von mindestens 21°. Die Tiefe der Massenbewegung wird, basierend auf Profilanalysen, Bohrungen und der Rekonstruktion der Oberfläche vor der Hangrutschung, auf 60 Meter geschätzt. Der separierte Teilbereich des gesamten Talzuschubes Perfuchsberg wird am besten als Gesteinsrutschung, welche durch zwei Trennflächen begünstigt wurde und aktive, sekundäre, seichtere Rutschungen im Hangfußbereich aufweist, klassifiziert. Bezugnehmend auf die kinematischen Analysen könnten die Brüche und Risse im oberen Bereich, hinter der Abrisskante, durch großräumiges Toppling hervorgerufen werden. Weiteres wurden im Bereich der steilen Abrisskante sekundäre Versagensereignisse wie Steinschlag oder Felsstürze aufgezeichnet.

In einem weiteren Bereich des Untersuchungsgebietes wurden während der Kartierung, Profilanalyse und der Interpretation von Laserscan Daten, große, offene Brüche, Risse und steile Felswände aufgezeichnet. Basierend auf ingenieurgeologischen Untersuchungen ist es wahrscheinlich, dass Trennfläche 3 (337/81°) und Trennfläche 4 (53/62°) die Versagensmechanismen begünstigen. Kinematik- und Sensitivitätsanalysen berechneten für die Trennflächen im Gleichgewichtszustand, einen Reibungswinkel von 15-20°, in Abhängigkeit von der Kohäsion der Trennflächen und den hydraulischen Bedingungen im Berg. Als Versagensmechanismus wird großräumiges Toppling in Verbindung mit sekundären Versagensereignissen, Steinschlag oder Felsstürzen an den steilen Felswänden,

angenommen. Die Größe der nach unten gestürzten Blöcke kann von riesigen Felsblöcken bis zu kleinen Steinen und Schutt variieren.

Sehr wahrscheinlich haben Quartäre Prozesse, wie die Übersteilung der Hangflanken und das große Wasserangebot nach der Gletscherschmelze, die komplexen Hangversagensprozesse verursacht und ausgelöst. Die derzeitige Aktivität und Bewegungsrate wird vermutlich signifikant von der Erosionsaktivität des Flusses Sanna im Hangfußbereich und von auftretenden Starkniederschlagsereignissen sowie der saisonal bedingten Schneeschmelze beeinflusst

Table of Content

Abstract IV
Kurzfassung V
Table of Content VII
List of Figures IX
List of Tables XII
List of Abbreviations XIII

1 Introduction 1
1.1 Purpose and Scope of Work 1

2 Site Conditions 2
2.1 Geographic Setting 2
2.1.1 Climate 3
2.1.2 Site Location 4
2.1.3 Topography 4
2.1.4 Vegetation 4
2.1.5 Human Settlements and Infrastructure 5
2.2 Regional Geological Setting 6
2.2.1 Tectonometamorphic Evolution 9
2.2.2 Quarternary Evolution 9
2.3 Geological Conditions in the mapping Area 11
2.3.1 Lithological Units 11
2.4 Previous Geotechnical Investigations 14
2.4.1 Geotechnical Properties of the Bedrock Units 15
2.4.2 Geologic Structure 16
2.5 Geomorphology 17
2.6 Regional Landslide Activity 22

3 Landslide Perfuchsberg 29
3.1 Laboratory Tests 31
3.1.1 Thin Section Evaluation 32
3.1.2 Direct Shear Tests 32
3.1.3 Triaxial Compression Tests 34

4 Landslide Analysis 35
4.1 Subsurface Interpretation 35
4.2 Engineering Geological Analysis 39
4.2.1 Key Block Analysis 39
4.2.2 Stability Analysis using “SWedge” 43
4.2.3 Stability Analysis using “Slide” 47
4.2.4 Stability Analysis using “RocTopple” 51
4.3 Subsurface Model 53

5 Discussion and Conclusions 56
6 References 59
8 Appendix 64

List of Figures

Figure 1: Detailed geographic map of the area around Landeck with the framed position of the study area and the orange colored four largest landslides in this region [modified after BEV]. 2

Figure 2: Climate Diagram of Landeck [modified after tirolatlas.at]. 3

Figure 3: Exact study area with the two areas of greater interest framed blue [modified after BEV 2015]. 4

Figure 4: Orthophoto showing the study area with its urban districts and important infrastructure [modified after BEV, 2015]. 5

Figure 5: Schematic profile through the Eastern Alps [modified after GeoDZ.com]. The approximate location of the cross section is shown in Figure 6. 6

Figure 6: Tectonic map of the Silvretta nappe and its adjacent units [modified after Schmid et al., 2012] with the approximate location of the cross section shown in Figure 5. 7

Figure 7: Detailed view of the Silvretta nappe and the differentiation into Silvretta crystalline, Venet complex and Landeck Phyllite according to Gruber et al. (2010) [modified after Bousquet at al., 2012]. 8

Figure 8: Map of the Upper Inntal during the last glacial maximum at Würm [after Van Husen, 1987]. 10

Figure 9: Geological and geomorphological map of the study area [base map from BEV, 2013]. 11

Figure 10: Lower hemisphere stereographic projection – great circles and poles - of the schistosity measured during field investigation. 16

Figure 11: Lower hemisphere stereographic projection - poles of the joint sets j1 to j5 with density contour lines. 16

Figure 12: View toward east: typical u-shaped valley, with characteristic terraces, e.g. in the north of Landeck. 17

Figure 13: Smooth and slightly curved morphology at the grasslands in Tobadill. 17

Figure 14: Dimension of breaks in the slope under the church of Tobadill. 18

Figure 15: Rockfall material northwestward of Tobadill. 19

Figure 16: Steep headscarp area. 19

Figure 17: Small flattened area with a smoother surface NNE of the headscarp. Behind the 20

Figure 18: Steep toe of the slope downward to the Sanna River with the railway track. 20

Figure 19: Detailed geomorphic map of the study area based on the laserscan data [modified after TIRIS, 2015]. The green lines represent the location of the cross sections (c.f. chapter 4). ... 21

Figure 20: Distribution of landslides Zintlwald, Niedergallmigg, Gfäll and Perfuchsberg around the study area [modified after TIRIS, 2015]. 22

Figure 21: Exact location of the landslide Zintlwald and the influenced infrastructure [modified after TIRIS, 2015]. 22

Figure 22: Profile of the landslide Zintlwald [modified after Henzinger et al., 2008]. 24

Figure 23: Hillshade map of the deep-seated rock slide system Niedergallmigg showing primary and secondary scarps, strike-slip faults (SSF1, SSF2, SSF3), geodetic monitoring targets and the trace of the cross section A-A' [after Zangerl et al., 2012]. 25

Figure 24: N-S cross section along A-A' showing the rock slide geometry, the actual and pre-failure topography, displacement vectors of geodetic targets and geological setting [after Zangerl et al., 2012]. 26

Figure 25: Geomorphic map of the landslide Gfäll and its upper region [after Strobl, 2015]. 27

Figure 26: Detailed Profile of the landslide Gfäll [modified after Strobl, 2015]. 28

Figure 27: Morphologic map of the landslide Perfuchsberg with its most noticeable structures based on laserscan data evaluation and the location of the cross section at the toe area [modified after TIRIS, 2015]. 29

Figure 28: Cross section of the toe area of the landslide Perfuchsberg [modified after Poscher, 1993]. 30

Figure 29: Exact location of the rock samples. 31

Figure 30: Exact position of the cross sections in the study area. 36

Figure 31: Estimated cross section after glaciation. 36

Figure 32 Estimated cross section after the valley got filled up with fluvio-glacial sediments and shortly before the landslide happened. 37

Figure 33: Present day cross section. 38

Figure 34: Graphic illustration of the removable blocks. The blue circle represent the reference circle, the black circles the joint planes and the dashed circle represent the excavation plane / the slope. All blocks which have no intersection with the slope (dashed circle) are highlighted and get identified as removable blocks. 40

Figure 35: Graphic illustration on which joint planes the determined removable blocks possibly slide. The removable blocks with the failure joint planes are highlighted. 40

Figure 36: Tables for analysis. The left table shows the free plane and the right table the sliding force for each removable block. 41

Figure 37: Stability analysis for the key block 110101. The blue circle represents the reference circle and R marks the resultant force vector. 41

Figure 38: SWedge analysis for the key block 110101 in different perspectives. 43

Figure 39: SWedge analysis for the key block 100100 in different perspectives. 44

Figure 40: SWedge analysis for the key block 100101 in different perspectives. 45

Figure 41: Graphic of the potential key block 101100. 45

Figure 42: Slide profile under dry conditions with the most likely failure plane. 47

Figure 43: Slide profile under medium water table conditions with the most likely failure plane. 48

Figure 44: Slide profile under high water table conditions with the most likely failure plane. 48

Figure 45: Material properties which lead to FS = 1 charted at the left diagram. The trend line indicates limit equilibrium conditions. The red sector represents the unstable parameter conditions and the green sector the stable conditions. 49

Figure 46: Material properties which lead to FS = 1 charted at the left diagram. The trend line indicates limit equilibrium conditions. The red sector represents the unstable parameter conditions and the green sector the stable conditions. 49

Figure 47: Material properties which lead to FS = 1 charted at the left diagram. The trend line indicates limit equilibrium conditions. The red sector represents the unstable parameter conditions and the green sector the stable conditions. 50

Figure 48: Stability analysis at the area under the church of Tobadill with respect to toppling. 51

Figure 49: Stability analysis with respect to toppling at Area 1. 52

Figure 50: Geologic cross section of Area 1 from the study area. The exact location of the cross section can be taken from Figure 30. 53

Figure 51: Cross section of the estimated internal structure of the landslide deposit. 54

Figure 52: Cross section under the church of Tobadill. The exact location of the cross section can be taken from Figure 30. 55

List of Tables

Table 1: Overview of the geotechnical properties (UCS, φ, c) from phyllitic rock samples (Venet complex) taken at the Strenger tunnel [modified after Button, 2004]. 14

Table 2: Summary of the geotechnical properties of the Landeck phyllite and Venet complex after Alber, Wierer (2011). 15

Table 3: Geotechnical properties of the unweathered light phyllite micaschist and weathered light phyllite micaschist in the study area following ÖNORM EN ISO 14689-1. 15

Table 4: Results from the direct shear test..... 32

Table 5: Results from the triaxial compression test..... 34

Table 6: Dip direction and dip angle of the determined planes 39

Table 7: Different FS due to different water pressures 44

Table 8: Comparison of the FS results obtained from the stability analysis using the software SWedge and the key block stability software. 46

Table 9: Assumed material properties..... 47

Table 10: Material properties of the “failure surface” without the water table which lead to FS = 1. 49

Table 11: Material properties of the “failure surface” with medium water table which lead to FS = 1. . 49

Table 12: Material properties of the “failure surface” with high water table which lead to FS = 1..... 50

List of Abbreviations

approx.	approximately
a.s.l.	above sea level
c	cohesion
c_{res}	residual cohesion
cf.	compare (lat. confer)
cm	centimeter
e.g.	for example (lat. exempli gratia)
EP	excavation plane
FS	factor of safety
i.e.	that is (lat. id est)
JP	joint plane
JRC	joint roughness coefficient
JS	joint set
kN/m^3	kilo Newton per cubic meter [Unit Weight unit]
kPa	kilo Pascal
m	meter
mm	millimeter
m/a	meter per year
m/min	meter per minute
m/s	meter per second
mm/a	millimeter per year
mm/s	millimeter per second
mio.	million
MPa	Mega Pascal
SP	space pyramid
UCS	uniaxial compression strength
v	Poisson ratio
°	degree
°C	degree in Celsius
ϕ	friction angle
ϕA	available friction angle
ϕM	mobilized friction angle
ϕ_{res}	residual friction angle
µm	micrometer

1 Introduction

1.1 Purpose and Scope of Work

The landscape around Landeck, Tyrol, is affected by several mass movements. Only few areas in Austria have such a high occurrence of deep-seated landslides. Some landslides are monitored in the course of different projects and are well understood from the geological and geotechnical perspective. [*Gruber et al., 2010*] For example the landslide Zintlwald in the eastern Stanzer valley has been worked out in detail and is constantly monitored in combination with an early warning system since the flood water event in 2005 [*Henzinger et al., 2008*]. There exists also a high state of knowledge for the landslide Niedergallmigg in the upper Inn valley southeast of Landeck [*Zangerl et al., 2012*].

Many other unstable slopes also affect infrastructure and settlements. They are however observed only punctually, including for example the mass movement Gfäll, at the very beginning of the Pauznaun valley and the mass movement Perfuchsberg, at the southwest of Landeck. [*Gruber et al., 2010*]

This master thesis is concerned with the landslide Perfuchsberg. The aim is, to determine the geological conditions, the failure mechanisms, causes and kinematics of the slope instability and to document the influence of the slope deformation on infrastructure and buildings.

For this purpose the following process steps have been carried out:

- Desk study of existing literature, investigation and measurement data, including topographical and geological maps, laserscan data and orthophotos
- Geological, structural und geomorphological field mapping and rock sampling
- Laboratory testing to receive comparable values, including:
  - Direct shear tests after *ÖNORM CEN ISO/TS 17892-10* and *ISRM (2013)*
  - Triaxial compression tests after *ÖNORM CEN ISO/TS 17892-8* and *ISRM (1983)*
- Analysis, interpretation and comparison of the testing results
- Slope stability analysis according to "*Block Theory" after Goodman and Shi (1985)* together with
- Failure mode analysis to define the preceded and occurring landslide processes.

2 Site Conditions

2.1 Geographic Setting

The study area is situated in the west of Landeck district, in Tyrol, Austria, in the Samnaun mountain range. Landeck is located in the Upper Inn valley.

The Upper Inn valley is a south-west to north-east directed valley and has a very narrow cross section in this part. It is bordered by the Northern Calcareous Alps in the north and by the Central Alps in the south. The larger lateral valleys are the Pitz valley and the Ötz valley entering the Upper Inn valley from the south, the Gurgl valley from the north and the Stanzer valley from the west. The Stanzer valley is drained by the river Rosanna, while the Paznaun valley is drained by the river Trisanna. Eventually, the Rosanna and Trisanna merge to the river Sanna, which flows from the west directly down the valley under the landslide Perfuchsberg until the river gets into the Inn at Landeck (Figure 1).

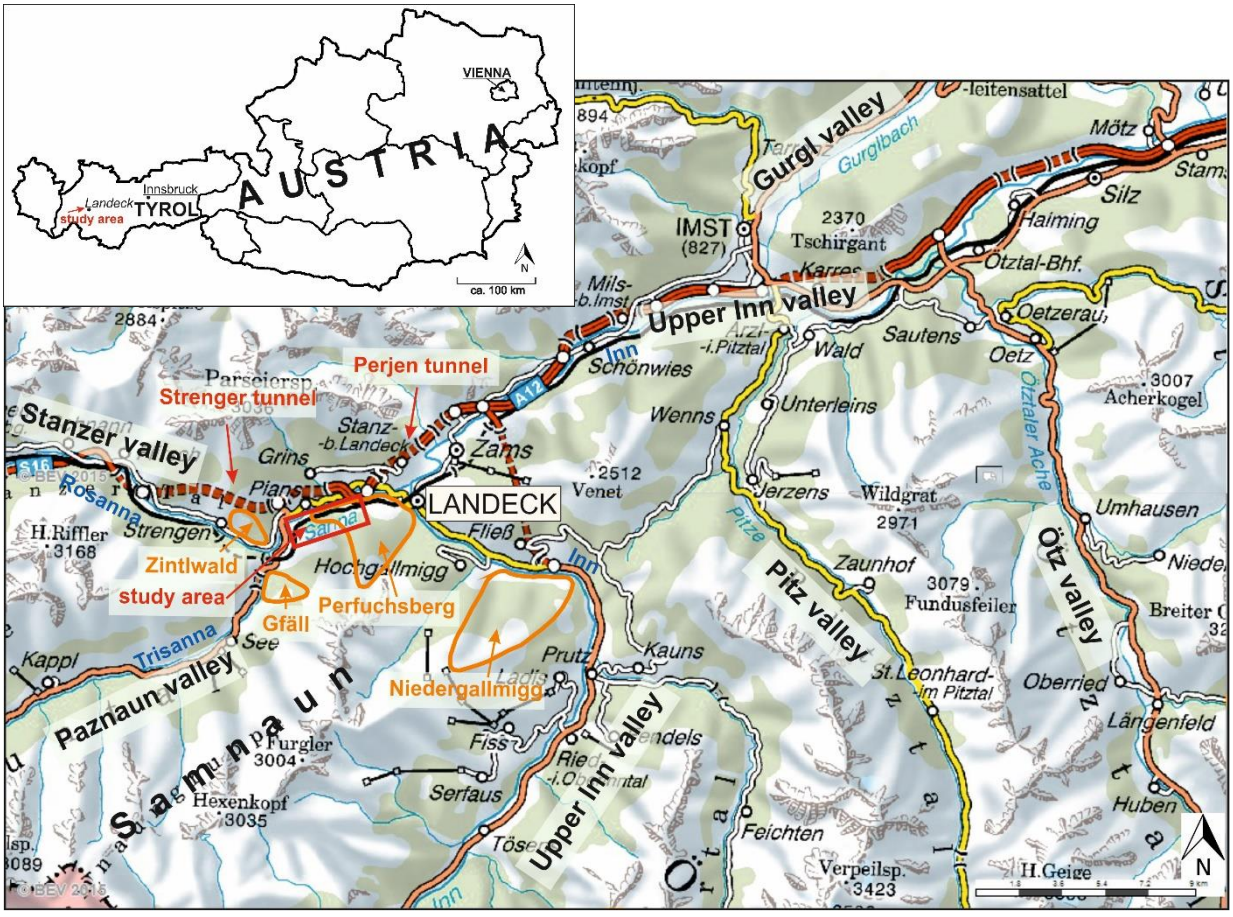

Figure 1: Detailed geographic map of the area around Landeck with the framed position of the study area and the orange colored four largest landslides in this region [modified after BEV].

2.1.1 Climate

Tyrol is subjected to the central European climate. It is influenced by both humid, oceanic climate from the west and dry, continental climate from the east [*Riegler, 2006*]. The climate is characterized by moderate temperatures with a summer maximum. The precipitation is distributed over the whole year, with the maximum occurring in summer [*cf. Figure 2*].

The next meteorological station at the town Landeck give a mean annual temperature of 8.7°C and a mean annual precipitation of 814 mm.

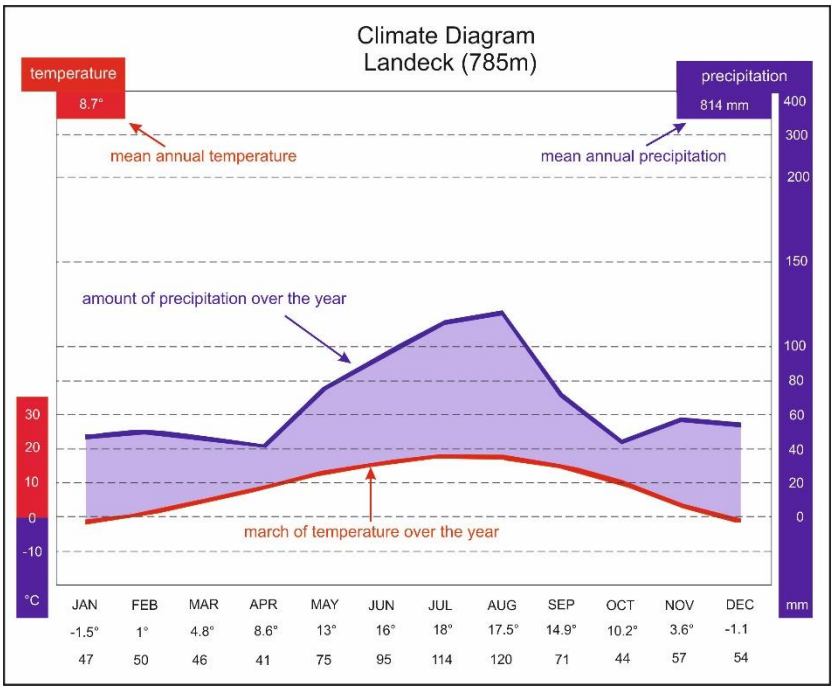

Figure 2: Climate Diagram of Landeck [modified after tirolatlas.at].

Additionally, the local climate is superimposed by alpine components, such as temperature reduction going along with increasing amount of precipitation with increasing elevation, different amount of precipitation on the stoss and lee slopes, different thermal insulation at the slopes, the inversion weather in winter and the warm falling wind (“Föhn”) in autumn and spring [*Riegler, 2006*]. Those phenomena give rise to differing microclimates in neighbouring valleys.

2.1.2 Site Location

The exact location and extension of the study area with its most important geographic features that are mentioned in the present thesis is shown in Figure 3.

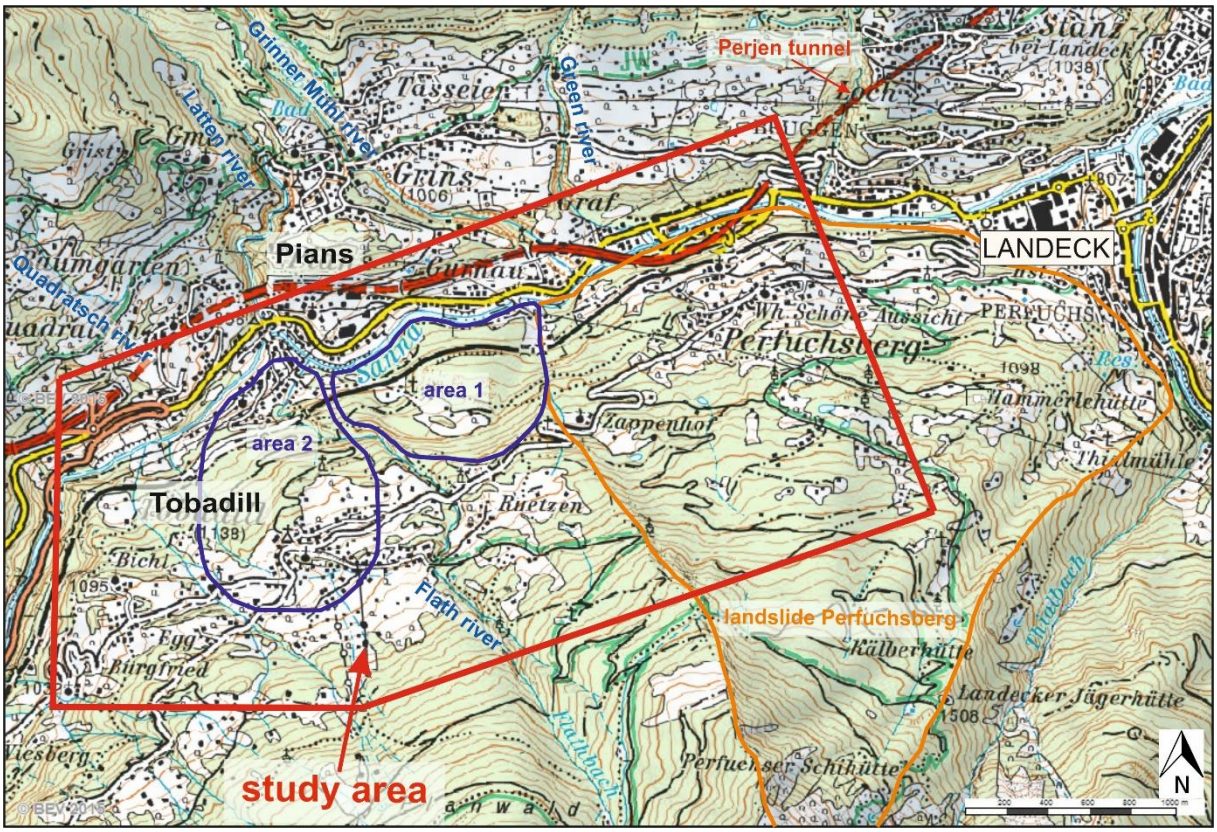

Figure 3: Exact study area with the two areas of greater interest framed blue [modified after BEV 2015].

2.1.3 Topography

The mapping area follows the Sanna stream from west to east, through the municipalities Pians, Tobadill and Landeck and has an area of about four km^2. The Sanna is representing the lowest point at the working area and has an elevation of about 790 m. On the orographic right side it goes up to 1,300 m and on the orographic left side up to 1,000 m. There are several tributary rivers flowing in the Sanna: These are from the south the Flath river and from the north the Quadratsch river, the Latten river, the Grinner Mühl river, the Hochrinner and the Green river.

2.1.4 Vegetation

The main part of the study are consists of a mix forest with spruces, pines, beeches, oaks, larches, alders and some firs, which sometimes is disrupted by free grasslands, human settlements and infrastructure. The grasslands are used for agriculture. The large boulders of the rockfall material are overgrown with lichens or mosses, whereas the younger ones are not covered by now.

2.1.5 Human Settlements and Infrastructure

The study area is next to the district capital Landeck (Figure 4). Landeck is the biggest city in the Tyrol Upland and represents an economic and cultural centre. Landeck has a large urban catchment and is the supply centre for thousands of people.

In the study area the urban districts Perfuchsberg, Tobadill, Grins and Pians are located. The small communities have their own administrative buildings, churches and village squares and are connected with narrow mountain roads.

In the valley the railway track from the ÖBB pass through. This railway track is the only and most important railway connection through the Stanzer valley respectively to Vorarlberg and has to keep workable anytime.

On the orographic left side of the Stanzer valley the highway with traffic connections, infrastructure and the Perjen tunnel are situated. In the course of those and other projects several geological and geotechnical investigations and monitoring were done and documented [*Alber & Wierer, 2011*].

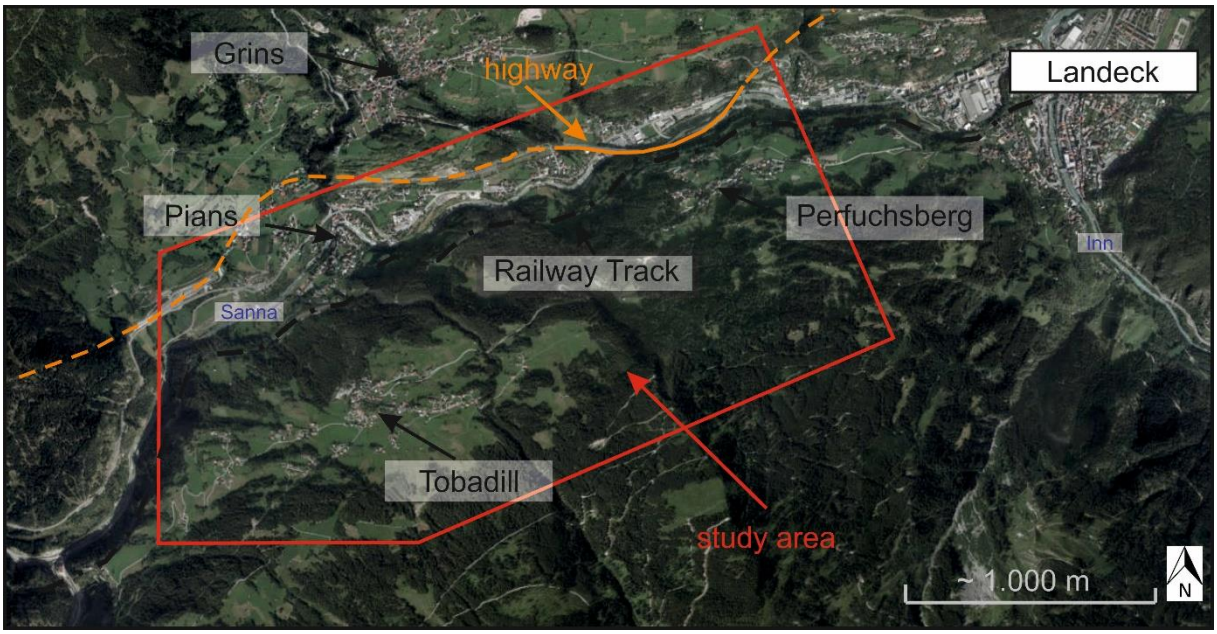

Figure 4: Orthophoto showing the study area with its urban districts and important infrastructure [modified after BEV, 2015].

2.2 Regional Geological Setting

The study area is situated in the Silvretta nappe, representing the western part of the Silvretta-Seckau nappe system. According to *Schmid et al. (2004) or Schuster (2004)*, tectonically, the Silvretta-Seckau nappe system constitutes the crystalline basement of the Upper Austroalpine unit. The Silvretta nappe lies as an about five kilometer thick slab on top of the Lower Austroalpine unit and the Penninic units. [*Gruber et al., 2010*]

The underlaying Penninic units appear at the Engadine window through the Austroalpine. This tectonic window with the sinistral Engadine line present the adjacent unit at the east and southeast. Tectonically, the Ötztal nappe overlays the Silvretta nappe at the east and the northern border to the Bavarian nappes of the Northern Calcareous Alps is exactly defined with the Stanzertal fault zone. From southwest the Err-Bernina nappe (Lower Austroalpine) and from west the Penninic units of Switzerland confine the Silvretta nappe (Figure 5). [*Gruber et al., 2010*]

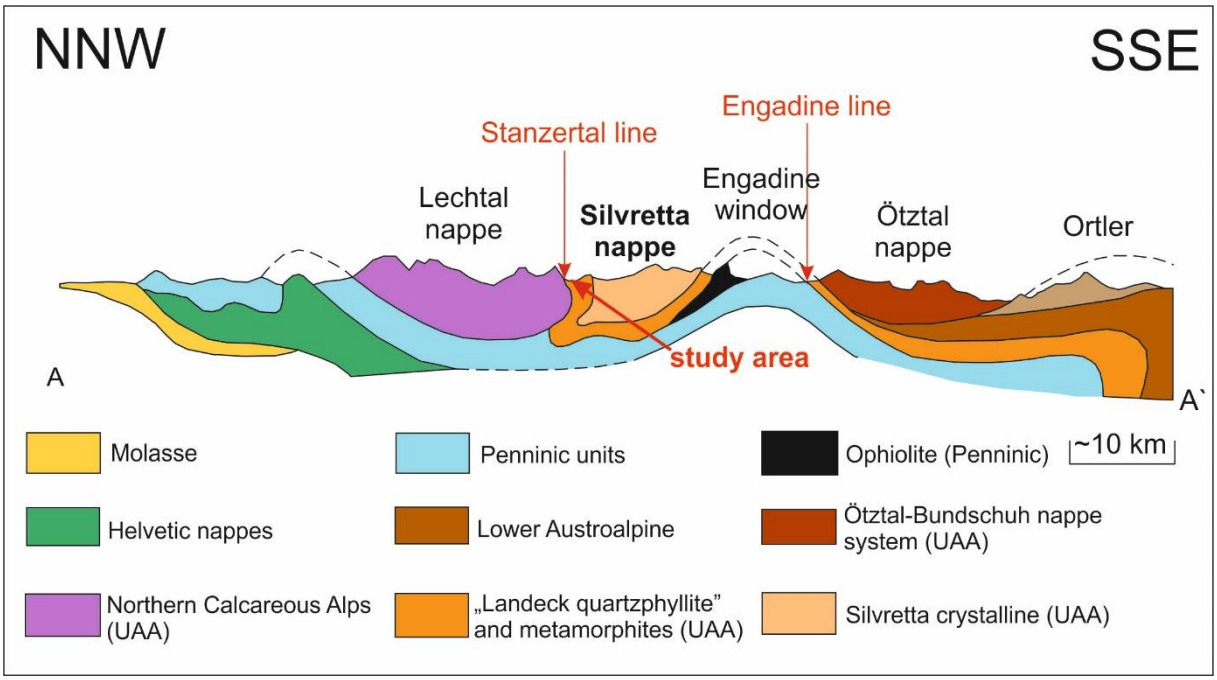

Figure 5: Schematic profile through the Eastern Alps [modified after GeoDZ.com]. The approximate location of the cross section is shown in Figure 6.

The Stanzertal line is a wide fault zone and border the Lechtal nappe (Northern Calcareous Alps) at the north from the Silvretta nappe at the south. It is a system of faults which are ENE-WSW to ESE-WNW striking. [*Gruber et al., 2010*]

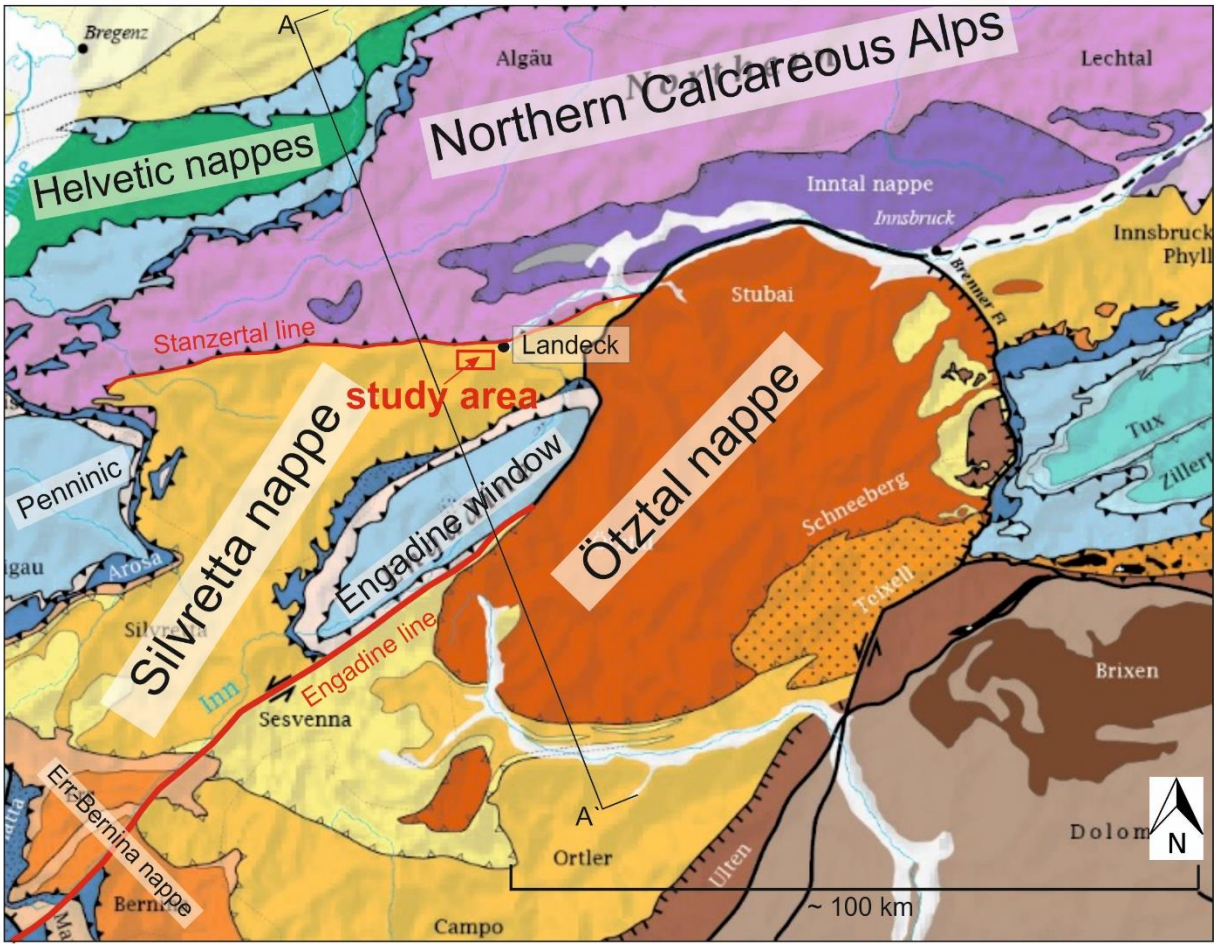

Figure 6: Tectonic map of the Silvretta nappe and its adjacent units [modified after Schmid et al., 2012] with the approximate location of the cross section shown in Figure 5.

Gruber et al. (2010) divides the Silvretta nappe into three different units (Figure 7), according to its tectonometamorphic evolution (c.f. chapter 2.3.1):

- The Silvretta crystalline constitutes the major part of the Silvretta nappe. The crystalline is composed of partly migmatic paragneisses, different mica schists and orthogneisses, lenses of amphibolites, metagabbros, eclogites, pegmatites, diabases and sporadic marbles. In the north-east, the Silvretta crystalline consists of metasediments (different mica schists and paragneisses). Orthogneisses and amphibolites only occur in small lamellas. [*Gruber et al., 2010*]
- The rock formations at the northern border of the Silvretta nappe, near the Stanzertal line, are related to the Venet complex and the Landeck Phyllite. The Venet complex is composed of phyllonitic micaschists respectively phyllonites. Those rocks are extensive foliated, jointed and folded. [*Gruber et al., 2010*]
- The light-colored phyllites, the so called Landeck Phyllite, are intensely foliated, sericite-chlorite phyllites. They occur only in a several hundred meter thick band northwards the Venet complex, with direct contact to the Stanzertal fault system and the Northern Calcareous Alps. [*Alber & Wierer, 2011*]

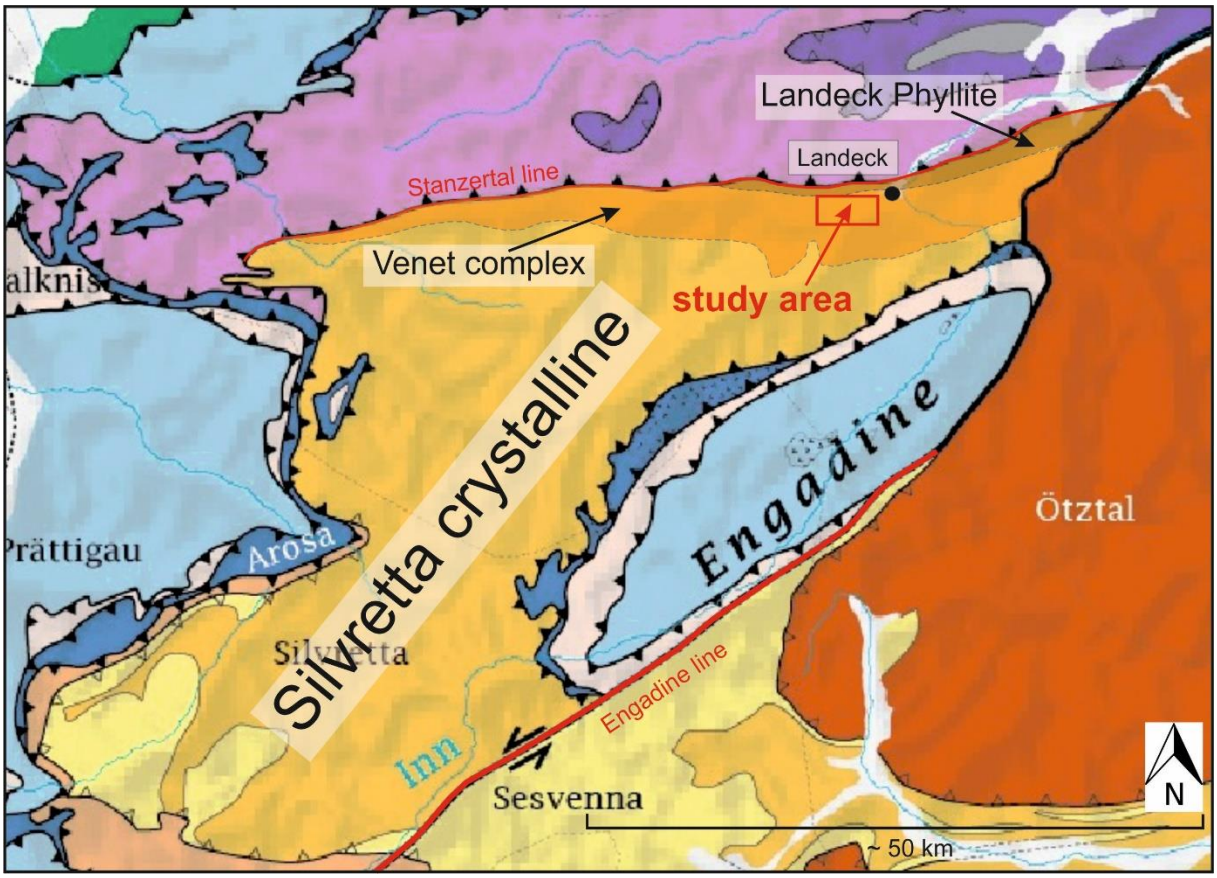

Figure 7: Detailed view of the Silvretta nappe and the differentiation into Silvretta crystalline, Venet complex and Landeck Phyllite according to *Gruber et al. (2010)* [modified after Bousquet at al., 2012].

2.2.1 Tectonometamorphic Evolution

The main internal deformation of the Silvretta crystalline took place during the Variscan orogeny (400 - 280 mio. years ago). The early Variscan high temperature metamorphism had its metamorphic peak 370 - 340 million years ago and the metamorphism conditions are assigned to an amphibolite- and/or eklogite facial regional metamorphism. The Eoalpine and Alpine (approx. 90 mio. years ago) metamorphism had no impact on large parts of the Silvretta crystalline. [*Maggetti & Flisch, 1993*]

The Venet complex received an intensive alpine retrograde overprint and deformation during the alpine metamorphic event (approx. 90 mio. years ago) and is extensive foliated, jointed and folded. [*Maggetti & Flisch, 1993*]

The Landeck Phyllite was affected by a prograde Alpine metamorphism (approx. 90 mio. years ago) with a temperature of about 300 - 350 °C and greenschist facial conditions. [*Maggetti & Flisch, 1993*]

2.2.2 Quarternary Evolution

Not only internal deformations and orogeny events gave the study area it´s present appearance. The glacial epochs (since 2.6 mio. years) and associated extensive erosion activity are also responsible for the morphology. [*Gruber et al., 2010*]

Since the Pliocene (5.3 - 2.6 mio. years ago) increasing erosion took place and high amounts of debris get carried out by streams. At the beginning of the Quarternary epoch (approx. 2.6 mio. years ago) the valley systems in the Alps has been established in large parts. Since the Middle Pleistocene (approx. 800,000 years ago) four glacial epochs are detected and are referred to as Günz, Mindel, Riss and Würm. They are characterized by a full glaciation of the Alps. [*Van Husen, 1987*]

The last glacial maximum was during the Würm glacial (14,000 years ago) and was initiated from the high mountain ranges. Starting from the source areas, the glaciers spread out through the existing valleys. At Landeck three valley glaciers, i.e. the Inn valley-, Stanzer valley- and Paznaun valley-glaciers merged. During the last glacial maximum the Upper Inn valley and its lateral valleys (Stanzer valley, Paznaun valley) were covered by approx. 2,400 meters of ice (Figure 8). Only the highest summits, the so called Nunatakker, were exposed. [*Gruber et al., 2010*]

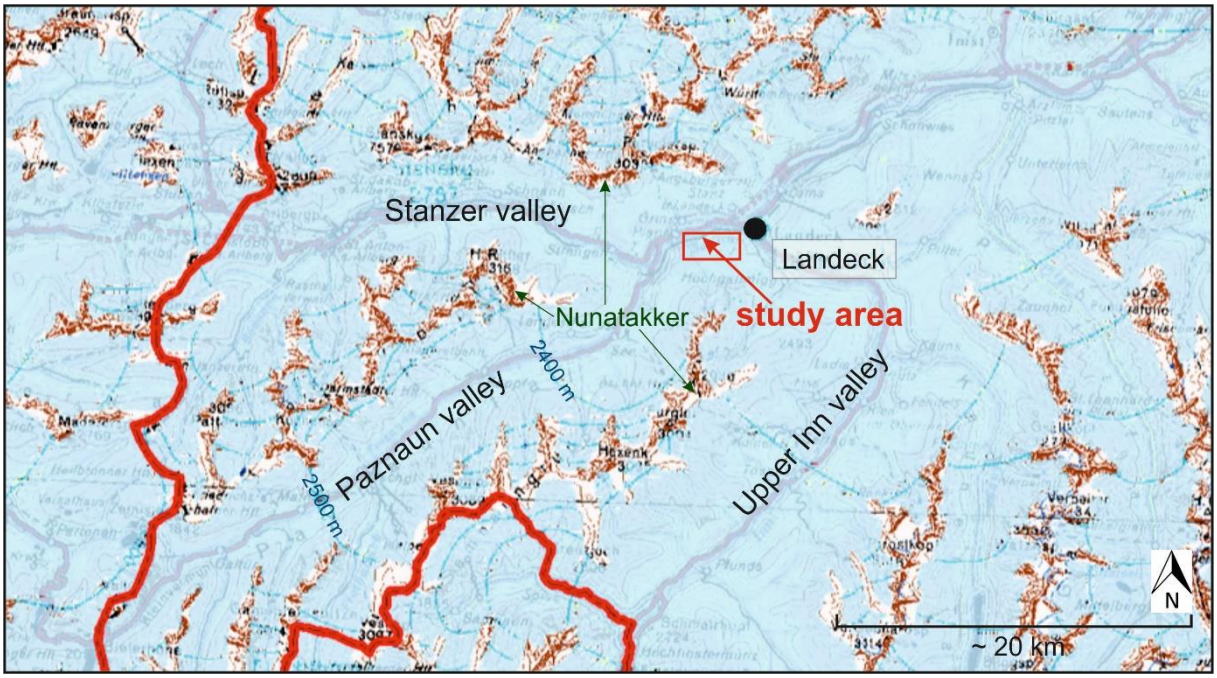

Figure 8: Map of the Upper Inntal during the last glacial maximum at Würm [after Van Husen, 1987].

At many locations the erosional and depositional forms of the ice age can be noticed: overdeepened U-shaped valleys, hanging valleys, cirques and horn peaks, whalebacks, glacial terraces, moraine deposits and glacial polish [*Gruber et al., 2010*]. The glacial overdeepening at Landeck is documented by drillings and refractions seismic measurements. The valley got filled up with fluvio-glacial sediments for approx. 100 meters [*Poscher, 1993*].

After the glacier retreated oversteepened slope flanks were left back. It is assumed that the large landslides have their origin in the early late glacial, when the glacial support was lost. Among the active landslides the alluvial erosion and avalanches and torrent activities during floodwater are primarily responsible for displacement of hard rocks and soils. Today the valley structures still get changed, streams get retained or redirected and transformations move forward. [*Gruber et al., 2010*]

2.3 Geological Conditions in the mapping Area

Figure 9 shows the detailed map of the project area at a scale of 1:10,000. The lithological units and quaternary deposits are explained in detail in the following chapter. As a base for the field mapping topographical (*ÖK 1:50,000*) and geological (*"Geologische Karte der Republik Österreich" 1:50,000, 2004, Kartenblatt 144 Landeck*) maps of the area around Perfuchsberg are used.

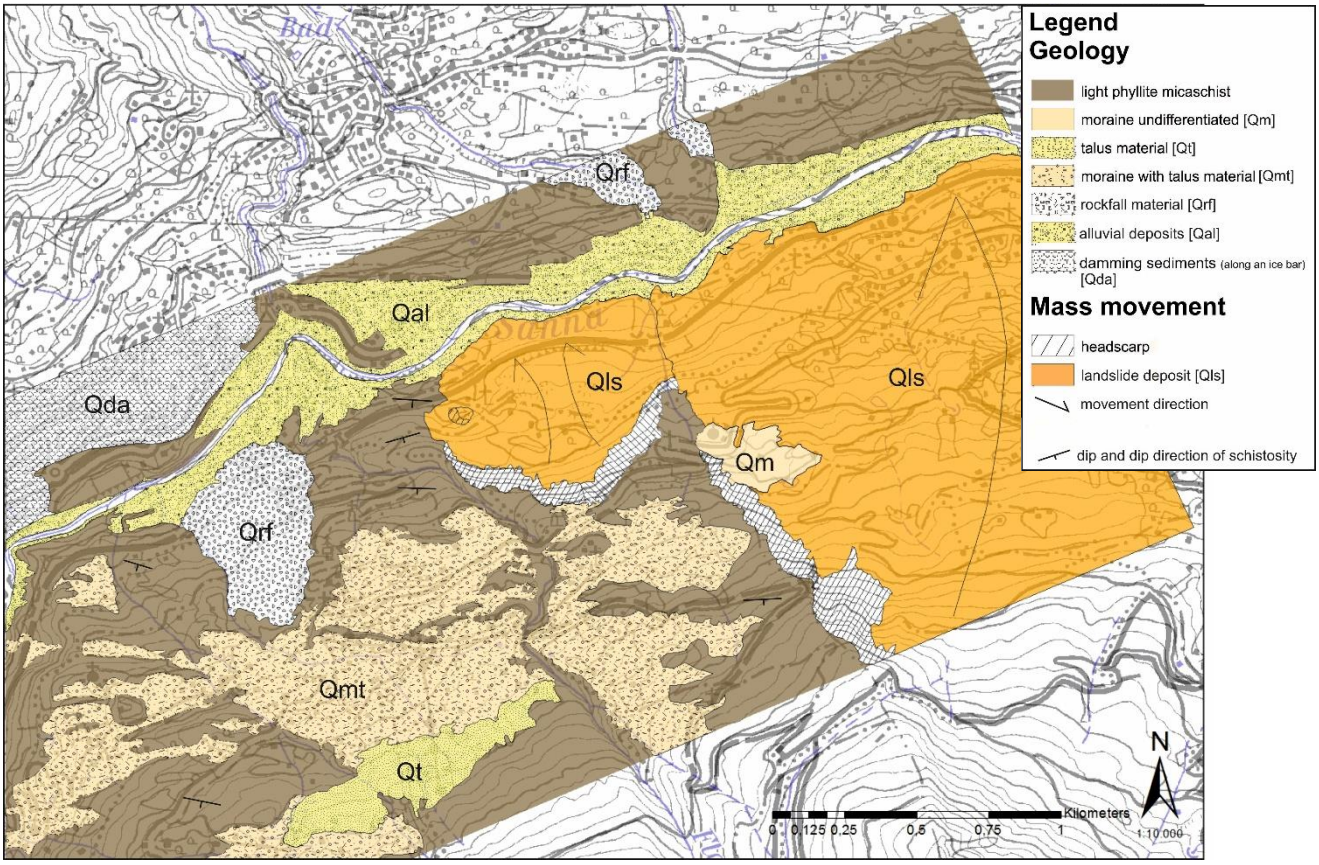

Figure 9: Geological and geomorphological map of the study area [base map from BEV, 2013].

2.3.1 Lithological Units

2.3.1.1 Quaternary Deposits

ALLUVIAL DEPOSITS [Qal]

The stream channel of the Stanzer valley consists of alluvial sediments. At some areas, e.g. around Grins, those sediments build up several terrace levels from late-glacial until recent. The deposits are made up mostly by mixed-grained sediments occasional disconnected by fine-grained layers. Where the tributary rivers flow in the Sanna inactive alluvial fans exist.

DAMMING SEDIMENTS ALONG AN ICE BAR [Qda]

The damming sediments were formed when the ice stream retreated and the dead ice blocks were left back. Through the plenty mass of easily erodible sediments as well as huge melt water amounts the loose material was deposited at the margin of the dead ice bodies. The damming-ice sediments represent a mixture of alluvium-glacial deposits and glacial-lacustrine accumulations. [*Gruber et al., 2010*] At the study area the damming materials consists of unconsolidated rock accumulations with a sandy-gravely grain composition of calcalpine and crystalline origin. At some places an incomplete cementation is noticed. The damming ice deposits in the western part of the study area, next to Grins and Pians, had a thickness up to 60 meters. Then the material got won for economic reasons [*Gruber et al., 2010*].

MORAINE UNDIFFERENTIATED [Qm]

Undifferentiated moraine is found east of Tobadill and includes glacial deposits from all glacial activity at the Würm glacial (approx. 14,000 years ago) until nowadays. That includes ground-, ablation-, lateral- and end moraines, because an accurate differentiation in field, due to rearrangement processes, mixing respectively covering processes, is very difficult. The deposit material is an unsorted mix of clay, silt, sand, gravel, stones and blocks. The bigger blocks are “swimming” without contact to each other in the finer grained matrix.

TALUS MATERIAL [Qt]

Talus deposits consist of angular rock fragments of different sizes. The size depends on the bedrock and rock properties, schistosity, joint planes, water content and alteration. The material breaks off, mainly by frost bursting, and gets transported downslope from steep rock faces or scarps only through gravitation. Whereas of course other processes, like heavy rainfalls or snow avalanches, have an important influence on rock falls and transport. At the south part of the project area talus deposits are mapped and the debris is build up in large part with coarse grained material (stones, blocks).

MORAINE WITH TALUS MATERIAL [Qmt]

Some moraine material is distributed over the bedrock and alternates in small scale with talus deposits. These sediment mix is referred as to moraine with talus material and occurs in the south part of the study area.

ROCK FALL MATERIAL [Qrf]

The area westward from the Flathbach is located under steep rock faces, where rock falls have occurred and are still possible. The deposit consists of very big boulders of rocks. The older blocks are covered already with vegetation (moss).

2.3.1.2 Bedrock

LIGHT PHYLLITE MICASCHIST

The geological formations, the Venet complex and the Landeck phyllite, get summarized with the term light phyllite micaschist, because an accurate distinction at a macroscopic scale in field is not possible. The retrograde overprinted, phyllonitic mica schists of the Venet complex and the prograde greenschist faciel phyllites of the Landeck phyllite look almost the same, with consideration to the tectonical and mineralogical conditioned lithological variation limit. [*Gruber et al., 2010*] For this reason the term “Landecker quartzite phyllite” was commonly used in the past.

This light phyllite is a high foliated, light grey to green-grey rock. It is intense folded with abundant crenulations. The main mineral content is dominated by muscovite, quartz and feldspar. Muscovite often occurs in continuous layers and / or covers the schistosity surfaces. Those layers cause a high anisotropy of the rock mass. Often the schistosity surfaces show fine foliation respectively crenulation.

At the outcrops all rock varieties have a light-ocher-brown, limonitic weathering cover. Quartz mobilisations form either lenses or banded, millimetres to centimetres thick segregations.

Depending on the tectonically shear strain and the sheet silicate to quartz/feldspar proportion the rocks can look very different. Variations from schisty and phyllitically to a gneiss habitus can happen every 50 cm but also after more than 10 meters.

The joint structure is dominated by the schistosity planes and the joint distance is about 5 to 30 cm. At highly deformed areas the distance gets lesser to only a few millimetres. The schistosity planes are rippled and smooth and often covered with sericite respectively muscovite.

The light phyllite micaschist is the only bedrock mapped in the study area.

2.4 Previous Geotechnical Investigations

Due to the construction of several construction projects, e.g. highway, railway, tunnels, extensive and detailed geological and geotechnical investigations were done. The following chapter summarizes the geotechnical results gained from the construction projects Strenger tunnel and Perjen tunnel.

Button (2004) analyses phyllitic rock samples from the “Landeck quartzphyllite” - Venet complex after *Gruber et al. (2010)* - obtained during construction of the Strenger tunnel, west of Landeck (Figure 1). The geotechnical properties - UCS, friction angle (φ) and cohesion (c) - are summarized in table 1. Both direct shear test and triaxial compression tests were performed. The direct shear test samples were tested parallel to the foliation.

Table 1: Overview of the geotechnical properties (UCS, φ, c) from phyllitic rock samples (Venet complex) taken at the Strenger tunnel [modified after Button, 2004].

		Direct Shear Test		**Triaxial Compression Test**	
	UCS [MPa]	**φ [°]**	**c [MPa]**	**φ [°]**	**c [MPa]**
Minimum	12	25	0.4	32	3.5
Maximum	55	28	0.6	44	5.4

During the design and construction of the first and second tube of the Perjen tunnel more geological and geotechnical information about the Landeck phyllite and Venet complex was detected.

Köhler (1983) describes the engineering geological situation of the phyllonites at the first tube of the Perjen tunnel: Because of the distinct foliation with laminar cleavage the mechanical strength of the phyllonites is low. The foliation planes can act as shear planes (planes of movement). They dip direction is southward and often they are covered with sericite. The phyllonites are very water sensitive. Also a low moisture content can lead to a loss of stability and an increases for the possibility of landslides. Although the water capacity of the phyllonitic rocks itself is low. The quartz or gneiss lenses and intercalations feature a higher stability and lower sensitivity to water. [*Köhler, 1983*]

Alber, Wierer (2011) (ASFiNAG) deal with the design and construction of the second tube of the Perjen tunnel. Three different rock types get distinguished: light phyllites, phyllonitic micaschists and schistose gneisses (equal to *Krainer et al., 2004*). Following

ÖNORM EN ISO 14689-1 the characteristics of the corresponding rock mass types were evaluated and summarized in Table 2.

Table 2: Summary of the geotechnical properties of the Landeck phyllite and Venet complex *after Alber, Wierer (2011).*

Rock Type	Rocks		Joints			
	UCS [MPa]	Weathering [0-4]	Spacing [mm]	Roughness	Aperture [mm]	Filling
Landeck Phyllite	5 - 50	0	< 20	planar, smooth	< 0.1	partly plastic fillings
Venet Complex	5 - 50	0	20 - 60	planar, smooth	< 0.1	partly plastic fillings

2.4.1 Geotechnical Properties of the Bedrock Units

The geotechnical properties of the bedrock - light phyllite micaschist - were determined during field work using field estimation methods according to ÖNORM EN ISO 14689-1 at seven different outcrops in the study area. Table 3 summarizes the geotechnical characteristics.

Table 3: Geotechnical properties of the unweathered light phyllite micaschist and weathered light phyllite micaschist in the study area following ÖNORM EN ISO 14689-1.

Rock Type	Rock		Joints				
	UCS [MPa]	Weathering [0-4]	Spacing [mm]	Roughness	Water	Aperture [mm]	Filling
Light Phyllite Micaschist (fresh)	5 - 25	1 - 2	60 - 600	undulating, smooth - rough	-	0 - 50	partly silty clay
Light Phyllite Micaschist (weathered)	< 5	3 - 4	< 60	stepped, rough	-	0 - 30	partly silty clay

Table 3 shows that there is a difference between the UCS of the unweathered/fresh light phyllite micaschist (5-10 MPa) and UCS of the weathered light phyllite micaschist (< 5 MPa). The fresh light phyllite micaschist indicates a higher mechanic strength and also larger spacing and apertures than the weathered micaschist. The joint roughness of the weathered michaschist is stepped and rough, whereas the fresh micaschist has undulated and both, smooth and rough, joint planes.

2.4.2 Geologic Structure

During field mapping numerous schistosity surfaces at different locations in the study area get determined and measured. A total amount of 42 schistosity measurements were done und shown in Figure 10. The schistosity shows a homogenous E-W to ESE-WNW striking, in average 175 degrees and dips to the south with a mean dip angle of about 63°.

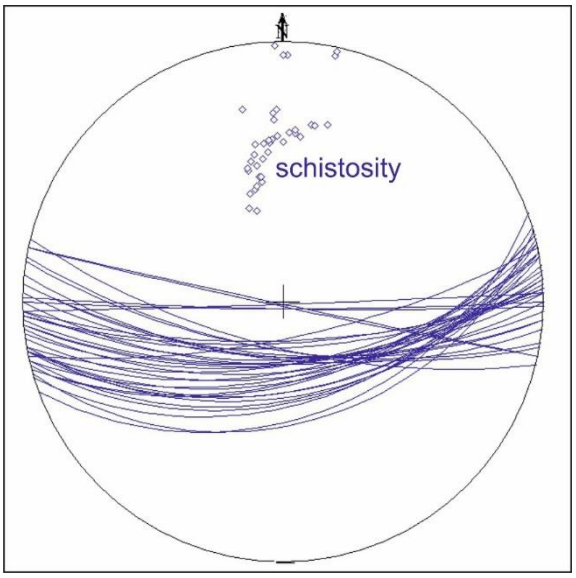

Figure 10: Lower hemisphere stereographic projection – great circles and poles - of the schistosity measured during field investigation.

The joint set systems were identified and recorded at certain outcrops, using field estimation methods following ÖNORM EN ISO 14689-1. Five different joint sets in addition to the schistosity get determined: Joint set 1 139/68°, joint set 2 219/51°, joint set 3 337/81°, joint set 4 53/62° and joint set 5 336/21°.

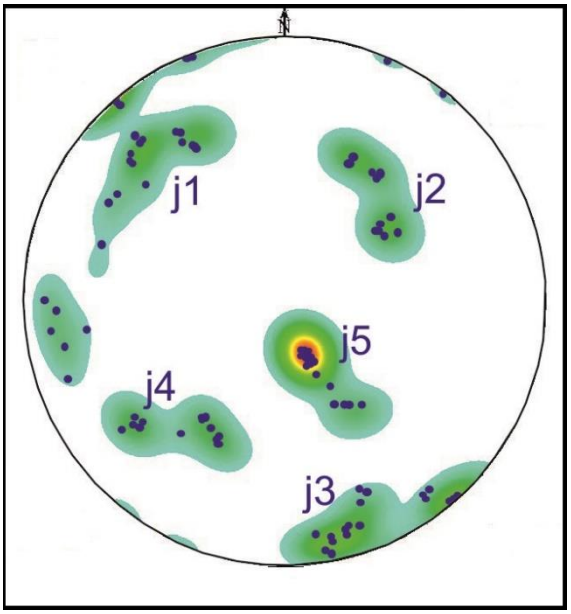

Figure 11: Lower hemisphere stereographic projection - poles of the joint sets j1 to j5 with density contour lines.

2.5 Geomorphology

During the last glacial epoch (Würm, approx. 14.000 years ago) the whole project area was covered by the glacier. The erosional activity of the ice formed the existing, rounded morphology with the typical u-shaped-valley. Good examples for the smooth and slightly curved physiography are shown at the grasslands in Tobadill and on the terrace in Pians and Grins, where sheepback rocks and glacial polish are found.

Figure 12: View toward east: typical u-shaped valley, with characteristic terraces, e.g. in the north of Landeck.

Figure 13: Smooth and slightly curved morphology at the grasslands in Tobadill.

Glacial sediments include moraines and late glacial damming sediments along an ice bar. Those sediments were eroded largely and occur only as local deposits, mixed with talus material or covered with talus material. They have a smooth and uniform morphology and an approx. slope inclination of 30°.

At the stream channel of the Sanna alluvial sediments are found. Those sediments originate from several late glacial until recent terrace levels. The surface is smooth and uniform with an inclination of approx. 4° at the Sanna level. At the tributary rivers, in very small scale, also alluvium occurs with a slope inclination that usually do not exceed 25°.

At the street, downhill from the church of Tobadill, large breaks, cracks and fractures are documented. They have a dimension of several meters and are distributed all over this area, also on the very front of the slope (Figure 14).

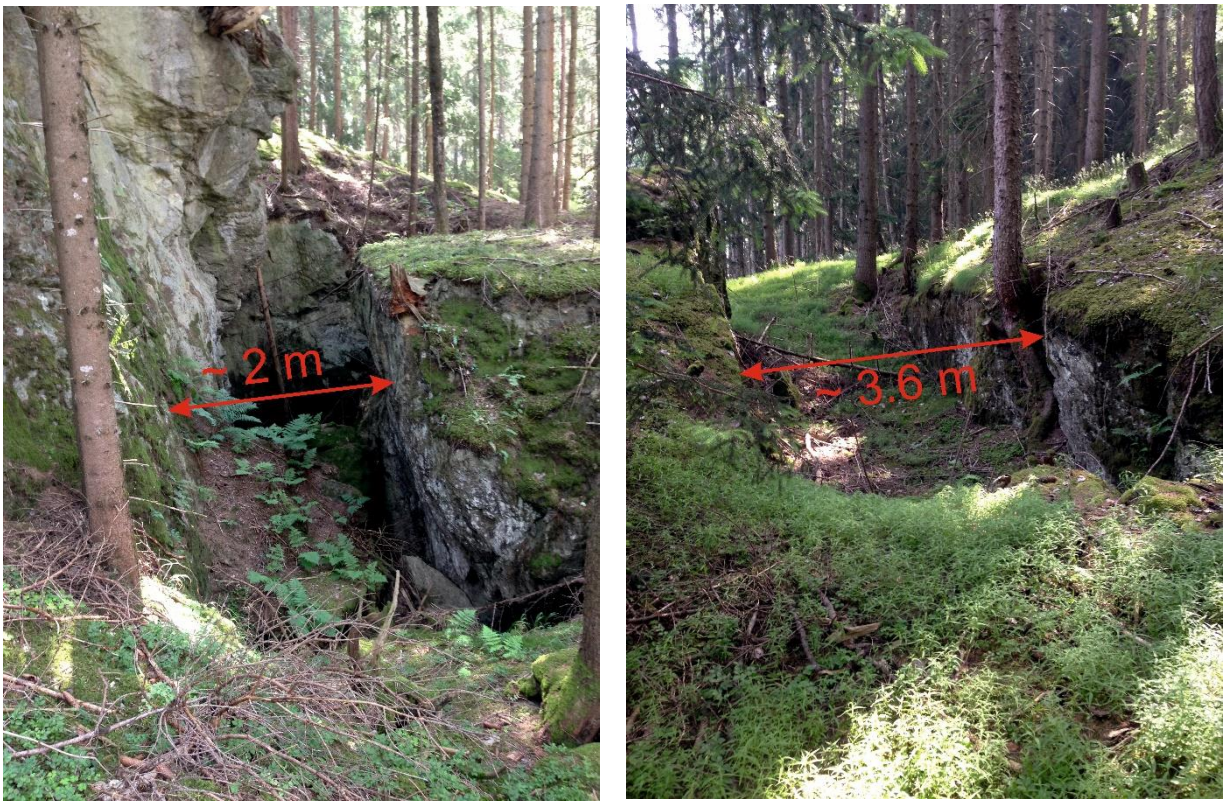

Figure 14: Dimension of breaks in the slope under the church of Tobadill.

The rockfall material, west- and northward the large cracks, are characterized by a rough and uneven morphology due to the existence of boulders and large rock fragments. The slope inclination is rather steep and about 35 – 40°.

Figure 15: Rockfall material northwestward of Tobadill.

Near the street to Tobadill, one kilometer eastward from Tobadill, a very steep part, with an approx. height of 70 meters and an extension of 800 meters is mapped (Figure 16). At this part the morphology is irregular and rough, destroyed rocks, boulders and trees are laying around and block of rocks are crumbling down from time to time. Below the steep slope a small flattened area with a smoother surface is located and then it goes again steep downward to the Sanna. On the way down small, about three metres high, “horst and graben” structures one after another are found.

Figure 16: Steep headscarp area.

Figure 17: Small flattened area with a smoother surface NNE of the headscarp. Behind the forest the headscarp area is located.

Figure 18: Steep toe of the slope downward to the Sanna River with the railway track.

Based on desk study and detailed field mapping Figure 19 shows the before mentioned geomorphic features on the laserscan data. The geomorphic map illustrates the exact location of the large breaks, cracks and fractures under the church of Tobadill. In the southeast noticeable structures of the slope get observed during laserscan evaluation and field investigations. Southward the steep headscarp areas small convex morphologies are found more frequently than concave slope structures. The two green lines are representing the location of the cross sections, which get analysed in the course of this thesis.

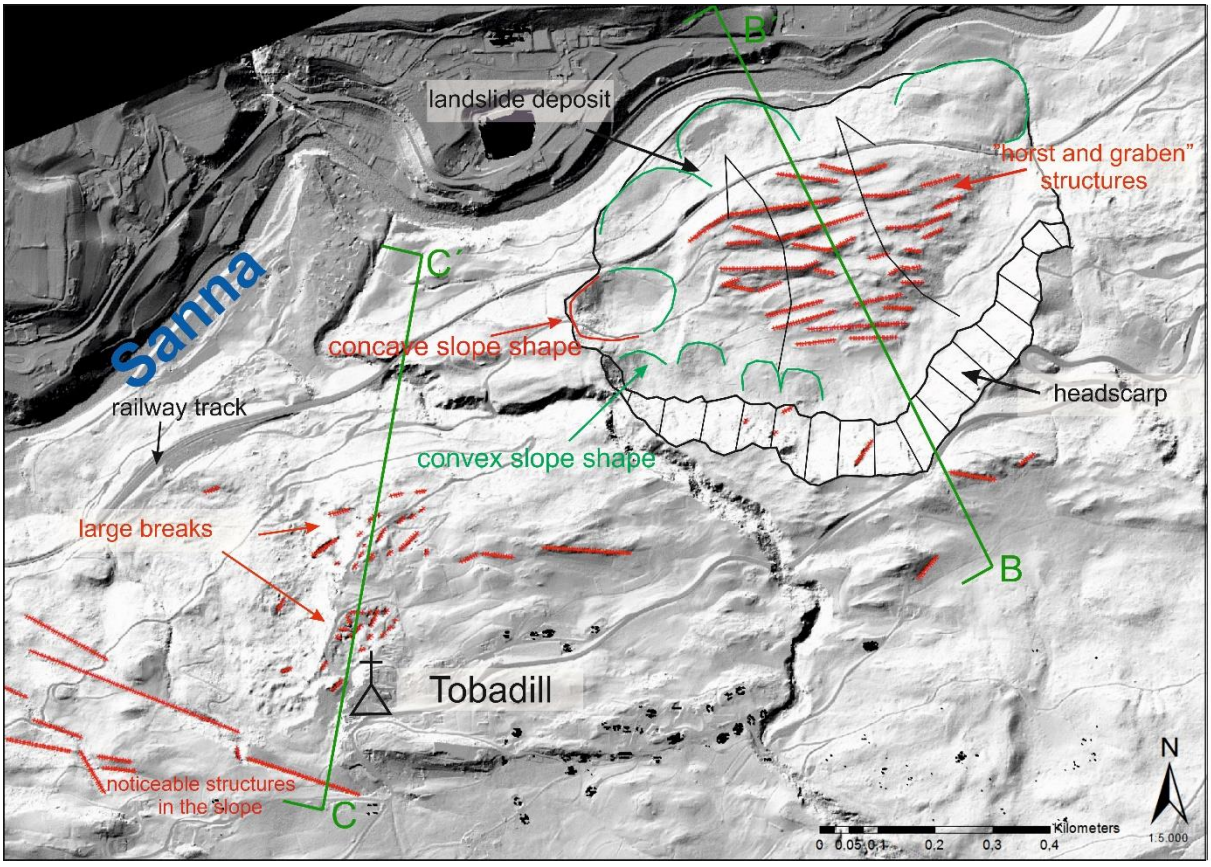

Figure 19: Detailed geomorphic map of the study area based on the laserscan data [modified after TIRIS, 2015]. The green lines represent the location of the cross sections (c.f. chapter 4).

2.6 Regional Landslide Activity

The area around Landeck is characterized by several landslide processes (Figure 20). In this chapter the reference examples Zintlwald and Niedergallmigg and furthermore the landslide Gfäll will be described.

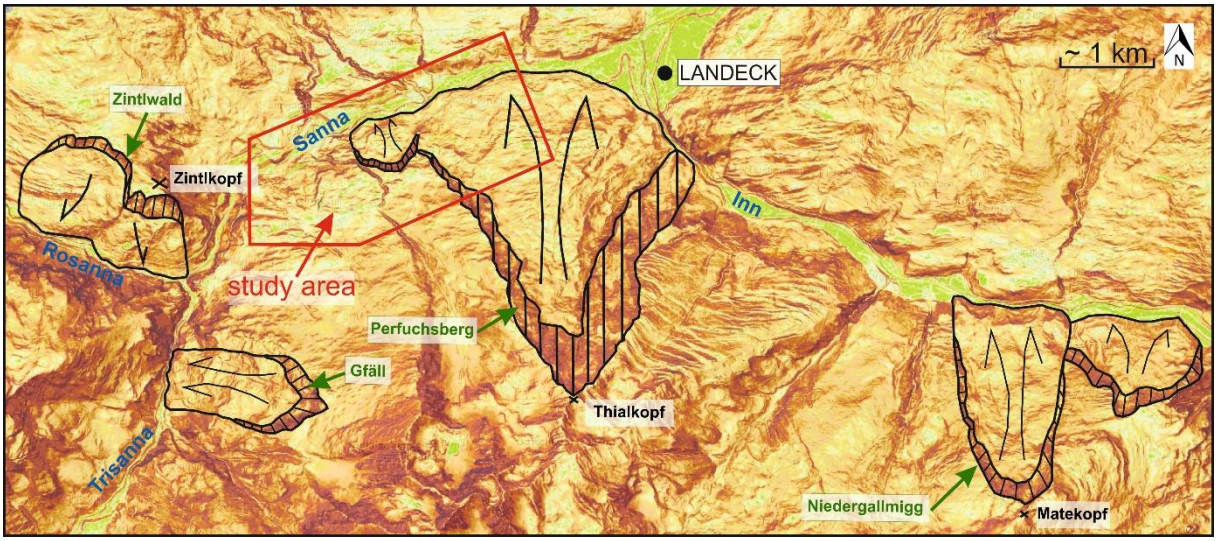

Figure 20: Distribution of landslides Zintlwald, Niedergallmigg, Gfäll and Perfuchsberg around the study area [modified after TIRIS, 2015].

ZINTLWALD

The mass movement Zintlwald is located in west of Landeck on the orographic left side of the Stanzer valley, directly upstream of the confluence from the streams Trisanna and Rosanna, south of the mountain Zintlkopf (Figure 21).

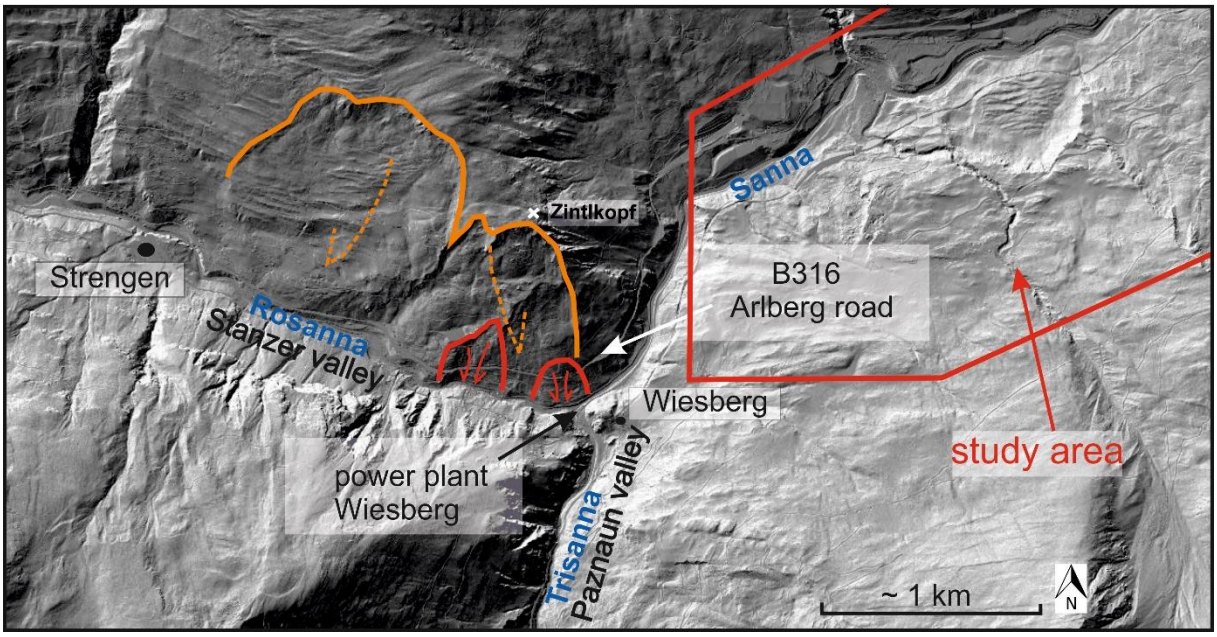

Figure 21: Exact location of the landslide Zintlwald and the influenced infrastructure [modified after TIRIS, 2015].

The rock mass consists of crystalline bedrock belonging to the Venet Complex of the Silvretta nappe [*Gruber et al., 2010*]. The lithology ranges from phyllites to quartzphyllonites to mica schists and some gneisses. Those rocks are intensely sheared and foliated. The schistosity and the dominant joint planes have a dip direction from SSW to SSE and a very steep dip angle. [*Gruber et al., 2010*]

In august 2005 heavy rainfalls in the Upper Inn valley, Vorarlberg and Eastern Switzerland lead to extreme runoffs in the Rosanna, the Trisanna and the Inn Rivers [*Gattermayer et al., 2005*]. Changes in the groundwater level and dramatic erosion along the streams by several meters led to the undercutting of slope toes and some landslides were (re)activated. The largest landslide was the Zintlwald slide. The movement had a length of 800 meters and a volume of 2.5 million cubic meters. The disturbed street section of the B316, Arlbergstreet, showed a local settlement of about eight meters and parts of the hydro station Wiesberg also were destroyed. [*Henzinger et al., 2008*]

Extensive investigation methods (field investigations, geodetic monitoring, reflection and refraction seismic, core borings with inclinometers and piezometers) enabled to design a geologic model: The bedrock is fragmented into slabs, which are floating in a more fragmented fine grained matrix (Figure 22). Those slabs have a higher seismic velocity than the matrix. The changeable subsurface conditions are also responsible for different groundwater situations when the groundwater level was rising due to the heavy rainfall. Furthermore, the valley is glacial overdeepened. It had a deeper and wider morphology before and has been filled up with loose material sediments, which are representing a perfect sliding underground. [*Henzinger, 2008*]

Current instrumentation and monitoring results indicate that deformations are still ongoing and about 40 centimetres per year at the Arlbergstreet and up to one meter per year in the head scarp area. Several stabilisation measures at the Rosanna (e.g. support of the river bed), rock fall protections, drainage procedures and repair activity at the Arlbergstreet are necessary to stabilize the slope or at least decelerate its movement. The controlling slope process has been described as a deep-seated creeping landslide. [*Henzinger et al., 2008*]

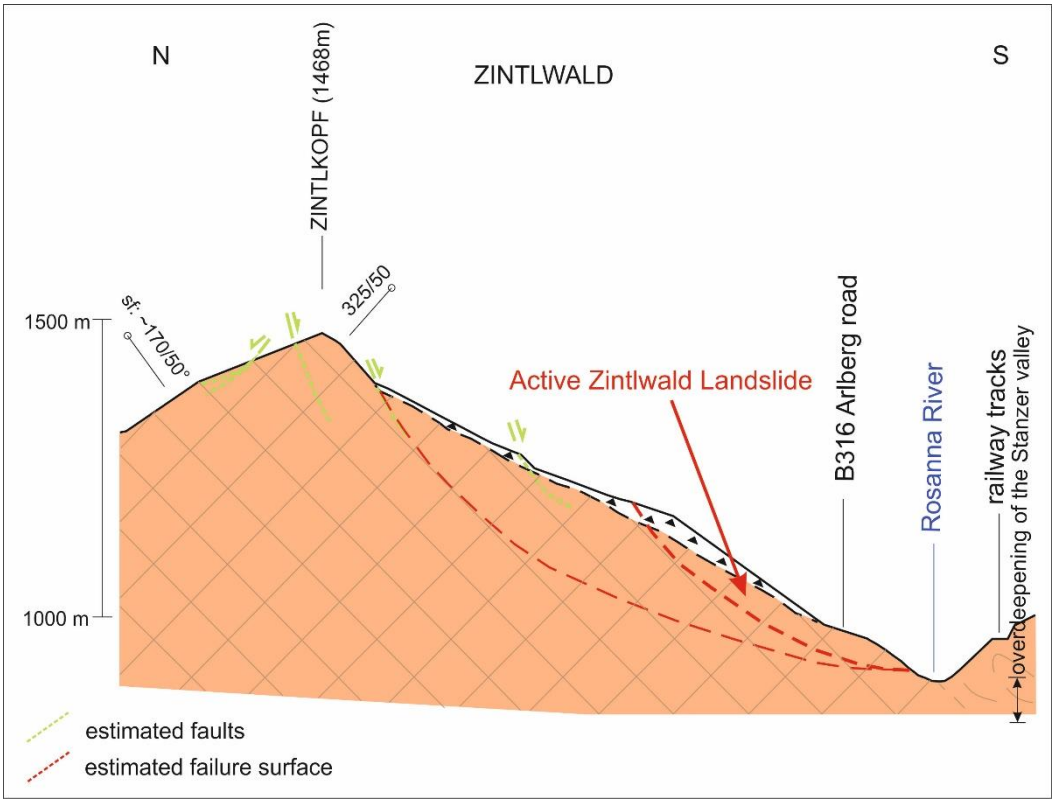

Figure 22: Profile of the landslide Zintlwald [modified after Henzinger et al., 2008].

NIEDERGALLMIGG

The landslide Niedergallmigg is situated in the Upper Inn valley approx. six kilometer southward of Landeck on the orographic left side of the Inn River and directed toward north. It has a vertical height of about 1,400 m, reaching from the Inn River (848 m a.s.l.) to the Matekopf (2248 m a.s.l.). The village Niedergallmigg (approx. 700 inhabitants), the Reschenbund street, the weir of the power plant Inn/Runserau and the Inn River, that gets eroded at the toe of the landslide, are in close contact respectively affected by the landslide Niedergallmigg. [*Kirschner, 2006*]

Geologically the landslide is located in the Silvretta nappe: The upper area (headscarp area) belongs to the Silvretta complex, consisting of biotite-muscovite schists and paragneisses, and the middle and lower part build up by phyllonitic micaschists, paragneisses and amphibolites of the Venet complex. The foliation is dipping to the southeast / south with rather flat dip angels. Due to the folding the dip direction can also vary to northwest and steeply dipping brittle faults that strike E-W also occur. Occasionally the bedrock is covered with quaternary deposits (e.g. moraine deposits, rockfall blocks). [*Zangerl et al., 2012*]

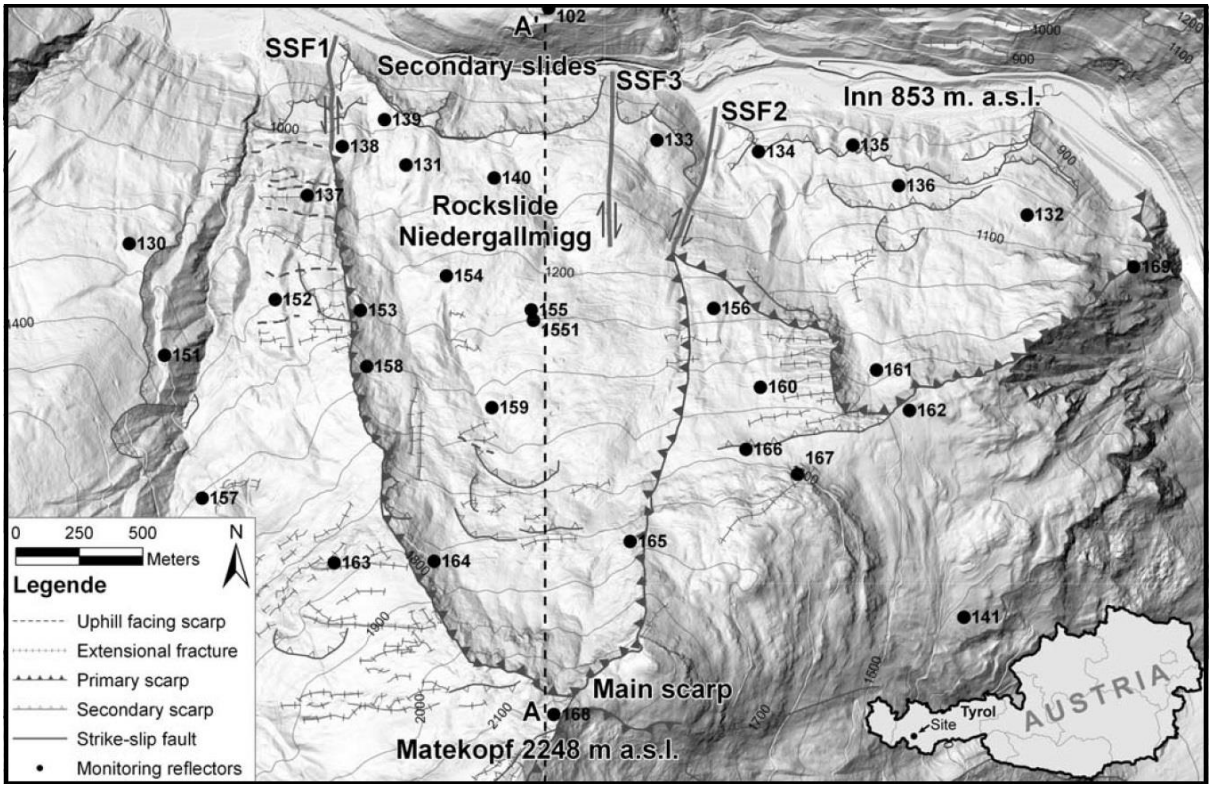

Figure 23: Hillshade map of the deep-seated rock slide system Niedergallmigg showing primary and secondary scarps, strike-slip faults (SSF1, SSF2, SSF3), geodetic monitoring targets and the trace of the cross section A-A' [after Zangerl et al., 2012].

Since 1974 the landslide gets monitored and controlled [*Kirschner, 2006*] and according to *Zangerl et al. (2012)* the landslide Niedergallmigg is divided into an eastern and western sliding mass (Figure 23). The western sliding mass shows movement rates up to 10 cm/year whereas the eastern sliding mass moves very slowly, only a few mm/year [*Kirschner, 2006*].

The landslide Niedergallmigg was initiated post-glacially and moved more than 200 m which lead to internal rock mass deformations (e.g. fragmentation, fracturing) and currently those fragments of hard rock form isolated sliding bodies. Results from reflection and refraction seismic indicate a maximum thickness of more than 300 m of the landslide. Two orthogonal joint sets, striking NE-SW and NW-SE, formed the existing headscarp and the existence of a discrete sliding zone, due to different seismic velocities between the sliding mass and the bedrock, is supposed. [*Zangerl et al., 2012*]

Zangerl et al. (2012) deduced that the landslide was sliding on the alluvial or fluvio-glacial sediments of the overdeepened Upper Inn valley and displaced the Inn River toward north. Further GIS-analysis show an enormous volume imbalance between the headscarp area and the sliding deposit area at the toe of the slope. The toe of the slope got eroded due to the high erosional rates of the Inn River. The volume increase at the toe is nearly three times smaller than the volume loss at the headscarp area. [*Zangerl et al., 2012*]

Changes in the slope topography, due to slope undercutting, or at the mechanical and hydrogeological conditions were leading to secondary slides at the toe of the slope (Figure 24). The composition is more like a soil, compared to the total landslide which is classified as rockslide. [*Zangerl et al., 2012*]

Due to the relatively high movements rates future slope instabilities are expected if the mean annual precipitation changes dramatically and/or the quantity of heavy rainfalls rises. Both phenomena lead to changes at the existing groundwater situation. [*Kirschner, 2006*]

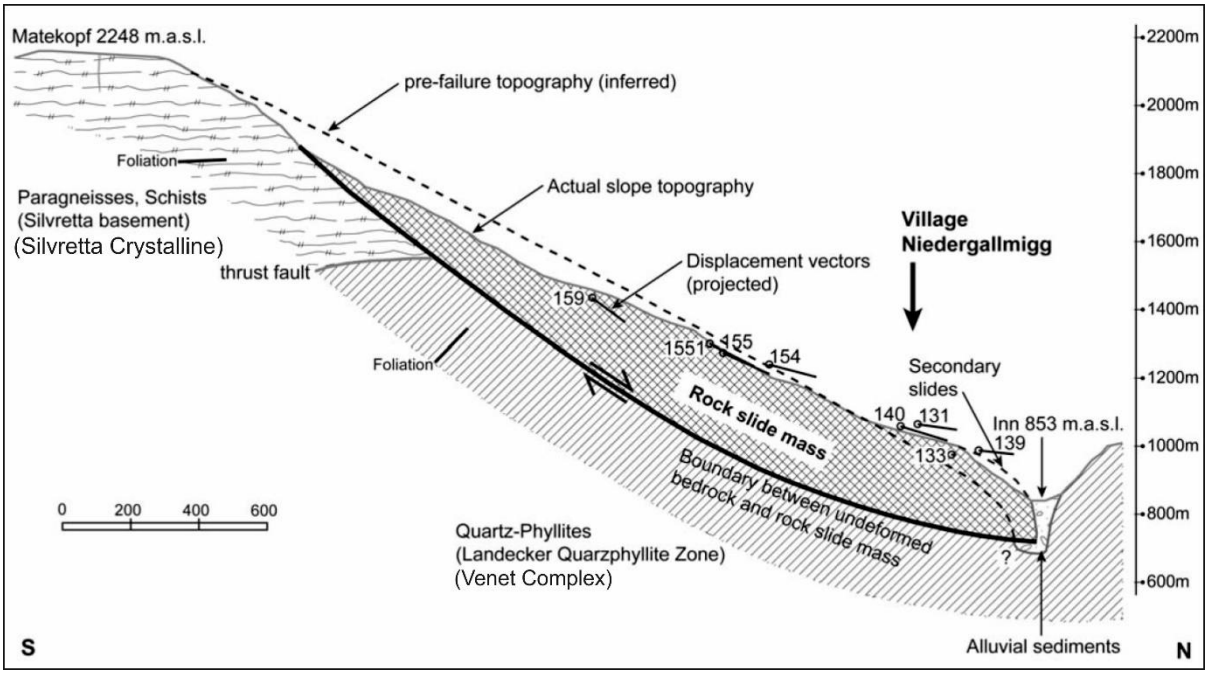

Figure 24: N-S cross section along A-A' showing the rock slide geometry, the actual and pre-failure topography, displacement vectors of geodetic targets and geological setting [after Zangerl et al., 2012].

GFÄLL

The landslide Gfäll is located on the orographic right side at the beginning of the Paznaun valley (Figure 25) and the valley morphology has a very narrow cross section in this sector. The bedrock consists of phyllonitic micaschist, paragneisses, biotite muscovite schists, amphibolites and cataclasites belonging to the Silvretta nappe (Venet complex and Silvretta crystalline). [*Strobl, 2015*]

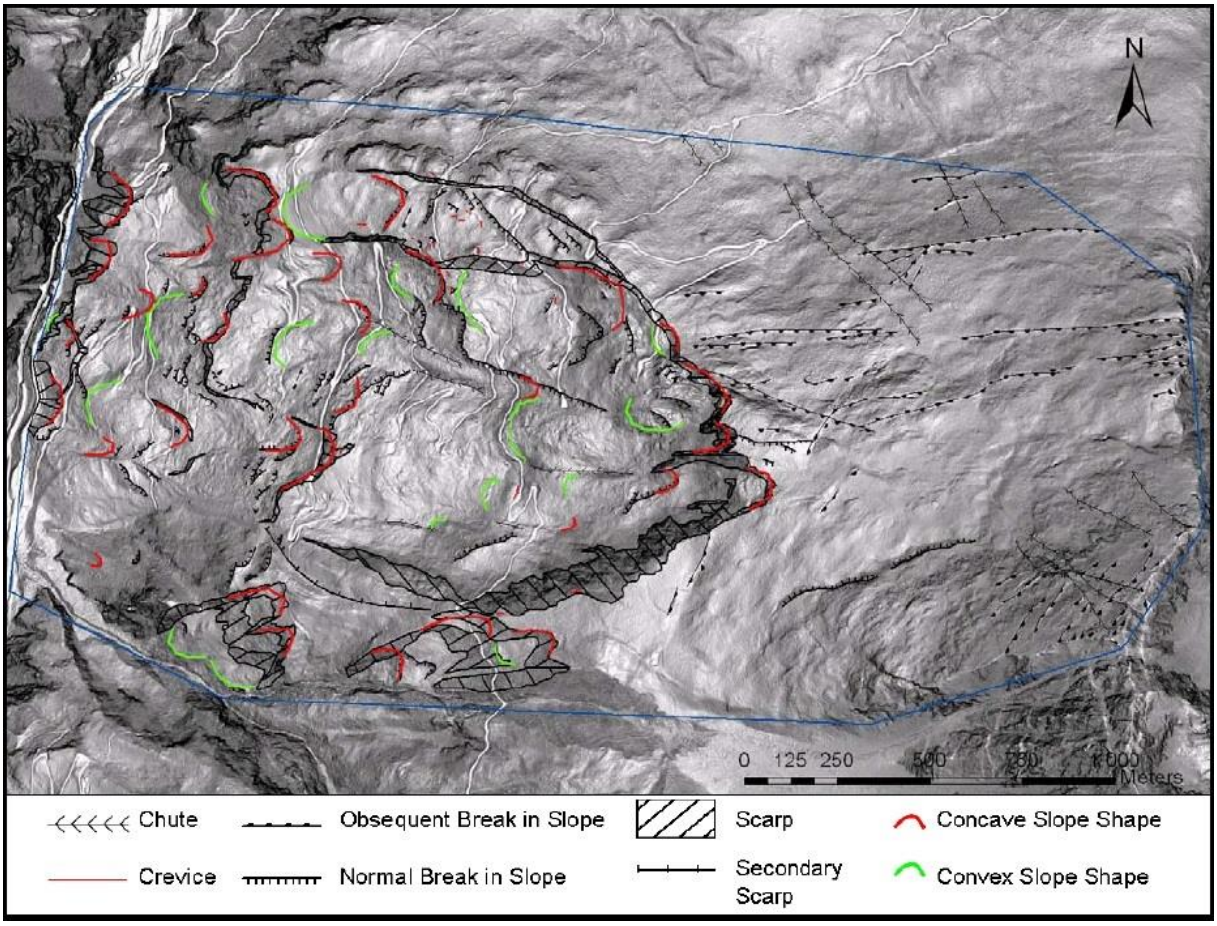

Figure 25: Geomorphic map of the landslide Gfäll and its upper region [after Strobl, 2015].

During the floodwater event in august 2005 parts of the slope got unstable and disturbed the street and the bridge in the valley. After this event field investigations, the monitoring and further analysis were initiated. According to *Strobl (2015)* two joint sets, striking approx. NE-SW and NW-SE, are forming the headscarp of the entire landslide Gfäll. "…On the basis of engineering geological investigations performed, it is suggested that the landslide initiated as wedge-shaped blocks sliding along a stepped failure surface. With continued displacements these steps (or asperities) were subsequently sheared during progressive movement of the landslide. A basal shear zone consisting of sheared rock material (kakirites) is then suggested to have developed. …" [*Strobl, 2015*] The estimated depth of the landslide is about 200 m. Based on engineering geological analysis the classified deep-seated rockslide Gfäll shows, with increasing distance to the headscarp area, an increasing disintegration of the landslide debris, which results in secondary (soil-like) slides at the toe of the slope (Figure 26). Actual these secondary slides are active. It is assumed that the erosion of the Trisanna River at the toe and changes at the groundwater situation (e.g. heavy rainfalls, snowmelts) have significant influence on the current movement of the landslide Gfäll.

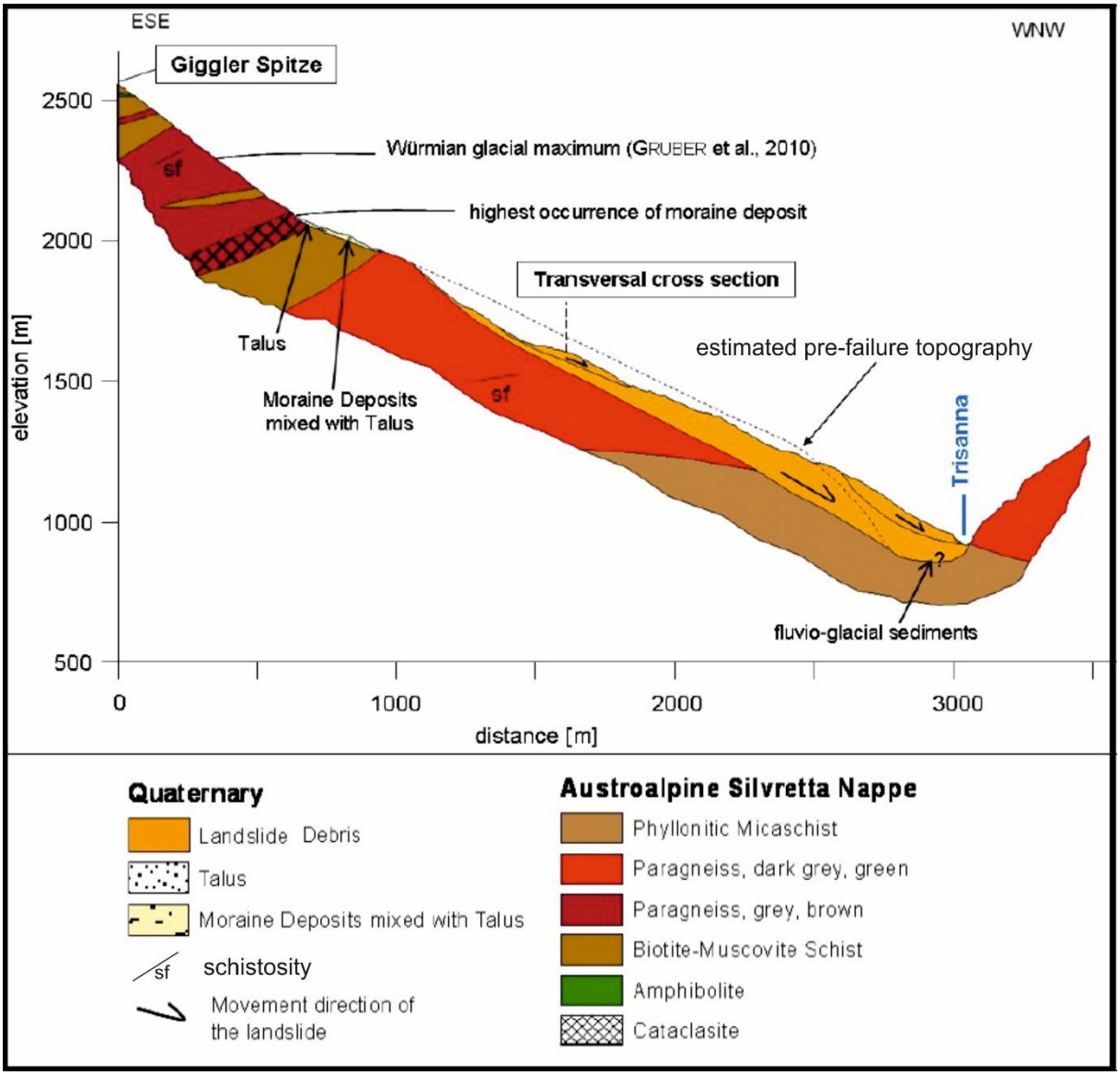

Figure 26: Detailed Profile of the landslide Gfäll [modified after Strobl, 2015].

3 Landslide Perfuchsberg

The entire landslide Perfuchsberg is located on the orographic right side of the confluence of the Stanzer valley and the Upper Inn valley, directly southwest of the town Landeck. The landslide extends from the mountain Thialkopf (2398 m a.s.l.) down to the Sanna (northward) and the Inn River (northeastward) (Figure 27). [*Gruber et al., 2010*]

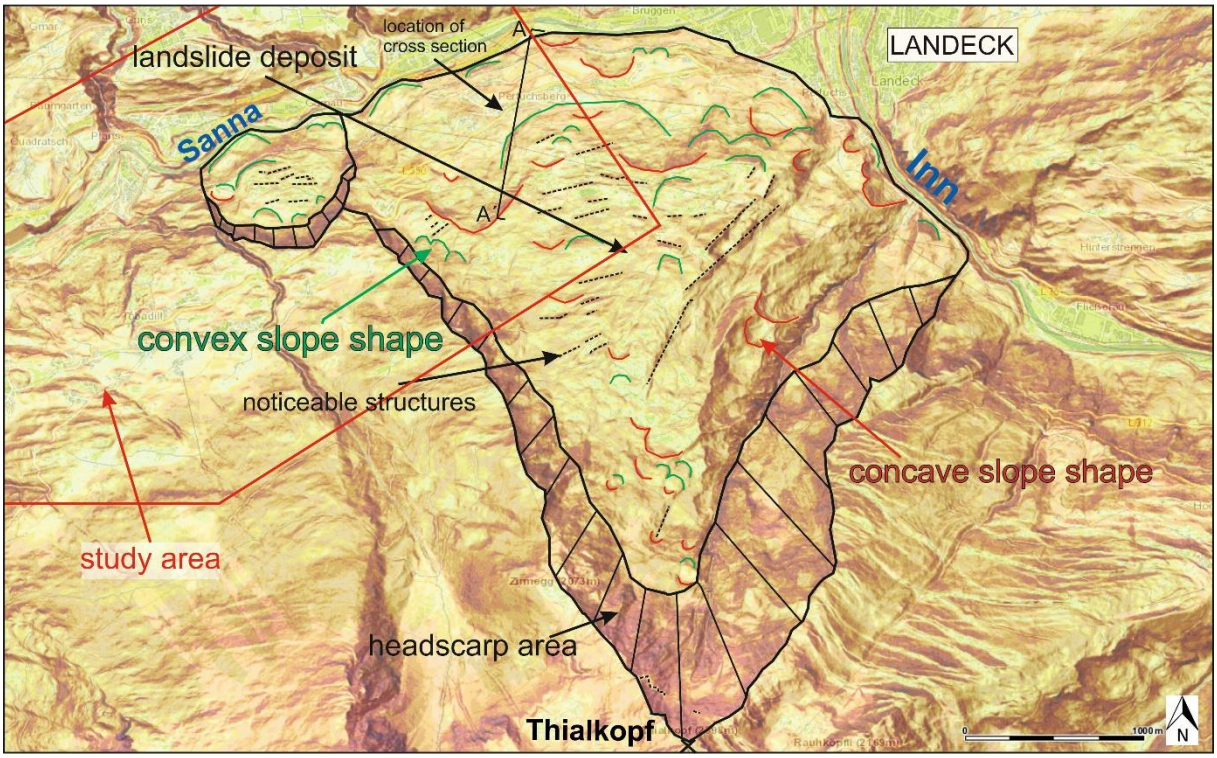

Figure 27: Morphologic map of the landslide Perfuchsberg with its most noticeable structures based on laserscan data evaluation and the location of the cross section at the toe area [modified after TIRIS, 2015].

The rock mass consists mostly of phyllonitic micaschists, generally striking E-W and dipping to the south, which are belonging to the Venet complex of the Silvretta nappe. The headscarp show a distinctive concave shape and behind the headscarp area (southward) mountain splitting phenomena, like tension cracks and trenches, occur. The convex shaped landslide deposit toward north has an area of approx. six to seven km^2. Secondary scarps at lower areas of the deposit indicate that parts of the entire landslide are still active or moving as separate slides. [*Gruber et al., 2010*]

From previous investigations (borings, refraction seismic), at the toe of the slope, it could be assumed that the landslide was sliding on the glacial overdeepened valley, which was filled up with fluvio-glacial deposits after the glaciation (Figure 28). The glacial overdeepening at this area get suggest with 100 m. [*Poscher, 1993*]

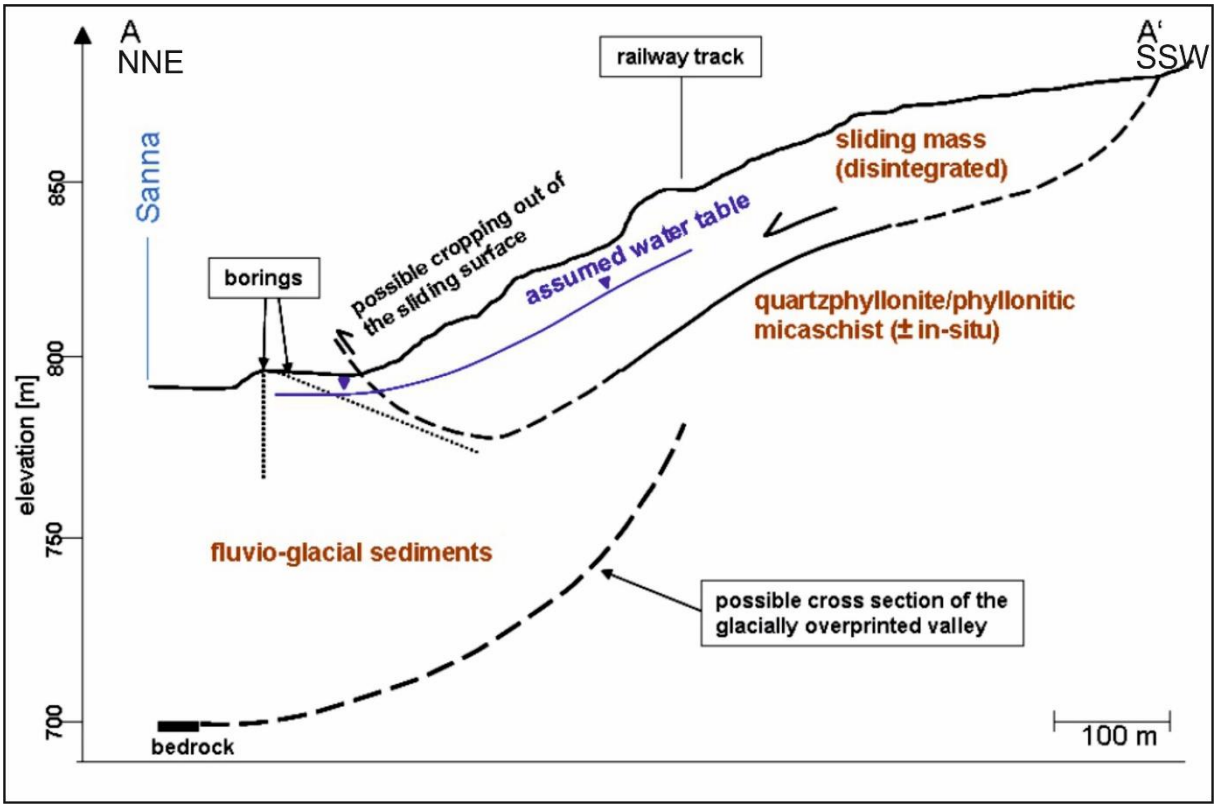

Figure 28: Cross section of the toe area of the landslide Perfuchsberg [modified after Poscher, 1993].

3.1 Laboratory Tests

For the laboratory tests rock samples are taken in the study area. The exact positions of the samples in field is shown in Figure 29 and the detailed sample list is attached.

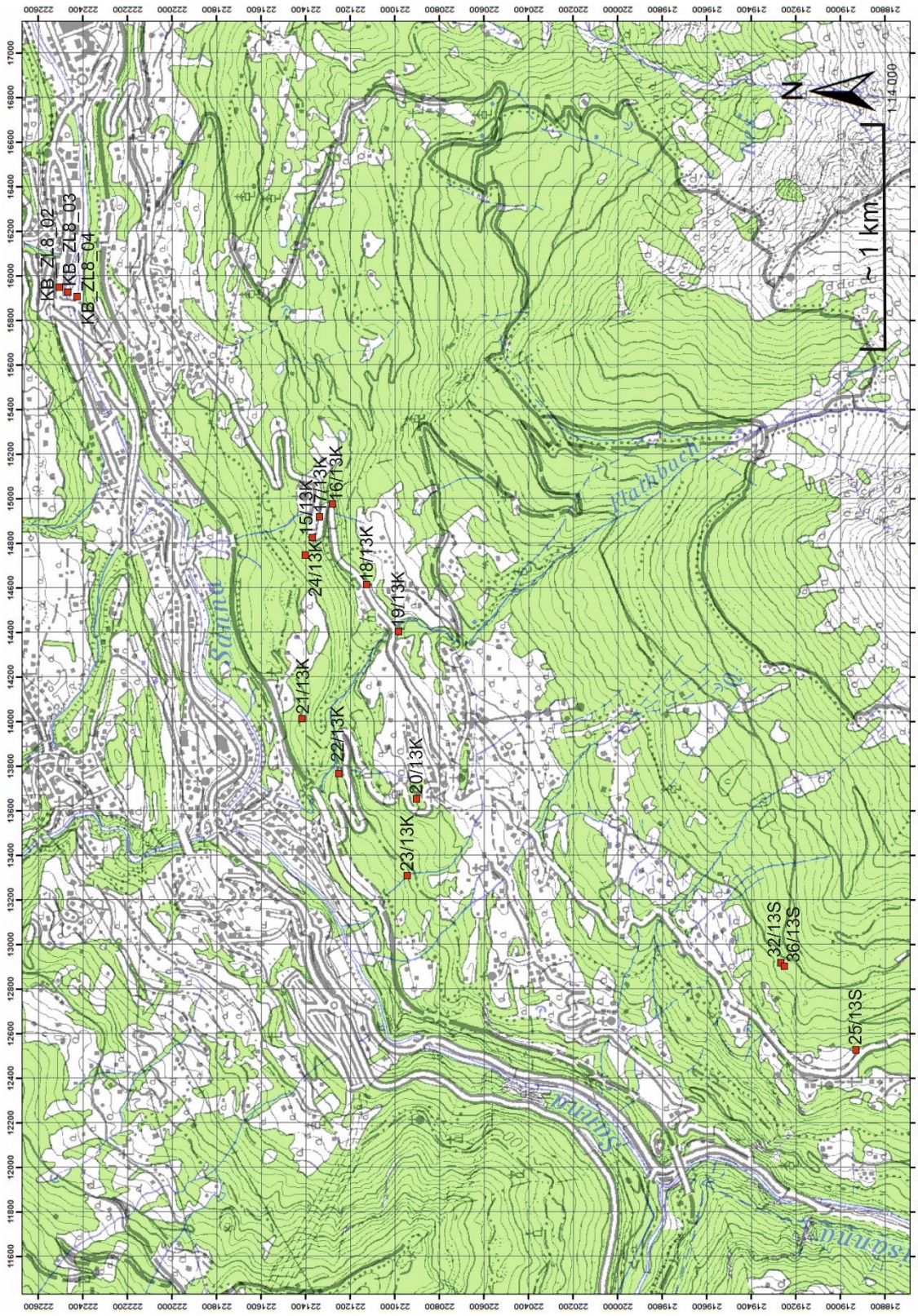

Figure 29: Exact location of the rock samples.

3.1.1 Thin Section Evaluation

Thin section evaluation was selected to confirm the field observations regarding to the exact type of bedrock, mineral composition, microstructure and other special features.

The rock samples 15/13K, 16/13K, 19/13K, 20/13K, 21/13K and 22/13K (Figure 29) are selected for the analysis with the polarization microscope. Detailed characteristics of each sample are shown at the appendix.

Due to the mineral compositions and the dominant microstructures all rock samples get characterized as micaschists. The main minerals are quartz, mica and feldspar and as accessory minerals occur rutile, tourmaline and iron-mineralizations. Several minerals feature deformed and sheared textures and all thin sections show the dominant and characteristic schisted microstructure.

3.1.2 Direct Shear Tests

Based on desk study and field investigations it is suggest that the schistosity and/or some joint planes are directly involved in the failure processes in the study area. Thus direct shear tests along foliation planes get performed, to receive a few reference values for the mechanic shear strength that can be compared to the testing results from previous projects. Those reference values are also needed as input parameters for further engineering geological analysis.

The direct shear test is performed with the rock samples 12/13, 18/13K, 22/13K, 25/13S, 32/13S and 36/13S. The sample 12/13 is a piece of a drill core from the Perjentunnel boring (KB-ZL8-03) while the others have been collected in the field (Figure 29). The following table (Table 5) shows the obtained shear parameters for each rock sample, measured and evaluated in the rock mechanical lab of TU Graz.

Table 4: Results from the direct shear test

Rock Sample	**JRC**	**Joint Roughness**	**Cross Section Area**	**φ**	**φ_{res}**	**c**	**c_{res}**
			[cm^2]	[°]	[°]	[MPa]	[MPa]
12/13	8	stepped - smooth	84.1	24.6	22.9	0.16	0.00
18/13K	4	planar - smooth	250.4	29.1	24.5	0.68	0.00
22/13K	6	undulating - smooth	193.5	24.1	23.7	0.23	0.00
25/13S	12	undulating - rough	237.9	39.7	26.2	2.00	0.00
32/13S	8	undulating - smooth	265.7	34.0	29.0	0.10	0.00
36/13S	10	undulating - rough	206.3	49.5	24.6	0.81	0.00

The measured friction angels (φ) and residual friction angels (φ_{res}) from the phyllonitic micaschist samples range between 24.1° and 29.1° (φ) and 22.9° and 24.5° (φ_{res}). The dark grey to green paragneiss samples feature higher amounts of friction angels and residual frictions angels of 34° and 49.5° (φ) and 24.6° and 29° (φ_{res}). For the cohesion (c) values between 0.1 MPa and 0.81 MPa for both lithologic units are calculated and the residual cohesion (c_{res}) does not occur. The joint roughness coefficient (JRC) vary between 4 and 10 and the shared surfaces are, in the majority of cases, smooth and undulating. Due to the defective test procedure at the rock sample 25/13S the results get not considered to avoid falsified values although the results are fitting to them of the other samples.

Button (2004) determined friction angels between 25° to 28° and cohesion values between 0.4 MPa to 0.6 MPa performing direct shear test along foliation planes of the “Landeck quartzphyllite” (Venet complex). This results correspond to the shear strength parameters from the study area.

3.1.3 Triaxial Compression Tests

The triaxial compression test is performed to receive reference values for the mechanical strength from the bedrock and to get input parameters for further slope stability analysis.

For the triaxial compression test the rock samples 02/13 and 08/13 are used. This samples are drill cores from Perjentunnel borings KB-ZL8-02 and KB-ZL8-04 [*ASFiNAG, 2012*]. The results are listed in table 6.

Table 5: Results from the triaxial compression test

Rock Sample	**UCS**	**φ**	**c**
	[MPa]	[°]	[MPa]
02/13	25.52	36.31°	7.08
08/13	31.15	41.62	7.92

The rock samples are taken from two different drill cores at the depth of 40 metres (02/23) and 18 metres (08/13), thus, the alteration and weathering has no influence on the mechanic stability of the samples.

The triaxial compression test calculates friction angels for the two rock samples of 36.31° and 41.62°, cohesions of 7.08 MPa and 7.92 MPa and uniaxial compressive strength (UCS) of 25.52 MPa and 31.15 MPa.

Compared with the test results given by *Button (2004)*: The friction angels (32° to 44°) correspond to this test results, but the cohesion values are not in the same range. They have lower values: 3.5 MPa to 5.4 MPa. The uniaxial compressive strength given by *ASFiNAG (2012a)* obtained a range of 5-50 MPa for the phyllonitic micaschists and gneisses (Venet complex). Also the results of the triaxial compression tests correspond to the results of previous geotechnical investigations.

4 Landslide Analysis

4.1 Subsurface Interpretation

The first step for constructing a detailed slope profile is to get to know the development of the slope and the valley. Together with different information and assumptions the pre-failure topography of the valley can be reconstructed:

- Based on desk study, analysis of remote sensing data and field observations it gets assumed that the exact opposite site of the study area was not influenced by large landslides. Therefor and according to the system of mass balance, meaning that the loss of rock mass volume in the upper headscarp area equals the volume increase at the toe area of the slope, the pre-failure profile line can get reconstructed approx. symmetrically to the exact opposite site.

- During the Würm glaciation (approx. 14,000 years ago) the whole region was covered by ice. Afterwards, when the ice cover was gone, a typical u-valley was left back. For the estimation of the depth of the Stanzer valley results from borings and geophysical investigations at the area of Landeck [*Poscher, 1993*] gets consulted: The overdeepening at Landeck is recorded by approximate 100 meters [*Poscher, 1993*]. Thus it gets assumed that the overdeepening several hundreds of meters upstream is approx. 75 meters.

- Furthermore it is assumed that the entire landslide Perfuchsberg and the landslide in the study area deflected the river Trisanna to the north. On basis of this the Sanna River gets reconstructed in the middle of the valley, somewhat northernly than today.

The exact position of the cross sections in the study area is shown in Figure 30 and the reconstructed pre-failure cross section after glaciation is shown in Figure 31.

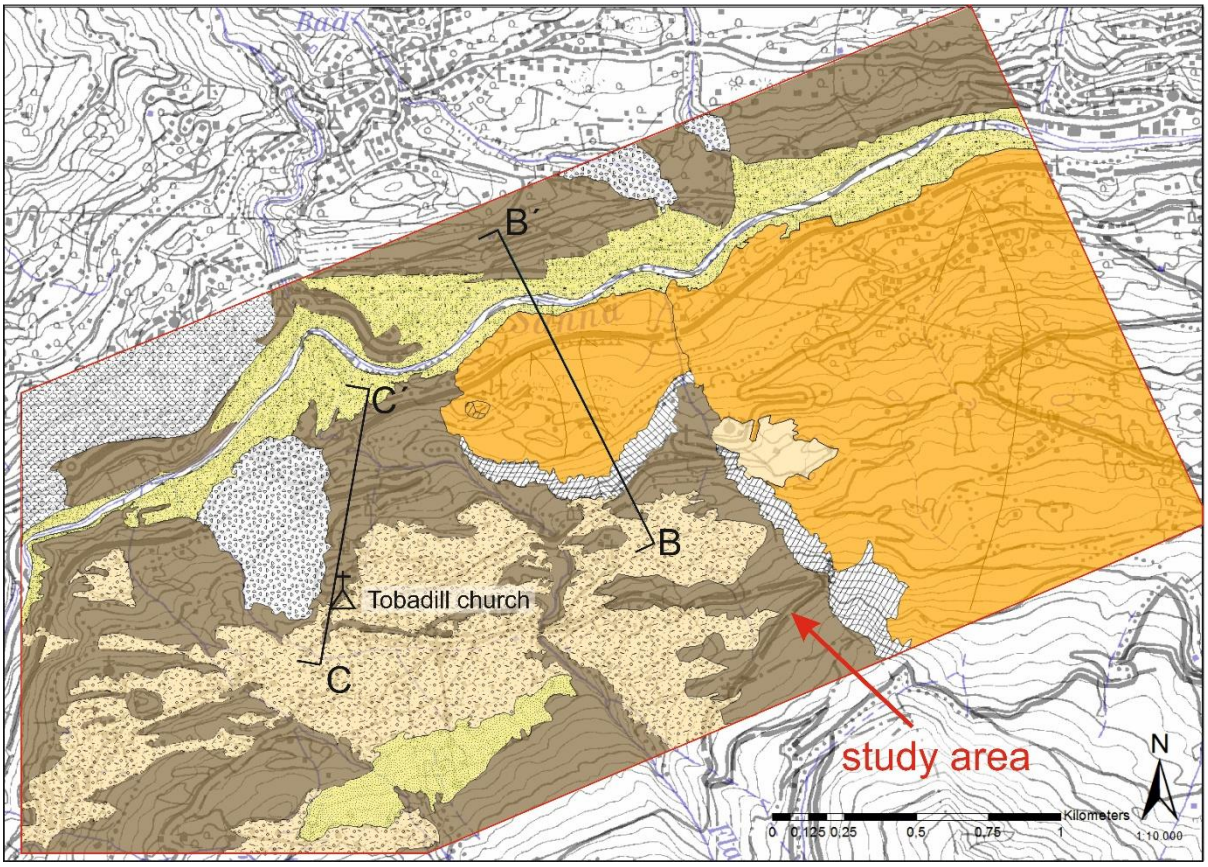

Figure 30: Exact position of the cross sections in the study area.

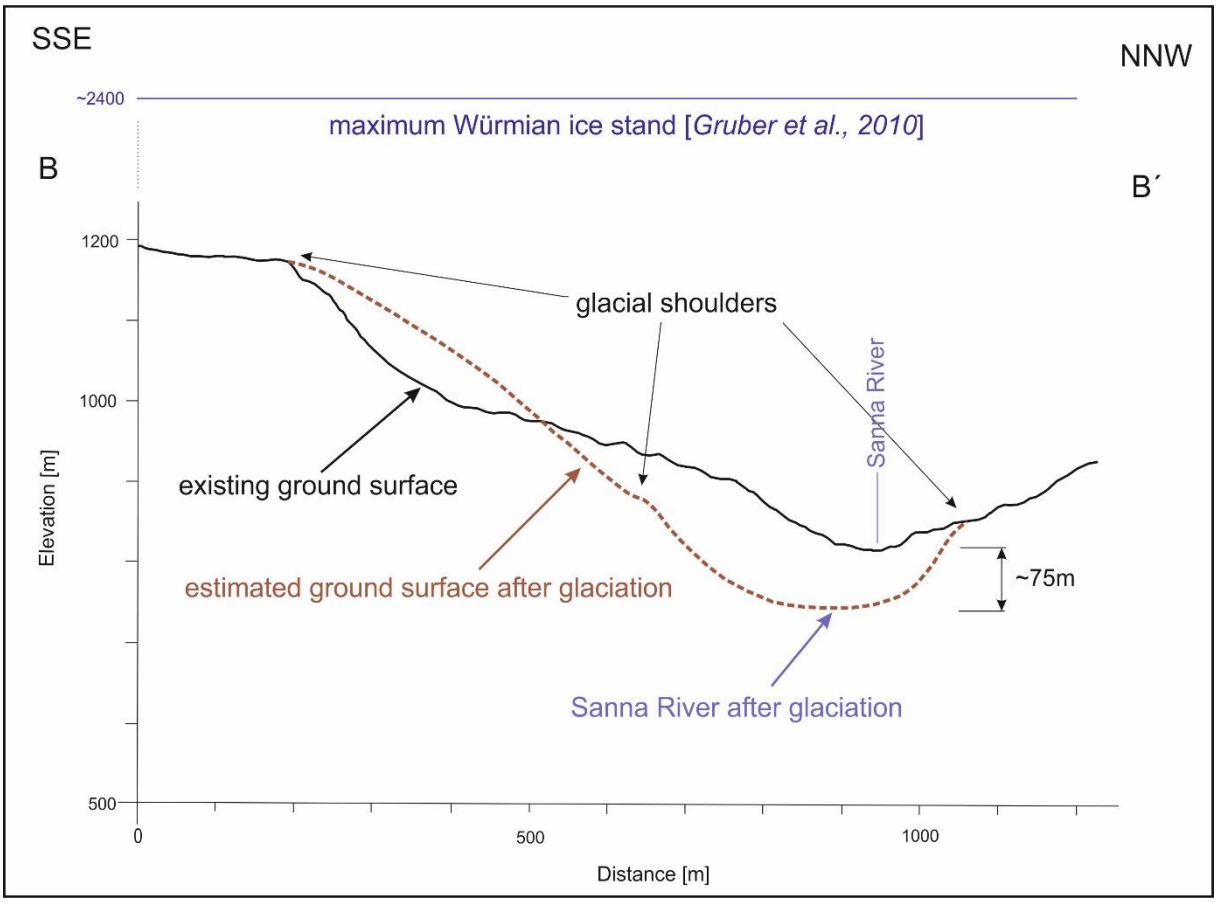

Figure 31: Estimated cross section after glaciation.

Borings and geophysical measurements at the level of the Sanna River in the area of Landeck [*Poscher, 1993*] detected both above and below the landslide mass alluvial Sanna deposits. Based on this it is expected that the Stanzer valley got filled up for a great part with fluvio-glacial sediments before the landslide has occurred. Figure 32 illustrates an estimated cross section shortly before the landslide happened.

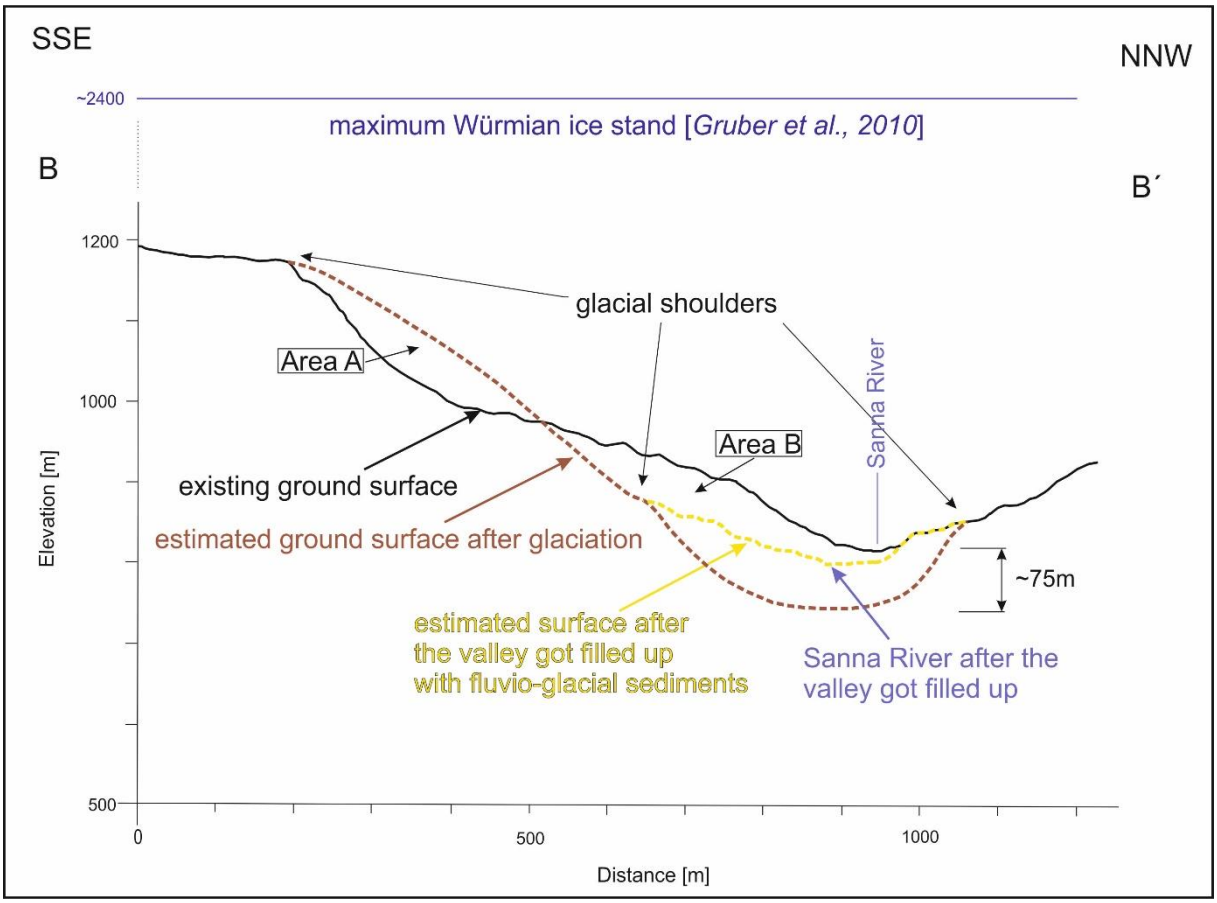

Figure 32 Estimated cross section after the valley got filled up with fluvio-glacial sediments and shortly before the landslide happened.

Figure 33 shows the present surface of the slope. The steep headscarp and the landslide deposit is well visible and the Sanna River was displaced to north.

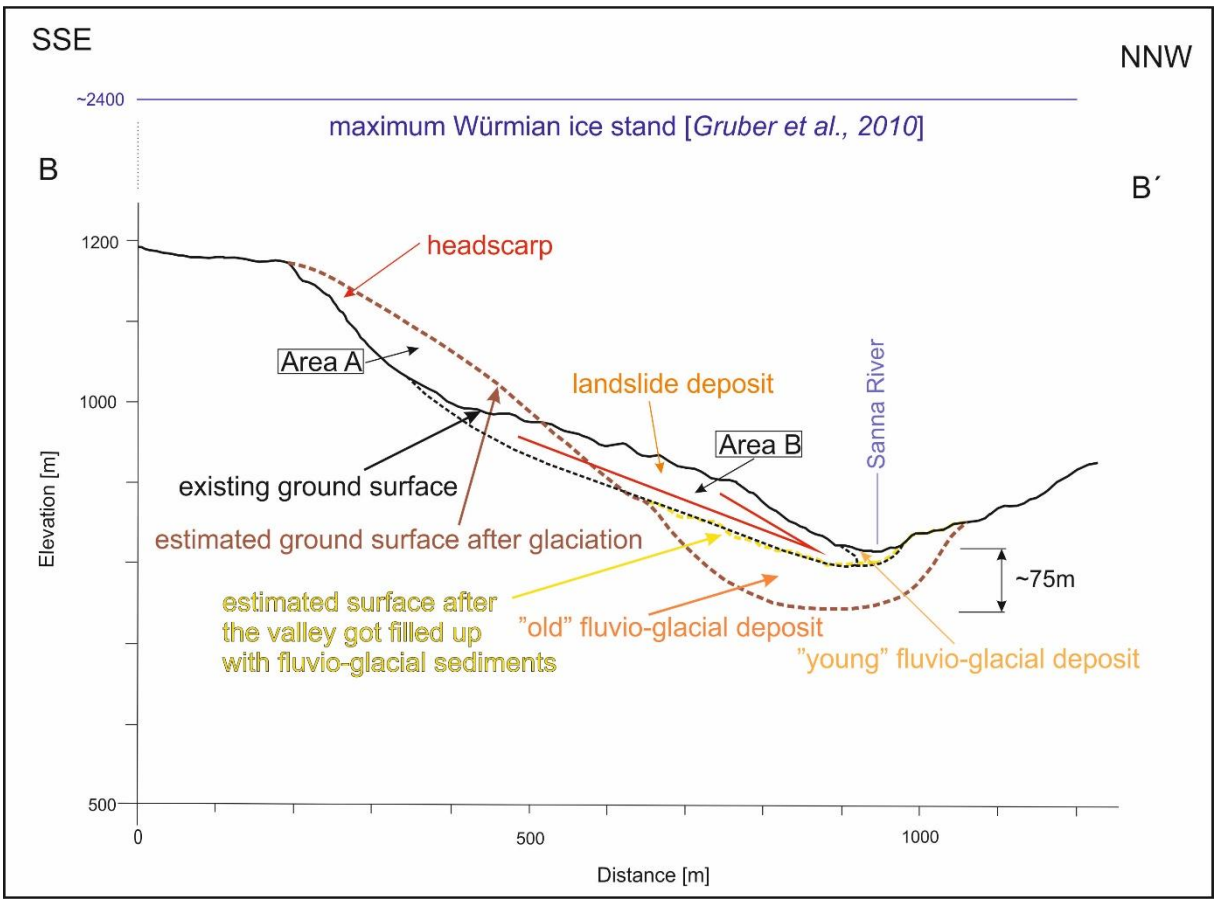

Figure 33: Present day cross section.

4.2 Engineering Geological Analysis

To analyse the involved slope instability processes and to support the results and interpretations that were made based on desk study, laserscan interpretation and field investigation including structural measurements, further engineering geological analysis are performed.

4.2.1 Key Block Analysis

Based on previous investigations the schistosity and the orientation of the joint sets led to the assumption that a failure on this planes or plane combinations is kinematically admissible. For this kinematic analysis a block theory software [*Liu, 2004*] is used.

For the Key Block Analysis the most important planes, schistosity and fault sets, get identified and measured during the field work. Also the dip direction and dip angle of the pre-failure slope get assumed during field work and in combination with the maps. The average dip direction and dip angle of the planes are shown at table 6.

Table 6: Dip direction and dip angle of the determined planes

Plane	Dip Direction	Dip Angle
Pre-failure slope	320	45°
Schistosity	175	63°
Joint set 1	139	68°
Joint set 2	219	51°
Joint set 3	337	81°
Joint set 4	53	62°
Joint set 5	336	21°

These joint sets 175/63° (schistosity), 139/68° (JS1), 219/51° (JS2), 337/81° (JS3), 53/62° (JS4) and 336/21° (JS5) combined with the estimated pre-failure slope (320/45°) led to the analysis that the blocks with the JP codes 100101, 101100, 110101 and 100100 form removable blocks. At the lower hemisphere projection “1” means the joint plane is inside the excavation plane/slope and “0” means the joint plane lies outside the slope. These blocks have no intersection with the slope and therefore they are removable (Figure 34).

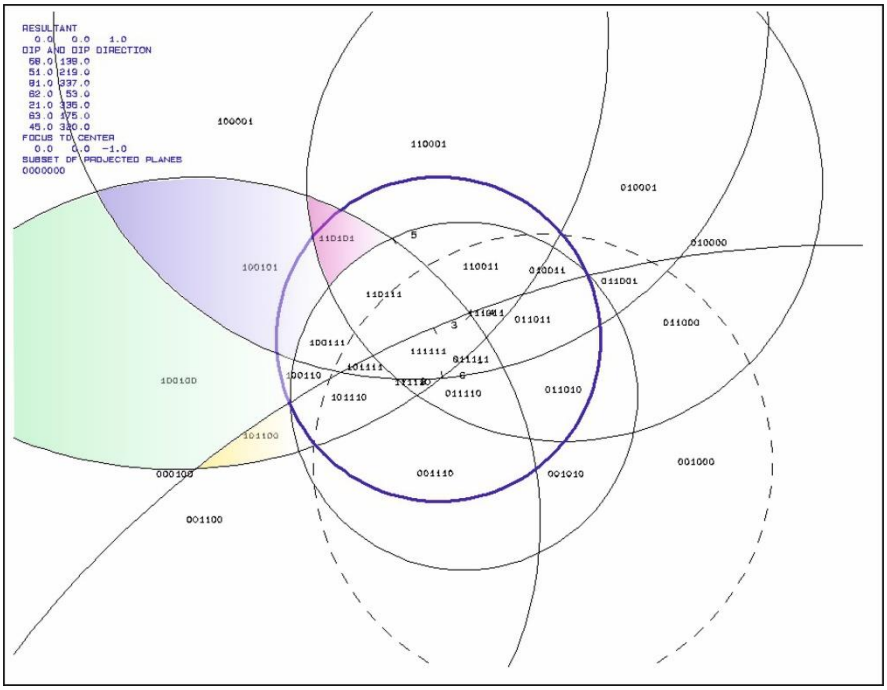

Figure 34: Graphic illustration of the removable blocks. The blue circle represent the reference circle, the black circles the joint planes and the dashed circle represent the excavation plane / the slope. All blocks which have no intersection with the slope (dashed circle) are highlighted and get identified as removable blocks.

At the second plot (Figure 35) the joint sets on which sliding is possible are determined. The block with the JP code 100101 slides on the intersection of joint set 2 and 5, block 101100 on 3 and 5, block 110101 on 4 and 5 and block 100100 slides on the intersection of 5 and 6 (schistosity). Based on this analysis, it is notable that the joint set 5 (336/21) is involved in every failure option.

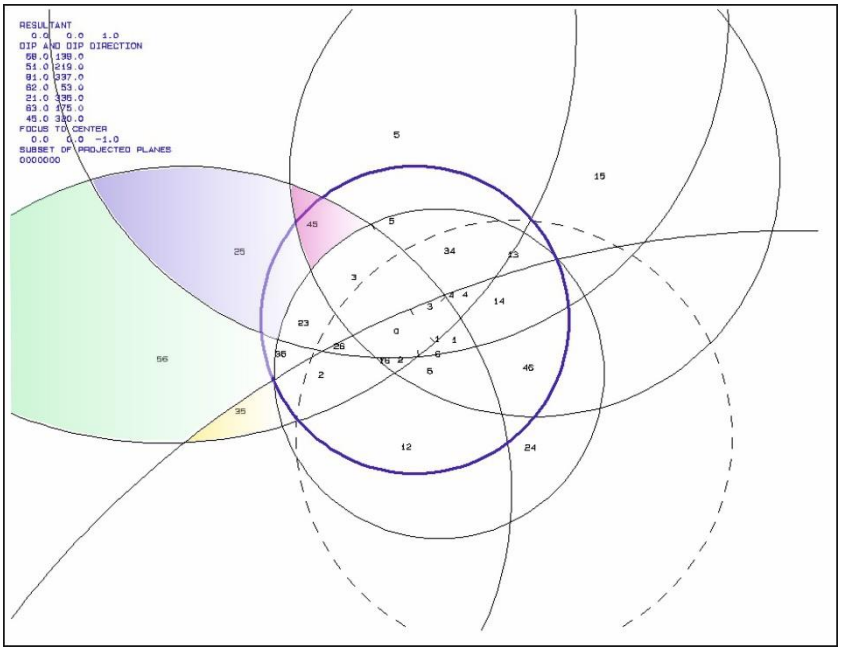

Figure 35: Graphic illustration on which joint planes the determined removable blocks possibly slide. The removable blocks with the failure joint planes are highlighted.

After wedge sliding is shown to be kinematically admissible for four removable blocks, mode analysis is performed. With the mode analysis type I key blocks (with a positive sliding force) can get distinguished from type II potential removable key blocks (with a negative sliding force). For an inserted friction angle of 23°, assumed from results from the laboratory tests, all blocks turned out to be type II potential removable key blocks.

Under the estimated friction angle of 20° also every determined removable block has a free plane but only the block with the JP code 110101 has a positive sliding force and is thus identified as key block (Type I). The other blocks get identified as potential removable key blocks (Type II) (Figure 36).

Table 5:Key blocks of free plane and concave slope

PYRAMID	PLANE 1	PLANE 2	CONCAVE SLOPE
0	0	1	0
1	0	1	0
2	0	0	0
3	0	1	0
4	0	1	0
5	0	0	0
6	0	1	0
12	0	0	0
13	0	0	0
14	0	0	0
15	0	0	0
16	0	1	0
23	0	1	0
24	0	0	0
25	1	0	0
26	0	1	0
34	0	1	0
35	1	0	0
36	0	1	0
45	1	0	0
46	0	0	0
56	1	0	0

SLIDING PLANE	SLIDING FORCE	SLIDING INTERVAL OF	TUNNEL
+0.00	+1.00	+302.86	+45.47
+1.00	+0.79	+314.60	+91.75
+2.00	+0.55	+253.21	+352.86
+3.00	+0.93	+292.11	+17.87
+4.00	+0.71	+327.84	+112.11
+5.00	+0.02	+0.00	+0.00
+6.00	+0.73	+344.96	+73.21
+12.00	+0.49	+0.00	+0.00
+13.00	-0.54	+0.44	+147.84
+14.00	+0.59	+6.07	+122.86
+15.00	-0.36	+73.21	+172.86
+16.00	+0.71	+271.75	+59.41
+23.00	+0.31	+225.47	+6.07
+24.00	-0.46	+42.00	+164.96
+25.00	-0.11	+197.87	+314.60
+26.00	+0.48	+239.41	+26.24
+34.00	+0.71	+352.86	+42.00
+35.00	-0.56	+180.44	+327.84
+36.00	-0.53	+206.24	+0.44
+45.00	+0.01	+222.00	+344.96
+46.00	+0.26	+17.87	+134.60
+56.00	-0.35	+186.07	+302.86

Figure 36: Tables for analysis. The left table shows the free plane and the right table the sliding force for each removable block.

STABILITY ANALYSIS

Stability analysis gets performed with another block theory software [*Liu & Kieffer, 2008*] plotting the contour lines of the friction angles corresponding to the joint planes on which failure is probably. From the resultant force vector R can be suggest to the friction angle (φM) that is required for failure.

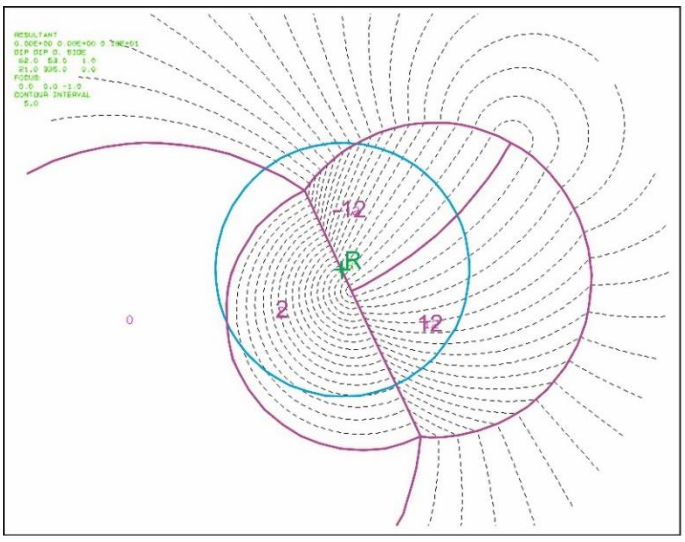

Figure 37: Stability analysis for the key block 110101. The blue circle represents the reference circle and R marks the resultant force vector.

With regard to figure 37 for key block 110101 wedge sliding on the intersection of joint plane 4 (53/62°) and joint plane 5 (336/21°) is admissible. The resultant force (R) represent a friction angle of 21°. Those 21° are required to stabilize the whole key block. If the available friction angle is greater than the required one, the factor of safety is greater than 1 (FS>1) and the key block 110101 will be stable. But if the available friction angle is lower than 21°, the factor of safety is lower than 1 (FS<1) and the key block 110101 is unstable.

$FS = \frac{tan\phi A}{tan\phi M}$ $FS = \frac{tan21}{tan21}$ FS = 1.0 stable

For an inserted friction angle of 23°, assumed from results from the laboratory tests, the block turn out to be stable with an FS = 1.11.

$FS = \frac{tan\phi A}{tan\phi M}$ $FS = \frac{tan23}{tan21}$ FS = 1.11

If the friction angle decreases e.g. to 20°. The FS = 0.95 and the block is no more stable or respectively expected to fail.

$FS = \frac{tan\phi A}{tan\phi M}$ $FS = \frac{tan20}{tan21}$ FS = 0.95

The potential key block 100100 is formed from joint plane 5 (336/21°) and the schistosity (175/63°). The mobilized friction angle from stability analysis has a rather small amount of 5° and thus the FS = 4.16, with an estimated available friction angle of 20°.

$FS = \frac{tan\phi A}{tan\phi M}$ $FS = \frac{tan20}{tan5}$ FS = 4.16

The other removable blocks are also stable with respect to the stability analysis. The potential key block 100101 has a FS = 1.46 and the block 101100 has a FS = 20.85.

$FS = \frac{tan\phi A}{tan\phi M}$ $FS = \frac{tan20}{tan14}$ FS = 1.46

$FS = \frac{tan\phi A}{tan\phi M}$ $FS = \frac{tan20}{tan1}$ FS = 20.85

4.2.2 Stability Analysis using “SWedge”

Based on key block analysis four potential removable key blocks and whose state of stability get identified. To support those results and to include another important stability parameter, the water pressure, into the block stability analysis, the program SWedge is used.

The program SWedge gets applied for stability analysis for the removable blocks with the JP codes 100101, 101100, 110101 and 100100. The two relevant joint sets, which are forming the wedge, the pre-failure slope and the shear parameters are inserted in the program and the Factor of Safety is calculated. Also sensitivity analysis can be performed to determine the correlation between the friction angles of the joint planes and the water pressure acting on them. It can be analysed how much water is needed for a failure, if the friction angle stays at the same amount.

For the type I key block 110101 the joint set 4 (53/62°) and joint set 5 (336/21°) are inputted. Figure 38 shows the plot of the wedge analysis. Assuming a friction angle of 21° and dry conditions the block is at limit equilibrium (FS = 1), what confirm the previous key block stability analysis.

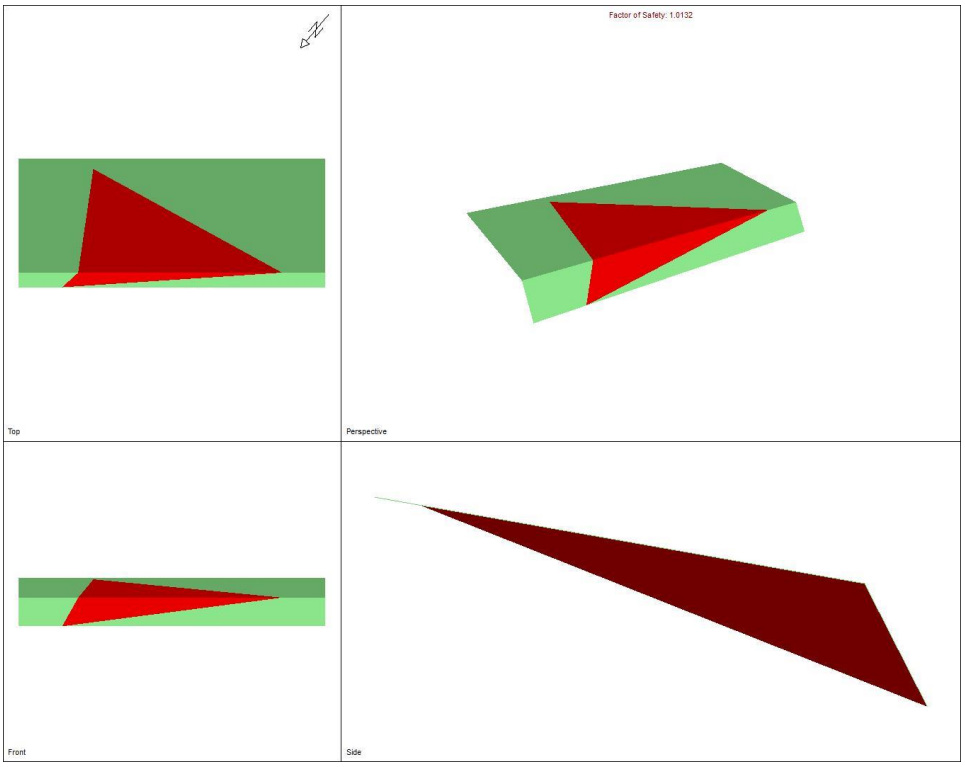

Figure 38: SWedge analysis for the key block 110101 in different perspectives.

With a friction angle of 20° and an added assumed water pressure, the Factor of Safety decreases (FS < 1) and the block becomes unstable. Table 7 shows the correlation between the factor of safety and the inserted water pressure at the same amount of friction angle. The FS decreases with inserting increasing water pressure.

Table 7: Different FS due to different water pressures

Water pressure	**Friction angle**	**Factor of Safety**
[MPa]	[°]	
0	20	0.96
0.48	20	0.95
0.80	20	0.90
1.12	20	0.80

The wedge of the potential removable type II key block with the JP code 100100 is illustrated at Figure 39. Assuming a friction angle of 20° and dry conditions the block is stable (FS = 4.29). Only with a rather small friction angle (< 3°) and a water pressure of approx. 0.4 MPa the limit equilibrium state (FS = 1) is obtained. The interpretation is, that the wedge formed by joint set 5 and the schistosity is kinematically removable but stable by friction.

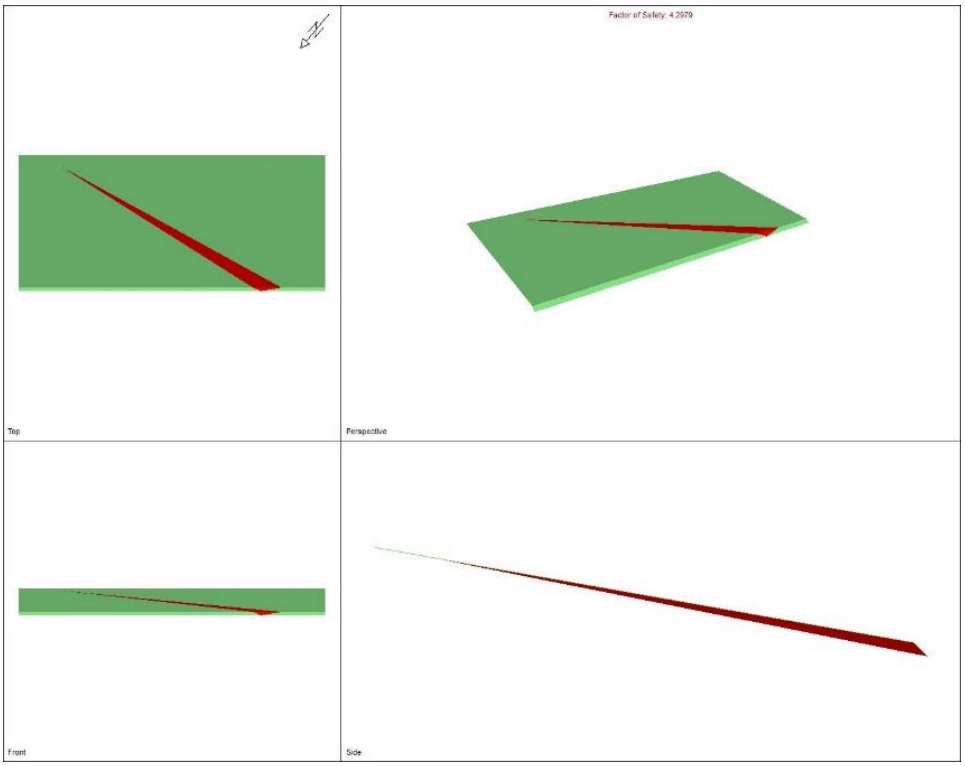

Figure 39: SWedge analysis for the key block 100100 in different perspectives.

The removable block 100101 has a Factor of Safety of 1.39 based on a friction angle of 20° (Figure 40). Water pressure can increase to approx. 1.13 MPa in order to reach limit equilibrium (FS =1). Only by reducing the friction angle and adding high water pressure the limit equilibrium state is reached. Failure only is expected if the friction angle drops down under 14° and the water pressure rises higher than 1.13 MPa.

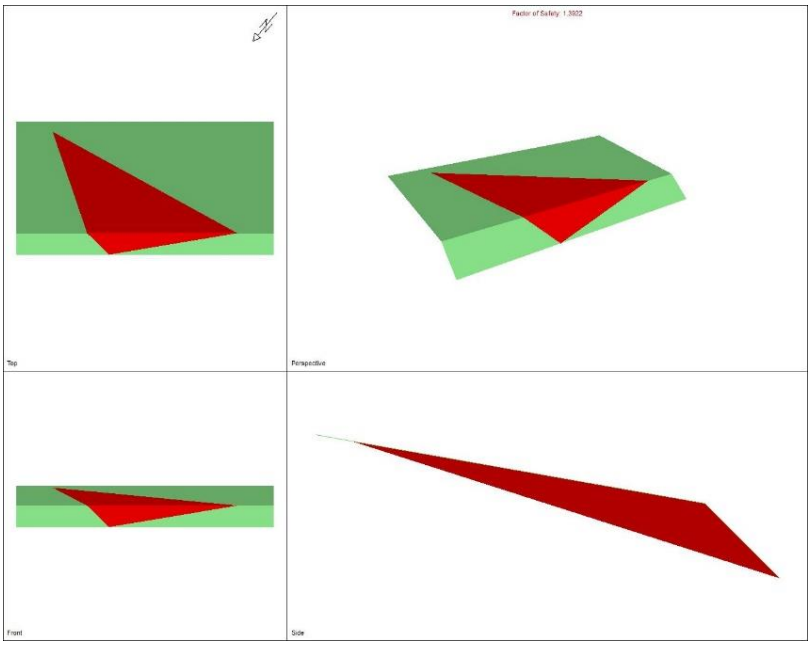

Figure 40: SWedge analysis for the key block 100101 in different perspectives.

The potential removable key block with the JP code 101100 (Figure 41) acts under the estimated field conditions very stable (FS > 20). Only at a drop with a friction angle to 5° and approx. 1.1 MPa water pressure the limit equilibrium state (FS = 1) is reached. A failure on the intersection of joint set 3 and 5 is much unexpected.

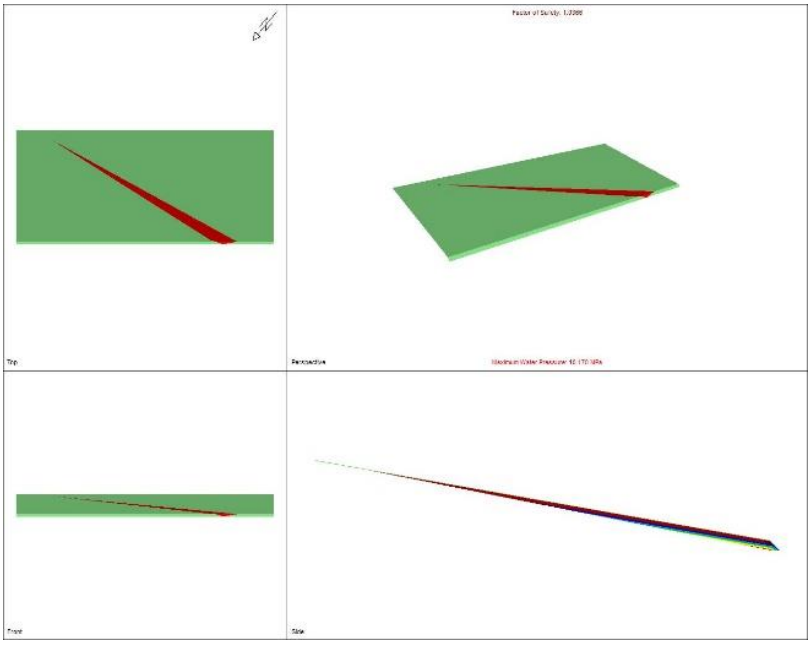

Figure 41: Graphic of the potential key block 101100.

The results from the stability analysis using SWedge correspond to the results obtained from key block analysis. The comparison is shown in table 8.

Table 8: Comparison of the FS results obtained from the stability analysis using the software SWedge and the key block stability software.

Potential Key Blocks	**Inserted Friction Angle**	**Key Block Analysis**	**Stability Analysis using SWedge**
[JP Codes]	[°]	**Factor of Safety**	**Factor of Safety**
11010	20	0.95	0.96
	21	1.0	1.0
100100	20	4.16	4.29
100101	20	1.46	1.39
101100	20	20.85	>20.0

All key blocks at the study area are, with regard to key block analysis and stability analysis using SWedge, stable with an inserted friction angle of 21°. The most critical key block is the block with the JP code 11010 formed from the joint plane 4 (53/62°) and joint plane 5 (336/21°). This type I key block has a FS = 1.0 with a friction angle of 21° and behaves therefor on its limit equilibrium state. If the friction angle of the joint plane decreases, e.g. to 20°, the block is unstable and failure is expected. The other potential key blocks act also with a friction angle of 20° stable.

4.2.3 Stability Analysis using “Slide”

The program SWedge interpret and compute the entire landslide area as one big wedge, which is based on previous investigations unlikely for this dimension. To analyse the whole area of landslide (Area 1) relating to the failure mechanism sliding the program Slide is performed.

The estimated pre-failure profile is used (cf. chapter 4.1) and for each different material, light phyllite micaschist, alluvium, failure surface area, suitable material characteristics get inserted. The assumed material properties from laboratory testing and literature [*Linser, 2009*] are listed in table 9.

Table 9: Assumed material properties

Material	Unit Weight	Friction Angle	Cohesion
	[kN/m³]	[°]	[kPa]
Micaschist	27	25	1000
Alluvium Deposit	27	25	1000
Failure Surface Area	26	20	200

The program analysis different sliding circles with regard to their safeness. The circle with the least safeness displays the critical sliding circle on which failure is most expected.

Under approximately dry conditions the most likely failure plane is shown in Figure 42.

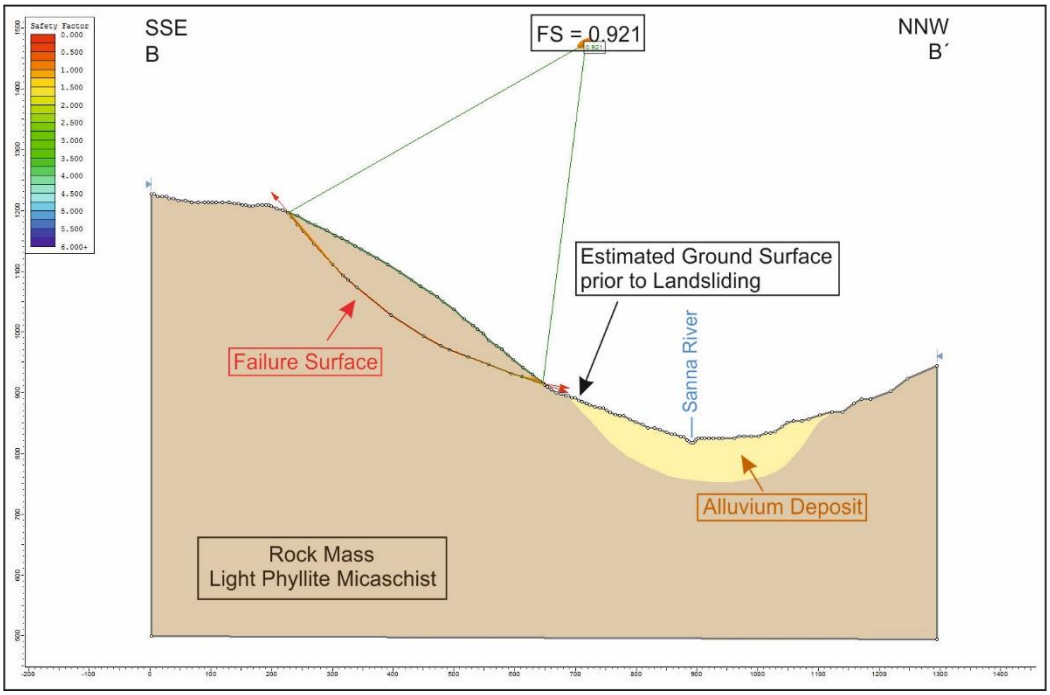

Figure 42: Slide profile under dry conditions with the most likely failure plane.

With the parameters denoted in table 9 a FS = 0.921 is obtained. The slope is not stable or safe and failure is expected. If a medium water table is inserted (Figure 43) the Factor of Safety decreases to 0.898 and with an added high water table (Figure 44) the FS = 0.857. This indicates that a rising water table reduces the resisting forces in the slope.

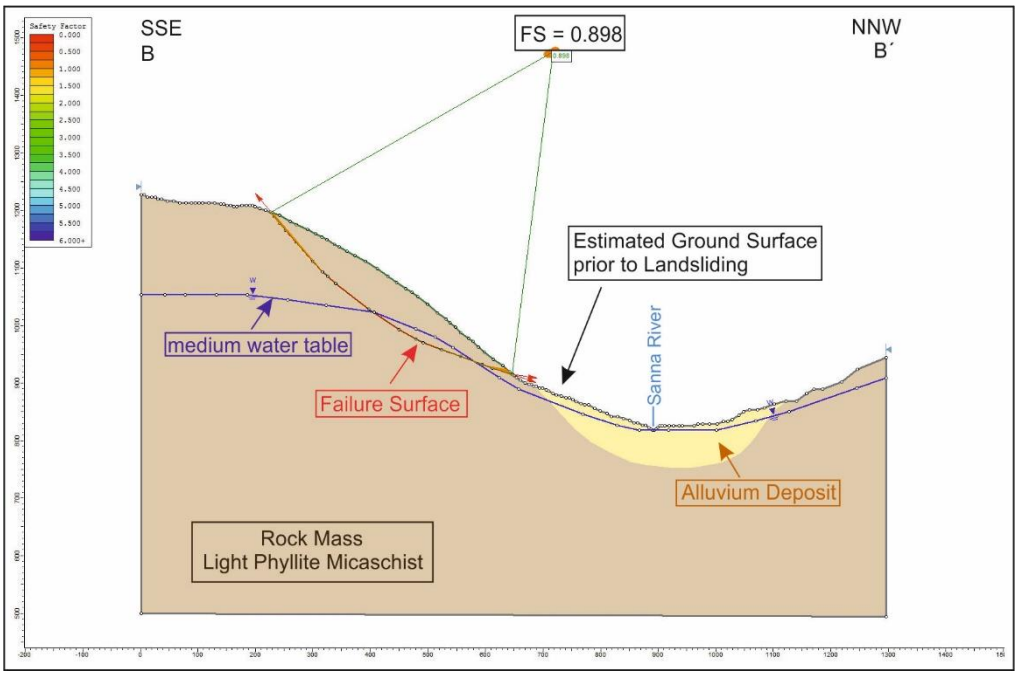

Figure 43: Slide profile under medium water table conditions with the most likely failure plane.

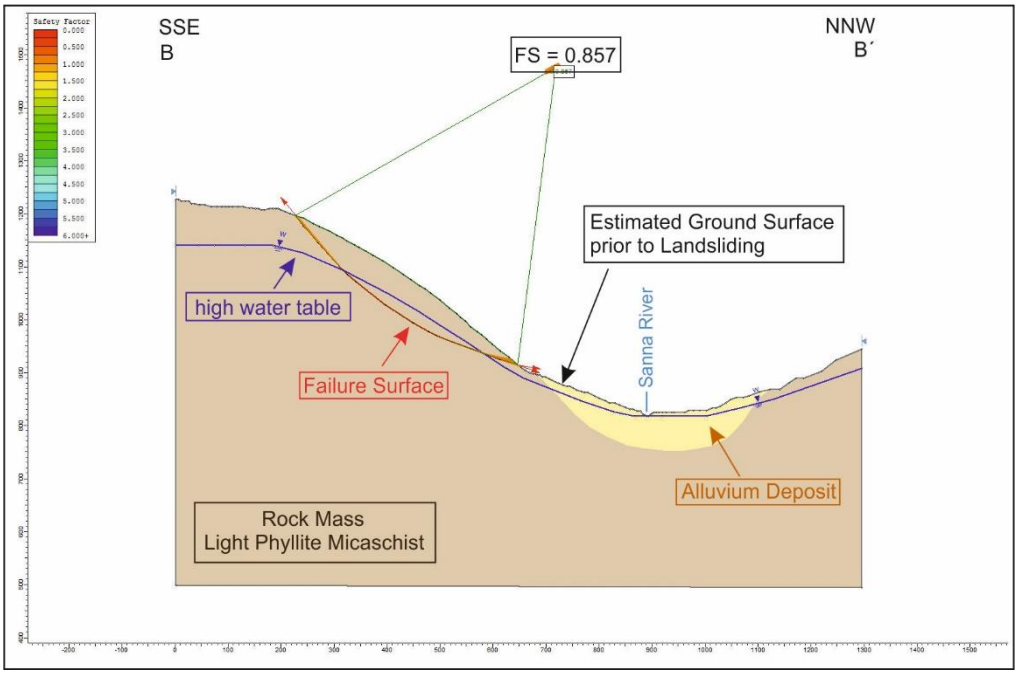

Figure 44: Slide profile under high water table conditions with the most likely failure plane.

The following variations of the material properties “failure surface”, listened at table 10, 11 and 12 led to the limit equilibrium state (FS = 1) of the slope. This analysis is done for dry conditions, an added medium water table and a high water table.

Table 10: Material properties of the “failure surface” without the water table which lead to FS = 1.

Factor of Safety	Friction Angle [°]	Cohesion [kPa]
FS = 1	15	344
FS = 1	20	248
FS = 1	25	146
FS = 1	30	35
FS = 1	3	600
FS = 1	12	400
FS = 1	23	200

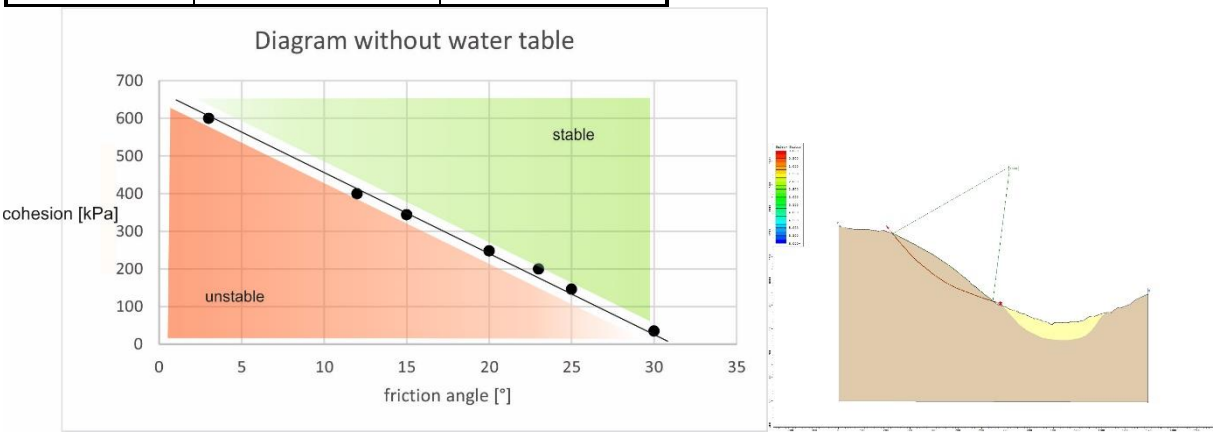

Figure 45: Material properties which lead to FS = 1 charted at the left diagram. The trend line indicates limit equilibrium conditions. The red sector represents the unstable parameter conditions and the green sector the stable conditions.

Table 11: Material properties of the “failure surface” with medium water table which lead to FS = 1.

Factor of Safety	Friction Angle [°]	Cohesion [kPa]
FS = 1	15	355
FS = 1	20	265
FS = 1	25	165
FS = 1	30	61
FS = 1	3	600
FS = 1	13	400
FS = 1	24	200

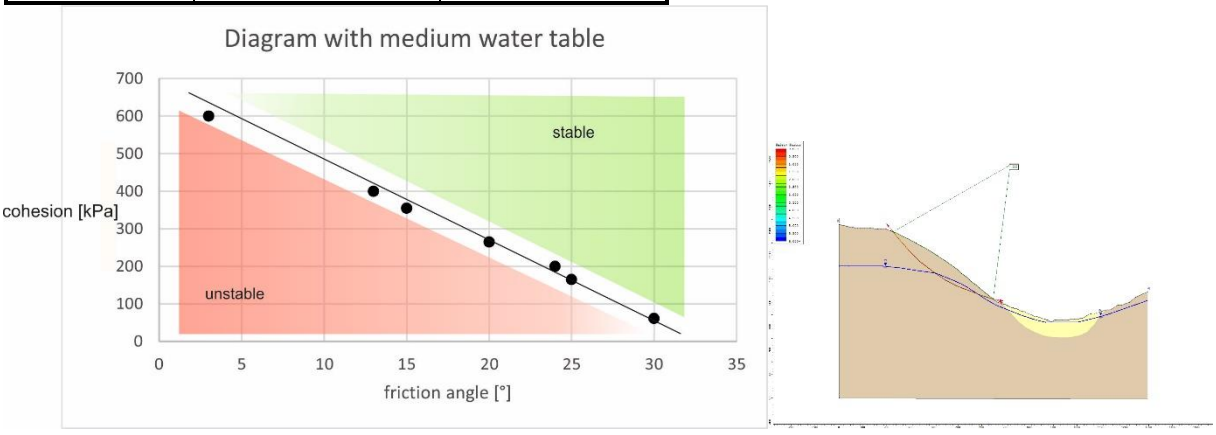

Figure 46: Material properties which lead to FS = 1 charted at the left diagram. The trend line indicates limit equilibrium conditions. The red sector represents the unstable parameter conditions and the green sector the stable conditions.

Table 12: Material properties of the “failure surface” with high water table which lead to FS = 1.

Factor of Safety	Friction Angle [°]	Cohesion [kPa]
FS = 1	15	373
FS = 1	20	287
FS = 1	25	196
FS = 1	30	96
FS = 1	3	600
FS = 1	14	400
FS = 1	25	200

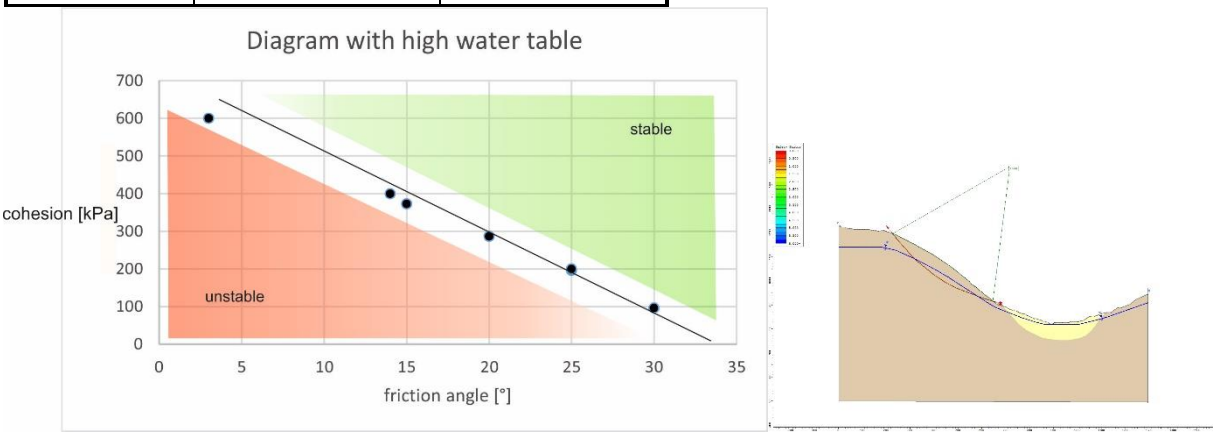

Figure 47: Material properties which lead to FS = 1 charted at the left diagram. The trend line indicates limit equilibrium conditions. The red sector represents the unstable parameter conditions and the green sector the stable conditions.

All diagrams show approximately linear correlation between the friction angle and the cohesion. The trend line represents the limiting state (FS = 1). The area above is characterised as stable (FS > 1) and the area below is unstable (FS < 1). Under the conditions, estimated in field and during laboratory testing, the slope is unstable also with respect to the different water tables. A failure is admissible.

If the water table rises the unstable area increases, the stable area decreases and so a higher failure potential is expected. With higher water tables, higher shear parameters, friction angle and cohesion, are needed to stabilize the entire slope.

4.2.4 Stability Analysis using “RocTopple”

The program RocTopple 1.0 [*Rockscience, 2013*] gets applied for the stability analysis at Area 2 right downhill from the church of Tobadill where the large breaks and cracks in the slope surface are observed during field investigations and laserscan interpretation. To find out if these cracks are caused by (deep-seated) toppling a kinematic and stability analysis using the software RocTopple is performed. Under the determined shear parameters of ϕ = 20° and c = 200 kPa and a very narrow, small spacing of about 5 m, the factor of safety is 0.844 (Figure 48). This result indicates that toppling is kinematically admissible.

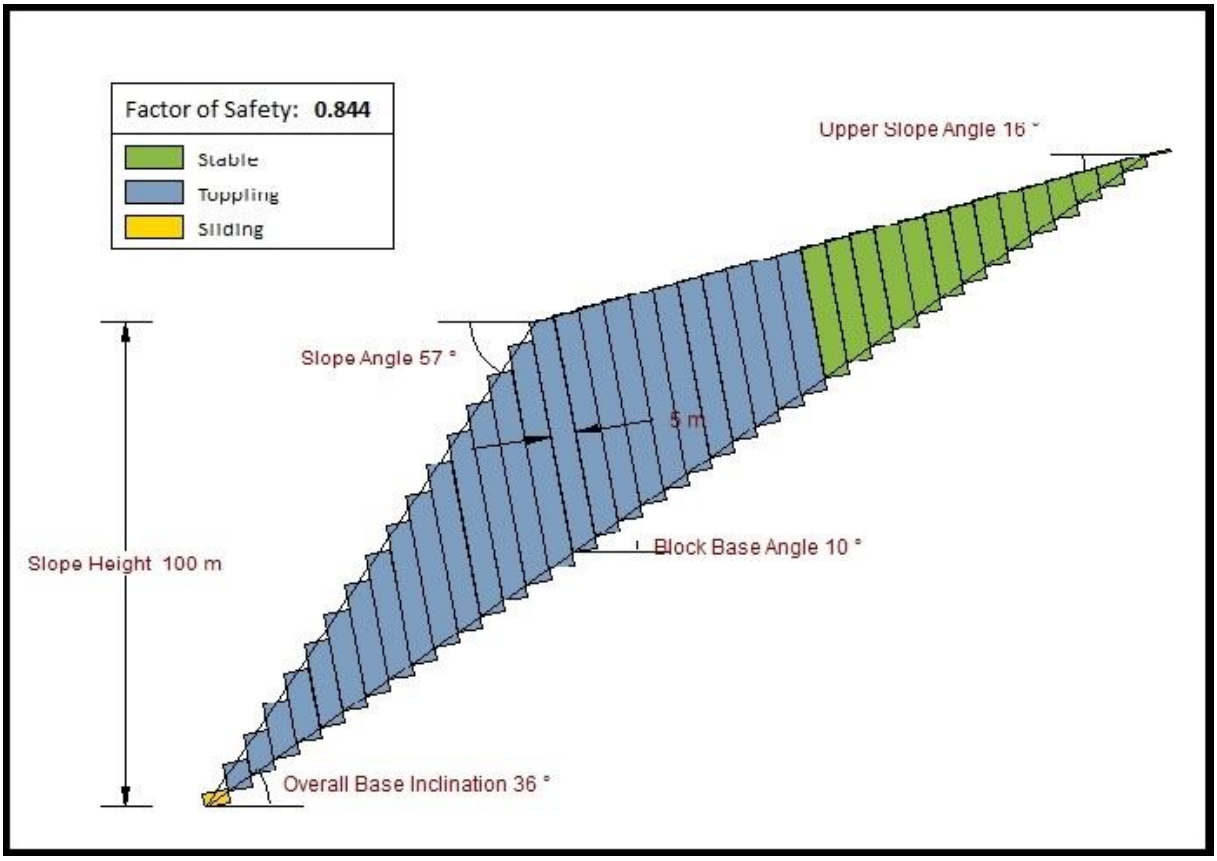

Figure 48: Stability analysis at the area under the church of Tobadill with respect to toppling.

Based on laserscan interpretation, field mapping and joint set orientation measurements joint set 3 (337/ 81°) and joint set 4 (53/62°) are significantly involved in the toppling processes.

To support previous analysis and to include the breaks at the headscarp area into the slope stability analysis the software RocTopple is also used for Area 1, the area of landslide. Under the determined shear parameters, slope characteristics and joint properties a factor of safety of 0.896 is computed (Figure 49). The factor of safety is lesser than 1 and also based on the analysis with RocTopple the expected failure mechanism at the front area of the slope is sliding. Figure 49 illustrates that at the upper area, behind the headscarp area, toppling is kinematically admissible and based on laserscan interpretation, field mapping and joint set orientation measurements joint set 3 (337/ 81°) affects the occurrence of toppling.

This result supports also the previous analysis. At Area 1 sliding is the estimated failure mechanism and at upper regions also (large scale) toppling is kinematically admissible.

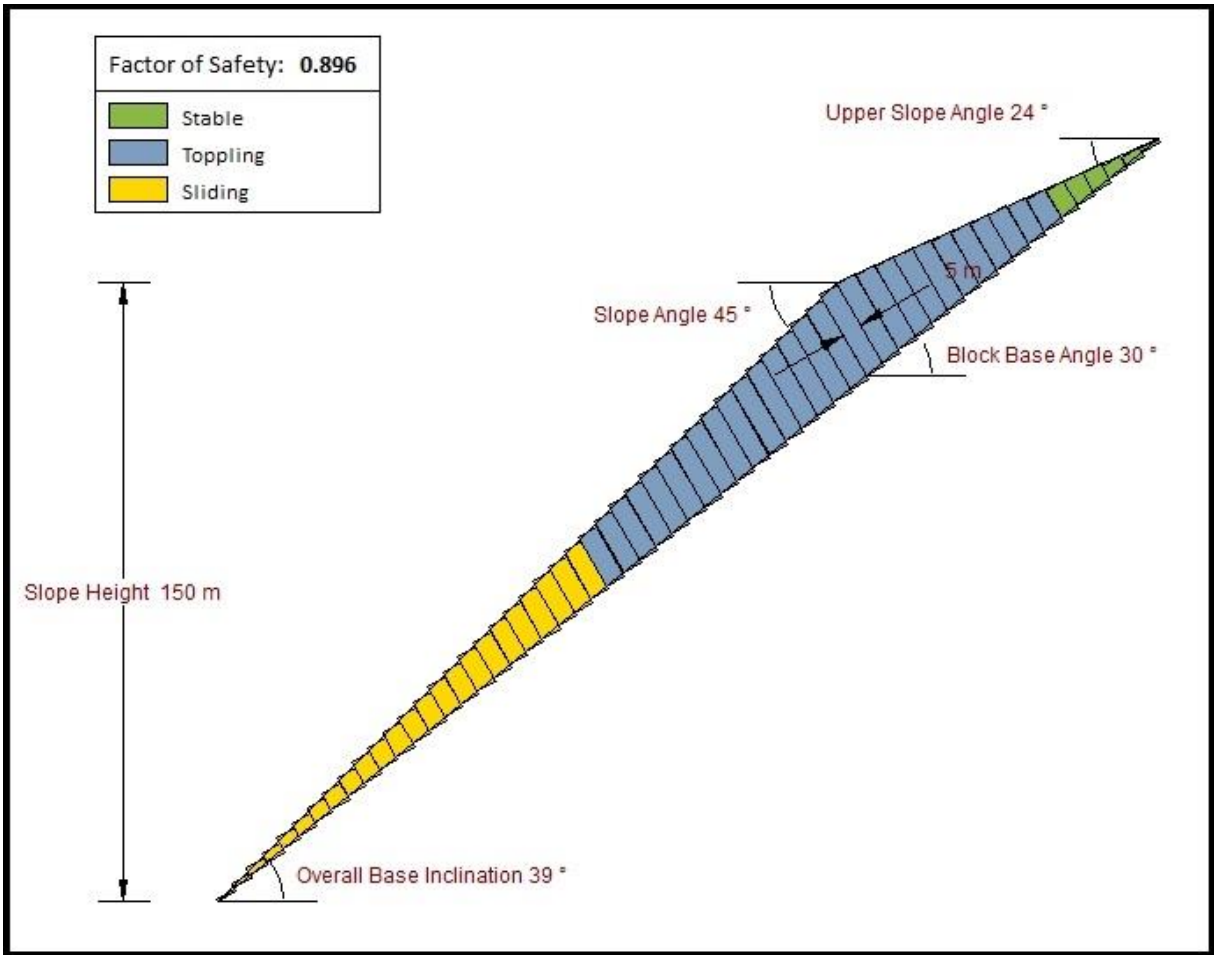

Figure 49: Stability analysis with respect to toppling at Area 1.

4.3 Subsurface Model

Based on subsurface interpretation and engineering geological analysis a model for the subsurface conditions and the depth of the landslide can be constructed. The geological and geomorphological cross section are provided for two different areas (Figure 30).

For Area 1 the maximum depth of the landslide get assumed with approx. 60 m (Figure 50). Based on previous investigations it is supposed that joint set 4 and joint set 5 initiated the landslide after the valley got filled up with fluvio-glacial sediments.

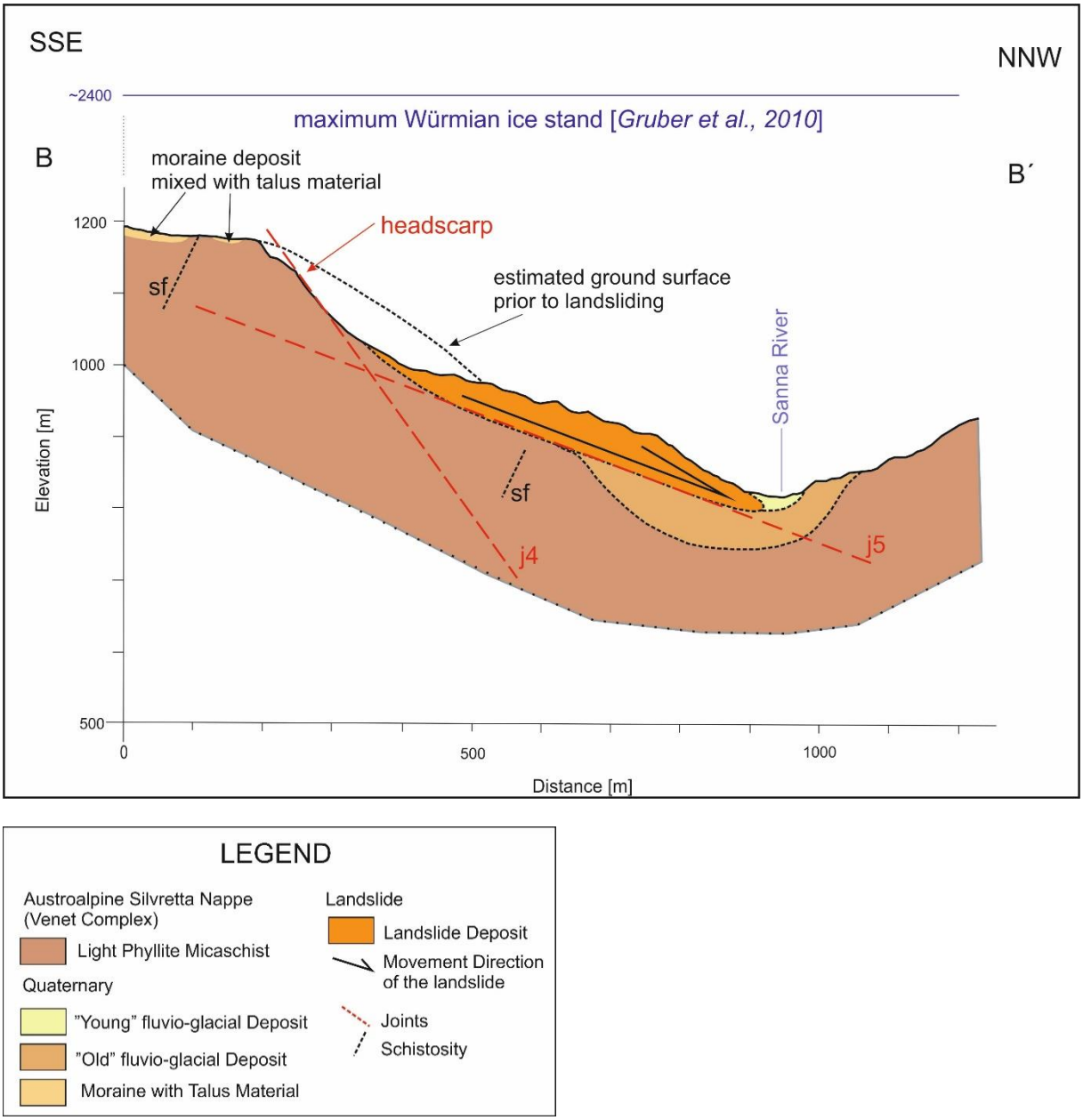

Figure 50: Geologic cross section of Area 1 from the study area. The exact location of the cross section can be taken from Figure 30.

Figure 51 illustrated the estimated internal structure of the landslide deposit. The significant transversal “horst and graben” structure of the deposit correspond to the orientations of the joint planes based on structural measurements and investigations. It is then suggest that the “horst and graben” structure is initiated and influenced by them (Figure 51).

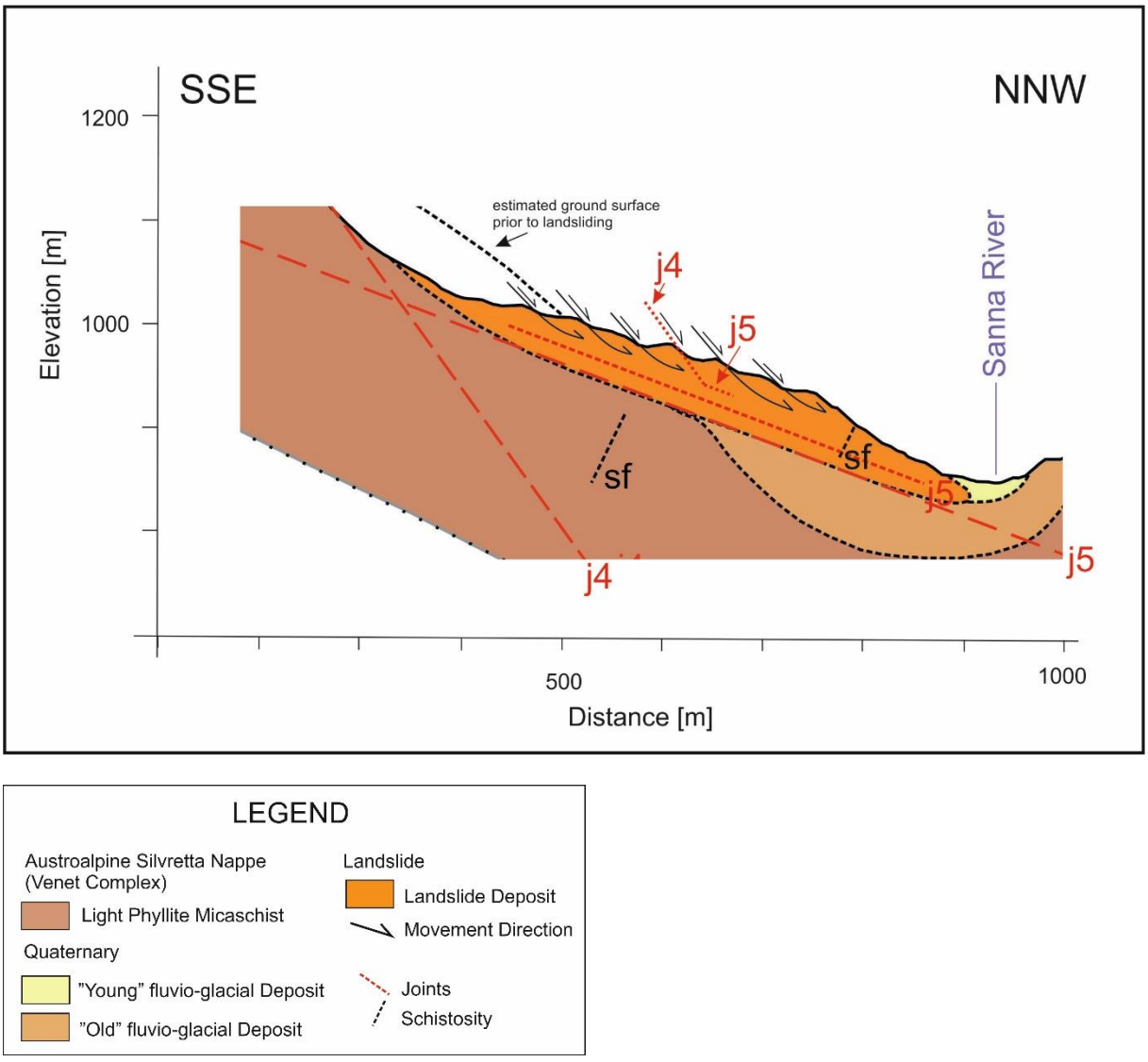

Figure 51: Cross section of the estimated internal structure of the landslide deposit.

The second coss section is constructed for the area under the church of Toadill where based on laserscan evaluation and detailed field investigations the large breaks, cracks and fractures occur. Based on structural and engineering geological analysis it is assumed that the cracks and the slope stability get significantly inluenced by joint set 3 and joint set 4 (Figure 52).

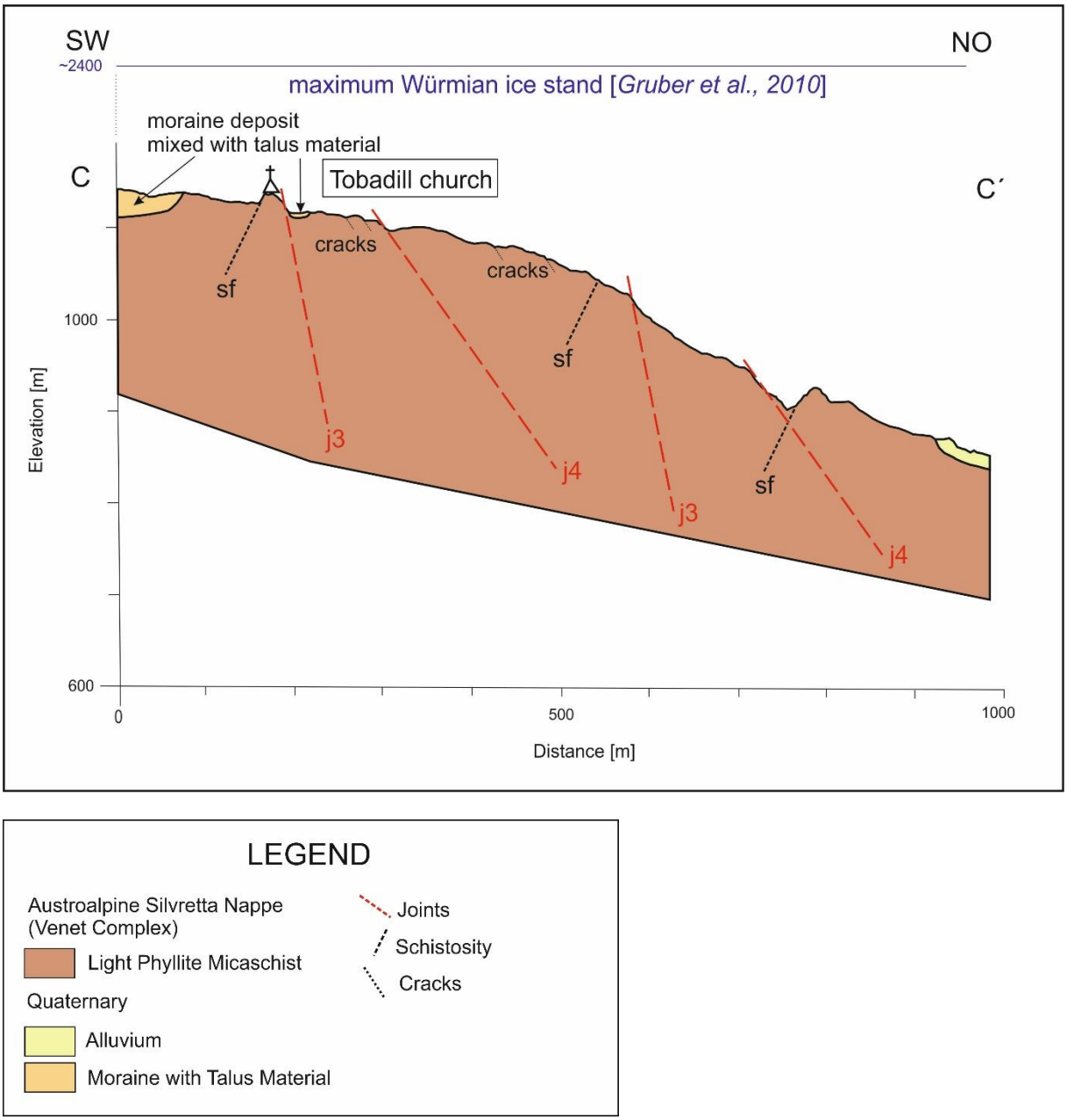

Figure 52: Cross section under the church of Tobadill. The exact location of the cross section can be taken from Figure 30.

5 Discussion and Conclusions

Based on desk study (e.g. laserscan data, ortophotos), detailed field mapping, structural geologic measurements and analyses, together with engineering geological investigations (including stability and kinematic analyses) an engineering geological and geomorphological evaluation of the study area has been performed. These studies revealed two main areas of greater interest: Area 1 is named “the landslide” and is located eastward from the small town Tobadill. Area 2 is situated downhill from the church of Tobadill.

Laserscan data and field observations show that Area 1 is characterized by a steep haedscarp area and an area with mass movement deposits. Based on field mapping, structural measurements and kinematic analysis the dip direction and dip angle of two joint sets favour the occurrence of the block sliding. On the basis of engineering geologic investigations performed, it is suggested that the landslide initiation was controlled by joint set 4 (53/62°) and 5 (336/21°). A basal shear zone is then suggest to have developed in close connection with joint set 5 (336/21°). Stability analyses using the software Slide compute a factor of safety <1 if the friction angle of the shear zone material is 20° and the cohesion 200 kPa. If water acting in the slope and the water table rises above the failure surface the factor of safety decreases further on. Based on cross section analysis, borings [*ASFiNAG, 2012b*] and the reconstruction of the pre-failure topography the depth of the landslide is interpreted to be approx. 60 m. The internal structure of the landslide deposit shows transversal “horst and graben” structures developed and featured from joint set 3 (337/81°) and joint set 4 (53/62)° referred to cross section and laserscan analysis and field investigations. At the toe area of the landslide shallow secondary slides are recorded during field mapping resulting from the disintegration of the landslide deposit rock mass. At this area also the railway tracks pass through and the ÖBB company documents higher abrasion and higher reparation efforts on the rail tracks at this sector. Due to the documentation of the ÖBB [*pers. Poscher*, 2013] and further indicators of movement observed during field investigations the secondary slides at the toe of the slope are supposed to be active. Based on investigations and engineering geological analysis the separated landslide from the entire Perfuchsberg landslide, get classified as a rockslide initiated by two joint panes. The breaks and cracks at the upper area, behind the headscarp, could be caused by (large scale) toppling referring to kinematic analysis. At the steep headscarp area secondary failure events like rock fall are expected.

Field investigations and cross section analysis illustrate that Area 2 is characterized by large open breaks in the ground surface and steep rock faces. Field mapping and structural measurements and kinematic analysis suggest that joint set 3 (337/81°) and joint set 4 (53/62°) are involved in this failure mechanism. Stability analysis using the software RocTopple calculate a factor of safety <1 if the friction angle of the rock mass is 20° and the cohesion 200 kPa. Based on engineering geological analysis it is suggest that the failure mechanism of Area 2 is (large scale) toppling on the steep rock faces as well as hundreds of meters behind the rock faces. Secondary failures like rock falling events take place on the steep rock faces and the size of the blocks vary from large boulders to small stones and debris referred to detailed field observations.

If the entire landslide Perfuchsberg with its separated slides get compared to the reference examples landslide Zintlwald [*Eder et al. (2006), Poscher et al. (2006), Henzinger et al. (2009)*], landslide Niedergallmigg [*Kirschner (2006), Zangerl et al. (2012)*] and landslide Gfäll [*Heißel et al. (2015), Strobl (2015)*] several similarities get identified:

- All landslides are composed of rock masses belonging to the Silvretta nappe (Venet complex, Silvretta crystalline). The lithology ranges from phyllites to quartzphyllonites to mica schists and gneisses with an intense sheared and dominant joint plane and schistosity affected structure.

- The valleys in which the landslides occur (Paznaun, Stanzer, Upper Inn valley) are showing glacial overdeepening of approx. 100 m, meaning that the river beds got filled up with fluvio-glacial sediments after the glaciation. Based on engineering geological analysis the fluvio-glacial deposit sets up the condition for slope ensuing slope instability.

- All four landslides show active portions (secondary slides) at the area, particularly along the slope toe. The erosion of the rivers and thus the change of the topography of the toes, in correlation with high rainfall, floodwater or snowmelt events are assumed to have significant influence on the present movement and stability of the active landslide portions.

Further investigation programs could be performed to obtain more detailed and exact information regarding to the precise depth of the landslide, the rock mass composition beneath the slope surface and the detailed characteristics of the suggest shear zone. This research and analysis program could be include:

- The depth of the sliding mass and its contact to the intact rock respectively the fluvio-glacial deposit could be detected with reflection and refraction seismic investigations.
- Further core borings down to the results obtained from the seismic investigations would allow to sample and test the shear zone and landslide material and to recheck the geophysical results.
- In the boreholes inclinometer could be installed to get the movement rates at the certain depth of the entire landslide or secondary slides. Active parts and parts with no displacement could be distinguished.
- To receive the exact movement rates, the total displacement vectors and to differentiate parts of higher and lower velocities a geodetic monitoring with surface measurement points over a long time (at least one year) could be required.

6 References

ALBER, WIERER (2011): Perjentunnel – Lötz Galerie, Bestandserhebung. ASFiNAG Bau Management GmbH, S16 Arlberg Schnellstraße AST Zams – AST Landeck West. Technischer Bericht.

ASFiNAG (2012a): S16 Arlberg Schnellstraße, Perjentunnel 2. Röhre, Gebirgsarten und Gebirgsverhaltenstypen. Technischer Bericht vom 27. April 2012, Planungsgemeinschaft Bernard - BK, 55 S.

ASFiNAG (2012b): S16 Arlberg Schnellstraße, Perjentunnel 2. Röhre, Bohrprotokolle – Geologische Aufnahme durch Bernard Ing.

BEV (2013): Bundesamt für Eich- und Vermessungswesen: KM50-R select, digital topographic map of Austria, mapping scale 1:50,000.

BEV (2015): Bundesamt für Eich- und Vermessungswesen, Austria Map online: www.austriamap.at.

BUTTON, E. A. (2004): A Contribution to the Characterization of Phyllitic and Schistose Rock Masses for Tunnelling. Gruppe Geotechnik Graz, Heft 22, 134 S.

BLUEMEL, M. (2004): Laboratory Testing for Soft Rock - a Challenge. Institute for Rock Mechanics and Tunnelling, Graz University of Technology, Austria.

CRUDEN, D.M. & VARNES, D.J. (1996): Landslide Types and Processes. National Research Council, Washington, D.C., 36-75.

EDER, S., POSCHER, G., PRAGER, C. (2006): Risk analyses and risk management - slope instabilities in alpine environments. ECI Geohazards - Technical, Econimical and Social Risk Evaluation, 18 - 21 June 2006, Lillehammer, Norway.

EGGER, H., KRENMAYR, H.G., MANDL, G.W., MATURA, A., NOWOTNY, A., PASCHER, G., PESTAL, G., PISTOTNIK, J., ROCKENSCHAUB, M., & SCHNABEL W. (1999): Geologische Uebersichtskarte der Republik Oesterreich. Geologischen Bundesanstalt, Wien.

GATTERMAYER, W., NIEDERTSCHEIDER, K., MAIR, G., FELDERER, W. (2005): Hydrogeologische Üebersicht, - August 2005. Landesbaudirektion, Abteilung Wasserwirtschaft - Sachgebiet Hydrographie.

GeoDZ (2010): Alpen - GeoDZ, Das Lexikon der Erde; www.geodz.com/deu/d/Alpen.

GOODMAN, R.E. & SHI, G. (1985): Block Theory and Its Application to Rock Engineering. Prentice-Hall, Inc., Englewood Cliffs, New Jersey.

GRUBER, A., PESTAL, G., NOWOTNY, A. & SCHUSTER, R. (2010): Erläuterungen zu Blatt 144 Landeck. Geologische Karte der Republick Österreich 1:50.000. Geologische Bundesanstalt, Wien.

GRUBER, WIERER (2012): Perjentunnel 2. Röhre, Vorprojekt 2012. ASFiNAG Bau Management GmbH, S16 Arlberg Schnellstraße AST Zams – AST Landeck West. Technischer Bericht.

HEIßEL, G., FIGL, T., GSTREIN, P., HENZINGER, J. & POSCHER, G. (2005): Gfällbrücke – Beurteilung der geologischen Situation. Ingenieurgeologisches Gutachten vom 10. September 2005, page 11.

HENZINGER, J., POSCHER, G., HEISSEL, G., MATTLE, B. (2008): Hangbewegung Zintlwald, 3 Jahre nach dem Anbruch.

ISRM. (1983): Suggested method for determining the strength of rock materials in triaxial compression. International Journal of Rock Mechanics and Mining Sciences & Geomechanics Abstracts, Vol. 20, No. 6, p. 285-290.

ISRM (2013): Suggested method for laboratory determination of the shear strength of rock joints: revised version. Rock Mechanics and Rock Engineering, Springer 2013.

KIRSCHNER, H. (2006): Endbericht zur Untersuchung von Massenbewegungen im oberen Inntal. Projekt A2.3, alpS - GmbH, Zentrum für Naturgefahren Management.

KÖEHLER, M., (1983): Perjentunnel (Landeck, Tirol): Baugeologische Verhältnisse, Prognose und tektonische Schlussfolgerungen. Geol. Paläont. Mitt. Innsbruck, 12, p. 249-267.

KRAINER, K., HAUSER, C., PAVLIK, W., PESTAL, G., NOWOTNY, A., ROCKENSCHAUB, M., UCIK, F.H. (2004): Geologische Karte der Republik Oesterreich 1:50.000, 144 Landeck. Geologische Bundesanstalt, Wien.

LINSER M. (2009): Speicherkraftwerk Kühtai, Beileitungsstollen. Geologisch/ Geomechanischer Bericht, TIWAK.

MAGGETTI, M. & FLISCH, M. (1993): Evolution of the Silvretta Nappe.- In: von Raumer, J. F. & Neubauer, F. (Eds.), 1993: Pre-Mesozoic Geology in the Alps, Part III, 469-484, Springer-Verlag, Berlin Heidelberg.

MURALHA, J., GRASSELLI, G., TATONE, B., BLÜEMEL, M., CHRYSSANTHAKIS, P., YUJING, J. (2013): ISRM Suggested Method for Laboratory Determination of the Shear Strength of Rock Joints: Revised Version. Springer-Verlag, Wien.

ÖNORM CEN ISO/TS 17892-8: Geotechnische Erkundung und Untersuchung - Laborversuche an Bodenproben - Teil 8: Unkonsolidierter undränierter Triaxialversuch (ISO/TS 17892-8:2004).

ÖNORM CEN ISO/TS 17892-10: Geotechnische Erkundung und Untersuchung - Laborversuche an Bodenproben - Teil 10: Direkte Scherversuche (ISO/TS 17892-10:2004).

ÖNORM EN ISO 14689-1: Geotechnische Erkundung und Untersuchung – Benennung, Beschreibung und Klassifizierung von Fels, Teil 1: Benennung und Beschreibung (ISO: 14689-1:2003).

PFIFFNER, O.A. (2009): Geologie der Alpen. 1. Auflage. Verlag: UTB, Stuttgart.

POSCHER, G. (1993): Neuergebnisse der Quartärforschung in Tirol. Geologie des Oberinntaler Raumes – Schwerpunkt Blatt 144 Landeck. Arbeitstagung Geol.B.-A., Wien, page 7 – 27.

POSCHER, G., MATTLE, B., HEISSEL, G. (2006): Hangbewegung Zintlwald, Geologisch / Geotechnischer Bericht – Risikobewertung. Amt der Tiroler Landesregierung, Gruppe Bau und Technik.

PRAGER, C., ZANGERL, C., PATZELT, G., & BRANDNER, R. (2008): Age distribution of fossil landslides in Tyrol (Austria) and its surrounding areas. Nat. Hazards Earth Syst. Sci., 8, 377 – 407.

PREUSSER, F., REITNER, J.M., SCHLÜECHTER, C. (2010): Distribution, geometry, age and origin of overdeepened valleys and basins in the Alps and their foreland. Swiss J Geosci 103; 407 – 426.

REITNER, J.M., GRUBER, W., ROEMER, A., MORAWETZ, R. (2010): Alpine overdeepenings and paleo-ice flow changes: an integrated geophysival-sedimentological case study from Tyrol (Austria). Swiss J Geosci 103; 385 – 405.

RIEGLER, Prof. Dr. F. (2006): Tirol Geographische Grundlagen. Pädagogische Akademie des Bundes in Tirol.

SCHMID, S.M., FÜEGENSCHUH, B., KISSLING, E. & SCHUSTER, R. (2004): Tectonic map and overall architecture of the Alpine orogen. Eclogae geol. Helv., 97, 93-117.

STROBL, S. (2015): Engineering geological aspects of the landslide Gfäll in the Paznaun valley (Tyrol, Austria).

TIRIS (2013): Tiroler Rauminformationssystem; Tiris Kartendienste: tirisMaps; Amt der Tiroler Landesregierung. www.tirol.gv.at.

TOLLMANN, A. (1977): Geologie von Österreich. Band 1. Die Zentralalpen. - Deuticke, Wien.

VAN HUSEN, D. (1987): Die Ostalpen in den Eiszeiten. Geol. B.-A., Wien.

VARNES, D.J. (1978): Slope movement types and processes. Landslides, Analysis and Control. Special Report 176, Transportation Research Board, Washington, 11-33.

ZANGERL, C., PRAGER, C. (2008): Influence of geological structures on failure initiation, internal deformation and kinematics of rock slides. ARMA 08-063.

ZANGERL, C., PRAGER, C., BRANDNER, R., BRÜECKL, E., EDER, S., FELIN, W., TENTSCHERT, E., POSCHER, G. & SCHÖENLAUB, H. (2008): Methodischer Leitfaden zur prozessorientierten Bearbeitung von Massanbewegungen. Geo.Alp, Vol. 5, S. 1 - 51.

ZANGERL, C., PRAGER, C., CHWATAL, W., BRÜECKL, E., KIRSCHNER, H. & BRANDNER, R. (2012): Kinematics and internal deformation of a slow deep-seated rock slide in metamorphic rock (Niedergallmigg, Austria).

INTERNET SOURCES

http://austria-forum.org/af/Community/Alles_%C3%BCber_%C3%96sterreich/Landkarte-%C3%96sterreich; retrieved on October 7th 2014

http://tirolatlas.uibk.ac.at/graphics/lieth/diag.py/chart?id=1371104; retrieved on October 8th 2014

http://www.geodz.com/deu/d/Alpen; retrieved on December 17th 2014

SOFTWARE USED FOR THE ENGINEERING GEOLOGICAL ANALYSIS

GS Geologische Software: FABRIC8; Wallbrecher E.

LIU, Q., 2004: Key block programs B2HPGL and B10HPGL. - modified after the methods and programs by GOODMAN, R. & SHI, G., 1989.

LIU, Q. & KIEFFER, D. S., 2008: Key block program B04HPGL. - modified after the methods and programs by GOODMAN, R. & SHI, G., 1989.

ROCSCIENCE, 2010: Slide 6.0.- Advanced Slope Stability and Groundwater Seepage Analysis.- Rocscience Inc.

ROCSCIENCE, 2013: RocTopple 1.0. - Toppling Analysis of Rock Slopes.- Rocscience Inc.

ROCSCIENCE, 2014a: SWedge 6.0. - 3D Surface Wedge Analysis for Slopes.- Rocscience Inc.

ROCSCIENCE, 2014b: Software tools for rock and soil. - Rocscience Inc.

8 Appendix

Appendix 1: Structural Measurements.....Appendix page 1
Appendix 2: Sample List.....Appendix page 2
Appendix 3: Thin Section Analysis .....Appendix page 4
Appendix 4: Laboratory Testing.....Appendix page 6
Appendix 5: Block Theory Analysis .....Appendix page 21

Appendix 1: Structural Measurements

Schistosity	
Dip Direction	Dip Angle [°]
186	65
190	69
181	87
164	40
165	55
170	50
168	74
177	70
178	73
177	72
160	42
163	47
166	48
167	49
189	69
192	88
192	89
180	63
178	65
169	52

Schistosity	
Dip Direction	Dip Angle [°]
170	50
170	52
182	66
184	66
184	67
167	58
172	58
169	60
190	69
194	70
180	87
178	89
173	63
170	63
165	56
169	56
175	63
170	63
176	64
174	60
175	64

Joint Set 1		Joint Set 2		Joint Set 3		Joint Set 4		Joint Set 5	
Dip Direction	Dip Angle [°]	Dip Direction	Dip Angle [°]	Dip Direction	Dip Angle [°]	Dip Direction	Dip Angle [°]	Dip Direction	Dip Angle [°]
158	90	204	51	316	90	39	55	326	42
159	90	218	90	352	84	22	51	328	41
140	89	203	90	339	70	49	63	320	45
140	90	232	45	342	80	34	46	336	25
101	62	241	44	320	84	91	80	337	18
129	57	239	39	322	84	88	77	332	20
116	64	232	40	322	85	24	49	335	19
120	63	217	50	317	90	24	50	333	39
132	65	218	51	318	90	34	45	330	32
134	67	233	37	345	79	35	46	338	15
132	66	234	38	346	80	50	61	336	16
139	68	215	50	346	81	52	64	339	14
140	68	204	51	337	72	53	62	340	20
139	70	203	49	340	74	53	68	334	19
152	63	204	51	351	85	74	75	338	18
151	64			350	81	78	76	337	18
151	60			354	80	82	69	339	17
154	58			350	82	83	79	342	13
155	56							340	14
								345	15
								342	14
								344	13
								336	20
								337	20
								336	20

Appendix 2: Sample List

Sample number	Position		Laboratory number	Investigation
Sample 01/13 KB-ZL8-04	x = 15820	y = 222423		
	Depth = 33.20 – 33.60 m			
Sample 02/13 KB-ZL8-04	x = 15820	y = 222423	02-13	Triaxial compression test
	Depth = 39.60 – 39.97 m			
Sample 03/13 KB-ZL8-02	x = 15886	y = 222508		
	Depth = 6.05 – 6.35 m			
Sample 04/13 KB-ZL8-02	x = 15886	y = 222508		
	Depth = 6.35 – 6.60 m			
Sample 05/13 KB-ZL8-02	x = 15886	y = 222508		
	Depth = 6.60 – 6.70 m			
Sample 06/13 KB-ZL8-02	x = 15886	y = 222508		
	Depth = 7.70 – 7.90 m			
Sample 07/13 KB-ZL8-02	x = 15886	y = 222508		
	Depth = 16.80 – 17.00 m			
Sample 08/13 KB-ZL8-02	x = 15886	y = 222508	08-13	Triaxial compression test
	Depth = 18.00 -18.30 m			
Sample 09/13 KB-ZL8-02	x = 15886	y = 222508		
	Depth = 18.75 – 18.90 m			
Sample 10/13 KB-ZL8-03	x = 15868	y = 222475		
	Depth = 16.00 – 16.55 m			
Sample 11/13 KB-ZL8-03	x = 15868	y = 222475		
	Depth = 16.55 – 16.75 m			

Sample number	Position		Laboratory number	Investigation
Sample 12/13 KB-ZL8-03	x = 15868	y = 222475	12-13	Direct shear test
	Depth = 17.35 – 17.47 m			
Sample 13/13 KB-ZL8-03	x = 15868	y = 222475		
	Depth = 21.07 – 21.20 m			
Sample 14/13 KB-ZL8-03	x = 15868	y = 222475		
	Depth = 22.50 – 22.75 m			
Sample 15/13 K	x = 14812	y = 221372	10828	Thin section
Sample 16/13 K	x = 14958	y = 221284	10830	Thin section
Sample 17/13 K	x = 14898	y = 221335		
Sample 18/13 K	x = 14625	y = 221149	18-13k	Direct shear test
Sample 19/13 K	x = 14485	y = 220980	10836	Thin section
Sample 20/13 K	x = 13612	y = 220856	10826	Thin section
Sample 21/13 K	x = 14061	y = 221401	10827	Thin section
Sample 22/13 K	x = 13710	y = 221265	22-13k	Direct shear test
Sample 23/13 K	x = 13299	y = 220909	10834	Thin section
Sample 24/13 K	x = 14787	y = 221400		
Sample 25/13 S	x = 12555	y = 218940	25-13s	Direct shear test
Sample 32/13 S	x = 12984	y = 219274	32-13s	Direct shear test
Sample 36/13 S	x = 12984	y = 219274	36-13s	Direct shear test

Appendix 3: Thin Section Analysis

Sample Number	Lab.Number	Main minerals	Accessory minerals	Structure
15/13K	10828	quartz biotite muscovite feldspar (plagioclase & kalifeldspar)	rutile tourmaline iron-mineralization	quartz: grey/ colorless, granulous, undulouse extinction; biotide: light brown/ brown, tabular/ elongated; muscovite: colorless/ light brown, tabular/ columnar; feldspar: colorless/ white, granulous; rutile: red/ brown, granulous; tourmaline: green (alternated), columnar; schisted structure, quartz-rich layers alternate with mica-rich layers, ion-mineralizations along joint planes, crenulation structure
16/13K	10830	quartz biotite muscovite feldspar (plagioclase & kalifeldspar)	tourmaline iron-mineralization	quartz: grey/ colorless, granulous, undulouse extinction; biotite: light brown/ brown, tabular/ elongated; muscovite: colorless/ light brown, tabular/ columnar; feldspar: colorless/ white, granulous; tourmaline: green (alternated), columnar; schisted structure with little folds, fine scaly micas, partial chloritized, tourmalines occur at the upper micalayers, at the same layer iron-mineralizations
19/13K	10836	quartz biotite muscovite feldspar (plagioclase & kalifeldspar)	rutile	quartz: grey/ colorless, granulous, undulouse extinction; biotite: light brown/ brown, tabular/ elongated; muscovite: colorless/ light brown, tabular/ columnar; feldspar: colorless/ white, granulous rutile: red/ brown, granulous fine grained, schisted structure, higher percentage of quartz
20/13K	10826	quartz biotite muscovite feldspar (plagioclase & kalifeldspar)	rutile tourmaline iron-mineralization	quartz: grey/ colorless, granulous, undulouse extinction; biotide: light brown/ brown, tabular/ elongated; muscovite: colorless/ light brown, tabular/ columnar; feldspar: colorless/ white, granulous; rutile: red/ brown, granulous; tourmaline: green (alternated), columnar; schisted structure, partial chloritized/ altered, higher percentage of biotide and feldspar, ion-mineralizations along joint planes

Sample Number	Lab.Number	Main minerals	Accessory minerals	Structure
21/13K	10827	quartz biotite muscovite kalifeldspar	rutile tourmaline iron-mineralization	quartz: grey/ colorless, granulous, undulouse extinction; biotite: light brown/ brown, tabular/ elongated; muscovite: colorless/ light brown, tabular/ columnar; kalifeldspar: colorless/ white, granulous, twins; rutile: red/ brown, granulous; tourmaline: green (alternated), columnar; schisted structure with little folds, minerals are adjusted/ have a direction, whole section is alternated
23/13K	10834	quartz biotite muscovite feldspar (plagioclase & kalifeldspar)	rutile	quartz: grey/ colorless, granulous, undulouse extinction; biotide: light brown/ brown, tabular/ elongated; muscovite: colorless/ light brown, tabular/ columnar; feldspar: colorless/ white, granulous; rutile: red/ brown, granulous schisted structure

Appendix 4: Laboratory Testing

Results from the direct shear tests:

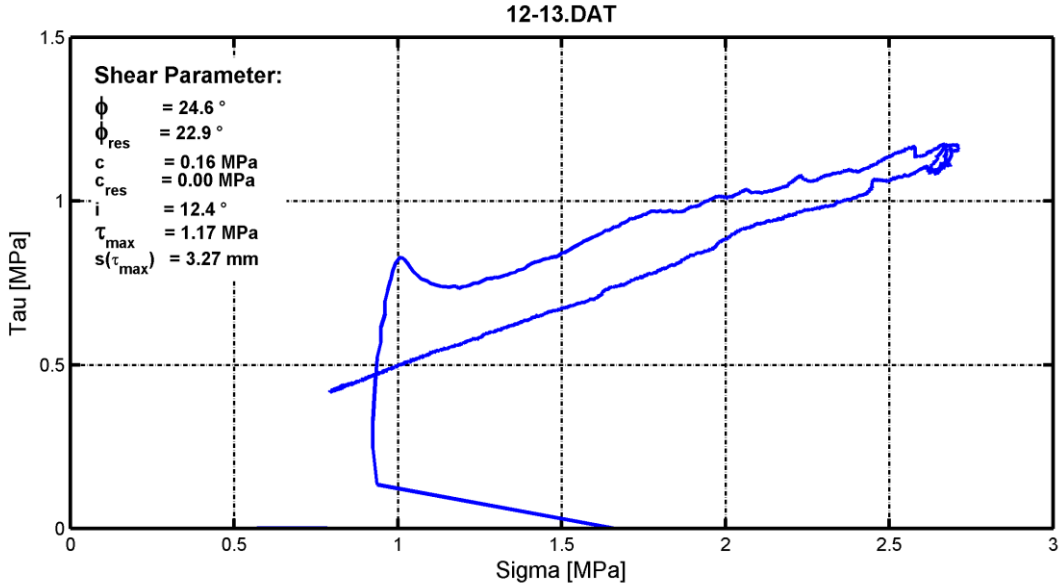

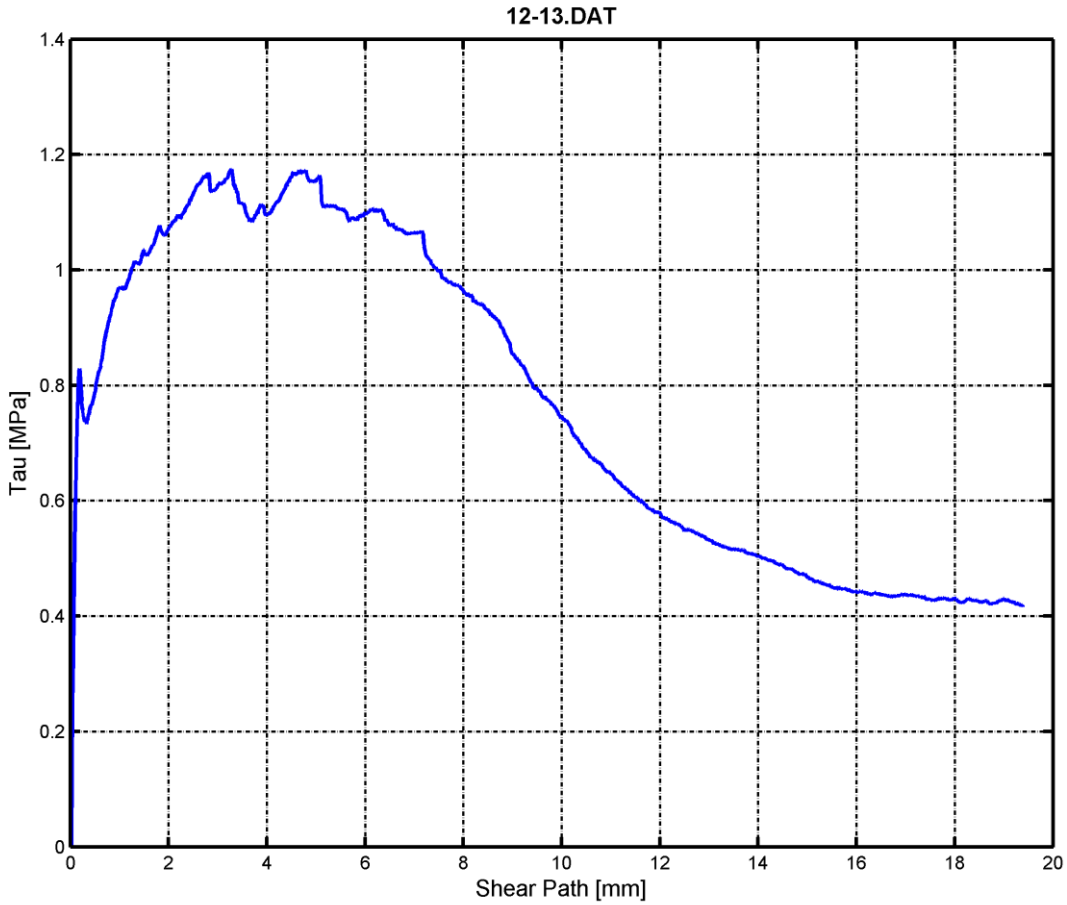

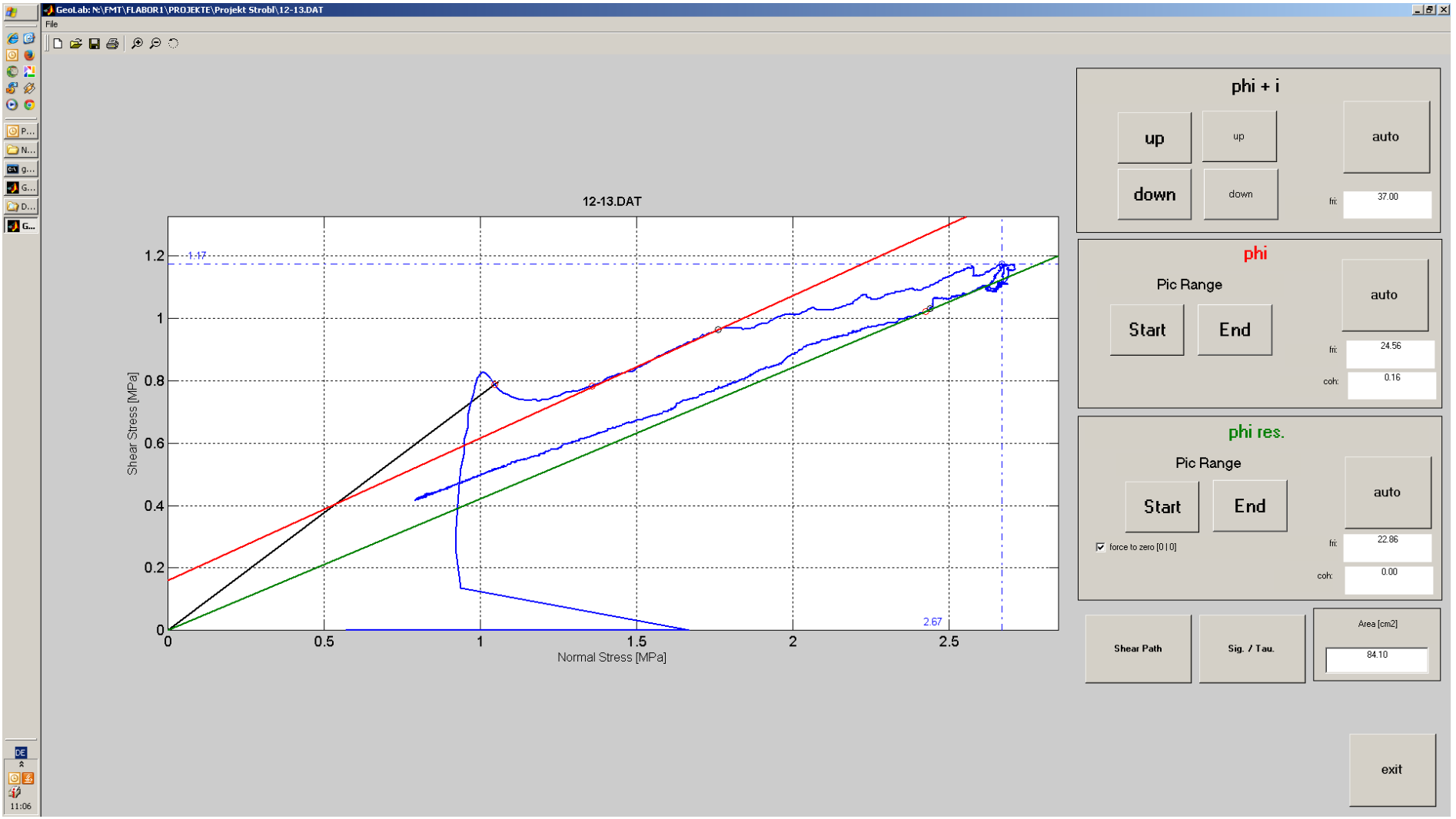
GeoLab: N:\FMT\FLABOR1\PROJEKTE\Projekt Strobl\12-13.DAT
File
12-13.DAT
Shear Stress [MPa]
Normal Stress [MPa]
1.17
2.67
0
0.2
0.4
0.6
0.8
1
1.2
0.5
1.5
2
2.5
phi + i
up
up
down
down
auto
fri:
37.00
phi
Pic Range
Start
End
auto
fri:
24.56
coh:
0.16
phi res.
Pic Range
Start
End
auto
force to zero [0 | 0]
fri:
22.86
coh:
0.00
Shear Path
Sig. / Tau.
Area [cm2]
84.10
exit

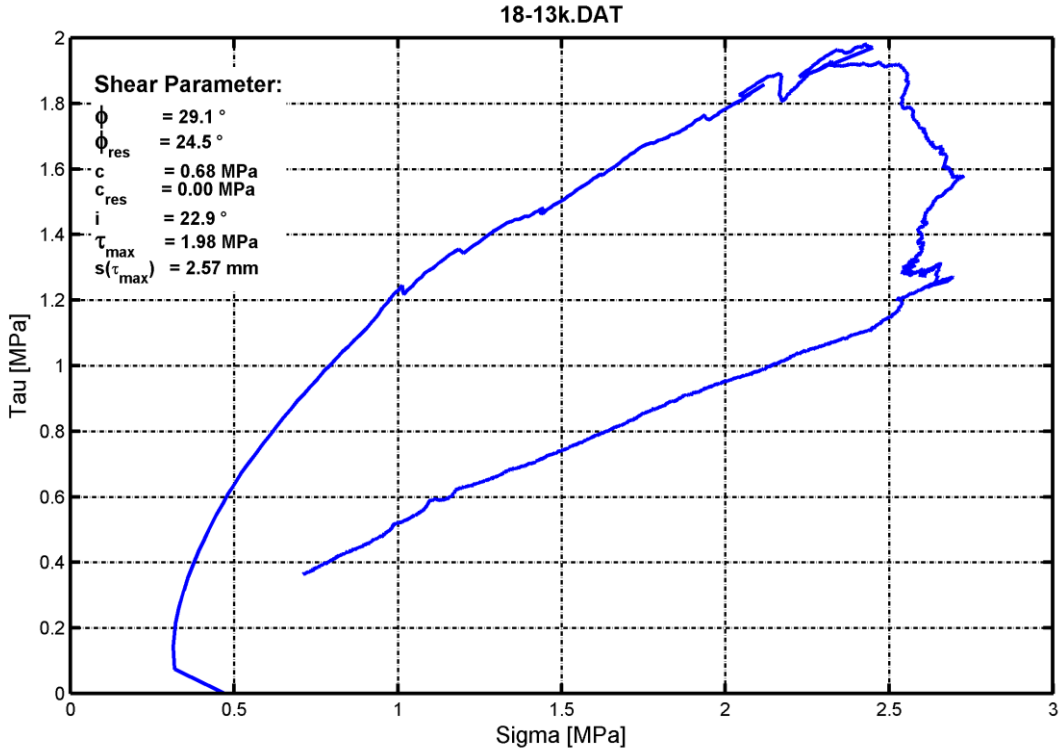
18-13k.DAT
Shear Parameter:
ϕ = 29.1 °
ϕres = 24.5 °
c = 0.68 MPa
cres = 0.00 MPa
i = 22.9 °
τmax = 1.98 MPa
s(τmax) = 2.57 mm
Tau [MPa]
Sigma [MPa]
0
0.2
0.4
0.6
0.8
1
1.2
1.4
1.6
1.8
2
0.5
1.5
2.5
3

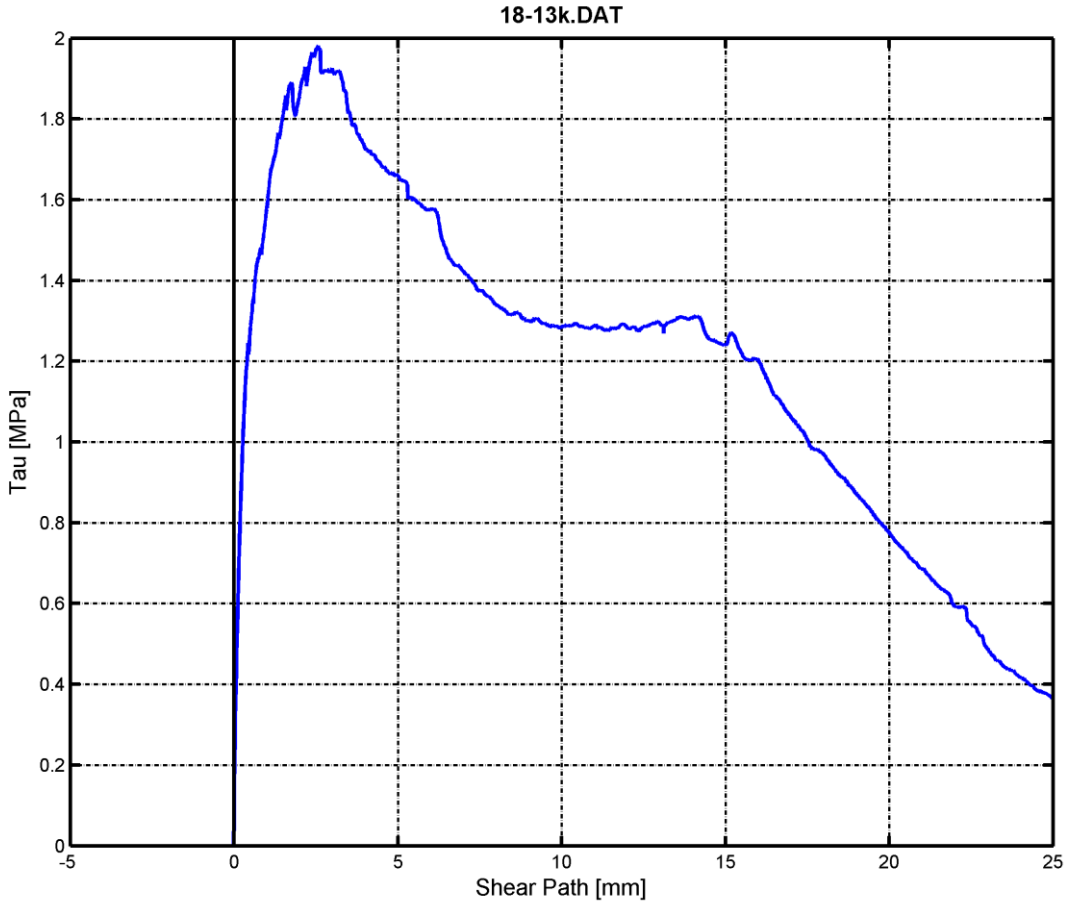
18-13k.DAT
Tau [MPa]
Shear Path [mm]
0
0.2
0.4
0.6
0.8
1
1.2
1.4
1.6
1.8
2
-5
0
5
10
15
20
25

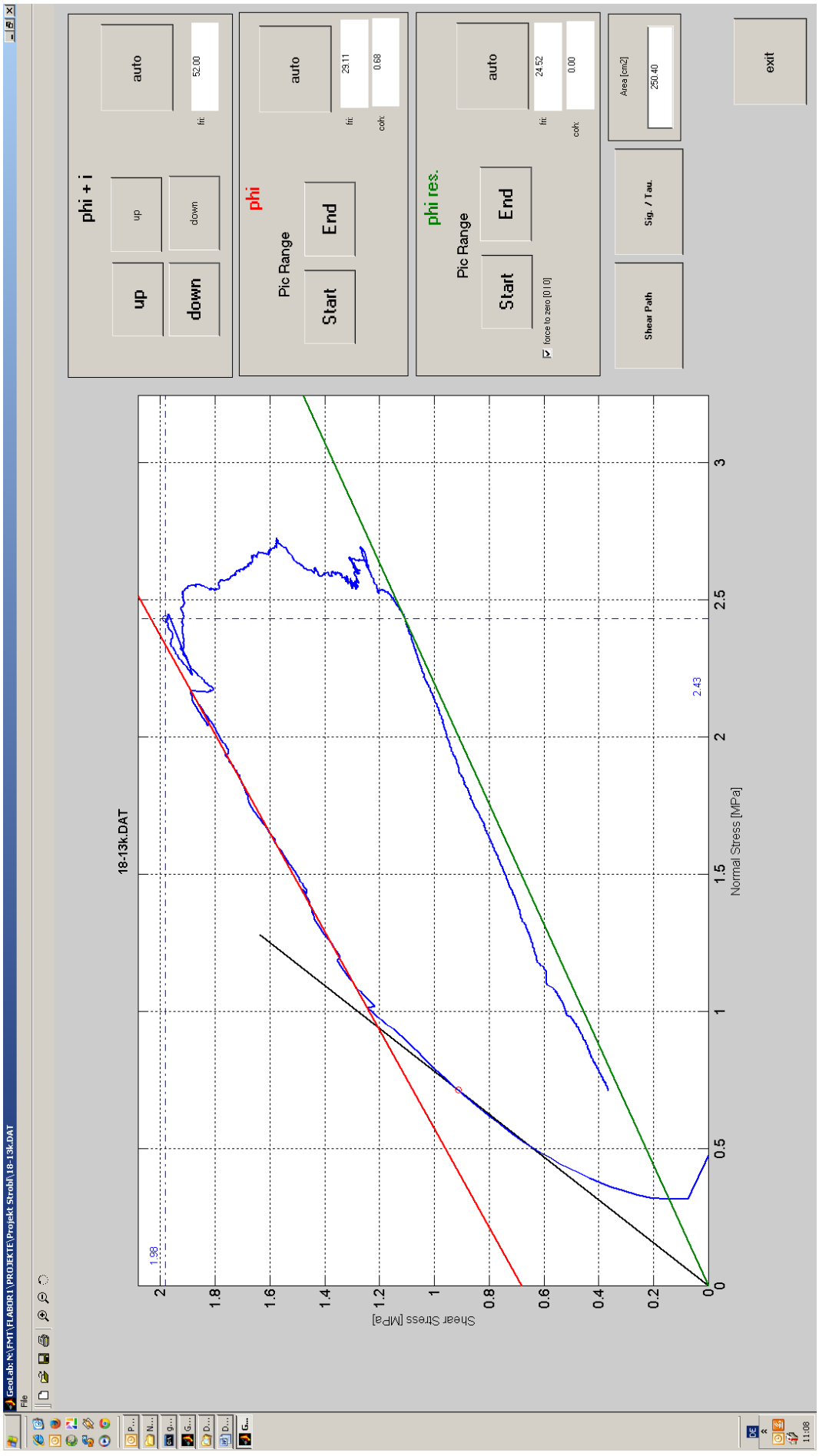
GeoLab: N:\FMT\FLABOR1\PROJEKTE\Projekt Strobl\18-13k.DAT
File
phi + i
up
down
up
down
auto
52.00
fi:
phi
Pic Range
Start
End
auto
29.11
fi:
0.68
coh:
phi res.
Pic Range
Start
End
auto
24.52
fi:
0.00
coh:
force to zero [0 | 0]
Shear Path
Sig. / Tau.
Area [cm2]
250.40
exit
18-13k.DAT
1.98
2.43
Shear Stress [MPa]
Normal Stress [MPa]
0
0.2
0.4
0.6
0.8
1
1.2
1.4
1.6
1.8
2
0.5
1.5
2.5
3
11:08

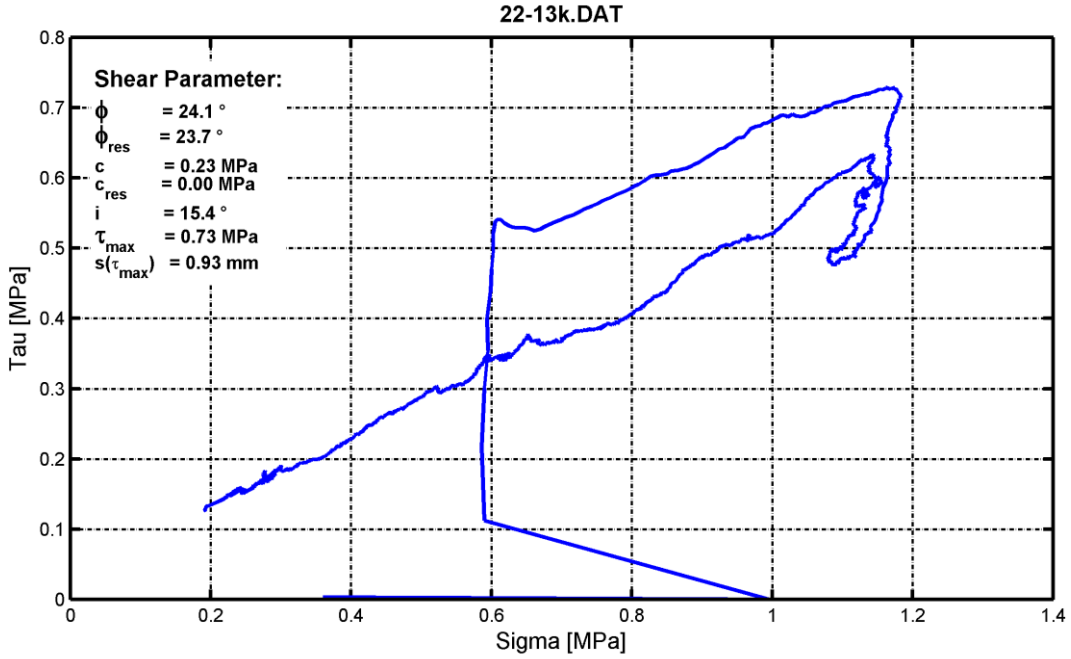
22-13k.DAT
Shear Parameter:
ϕ = 24.1 °
ϕres = 23.7 °
c = 0.23 MPa
cres = 0.00 MPa
i = 15.4 °
τmax = 0.73 MPa
s(τmax) = 0.93 mm
Tau [MPa]
Sigma [MPa]
0
0.1
0.2
0.3
0.4
0.5
0.6
0.7
0.8
0.2
0.4
0.6
0.8
1
1.2
1.4

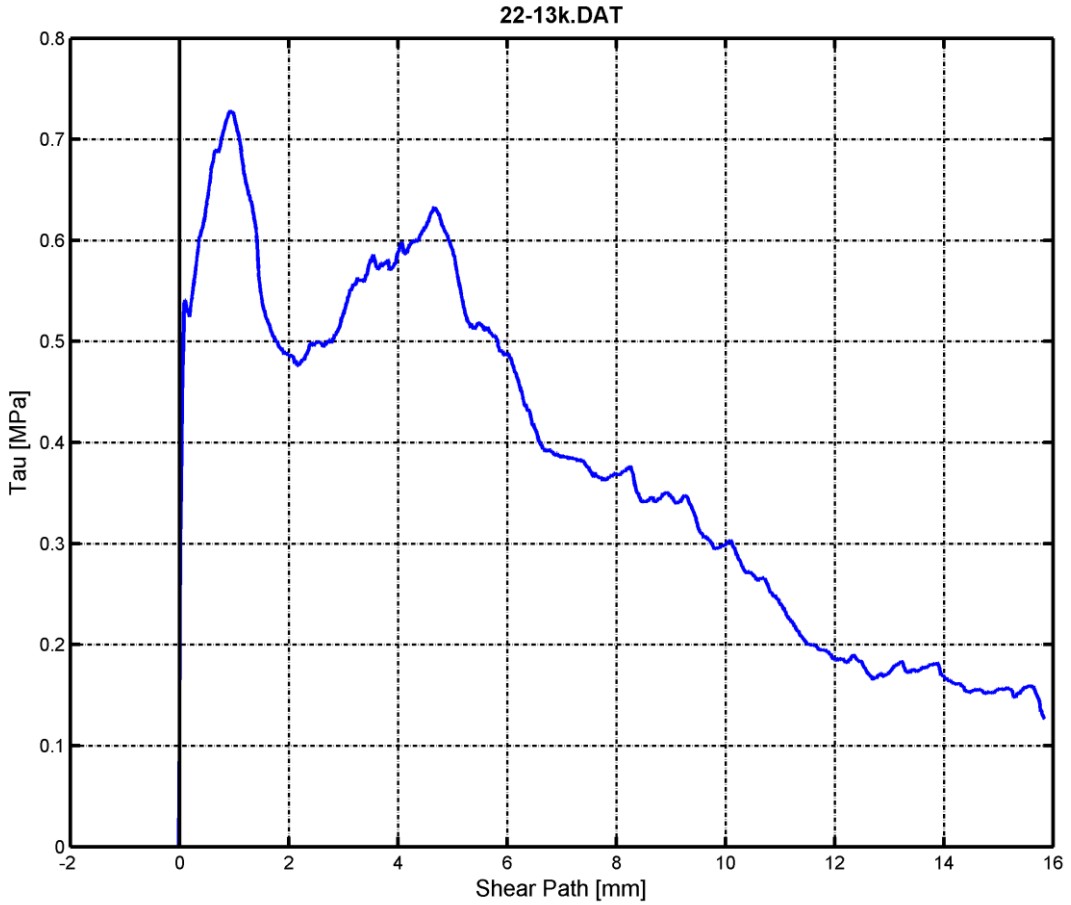
22-13k.DAT
Tau [MPa]
Shear Path [mm]
0
0.1
0.2
0.3
0.4
0.5
0.6
0.7
0.8
-2
0
2
4
6
8
10
12
14
16

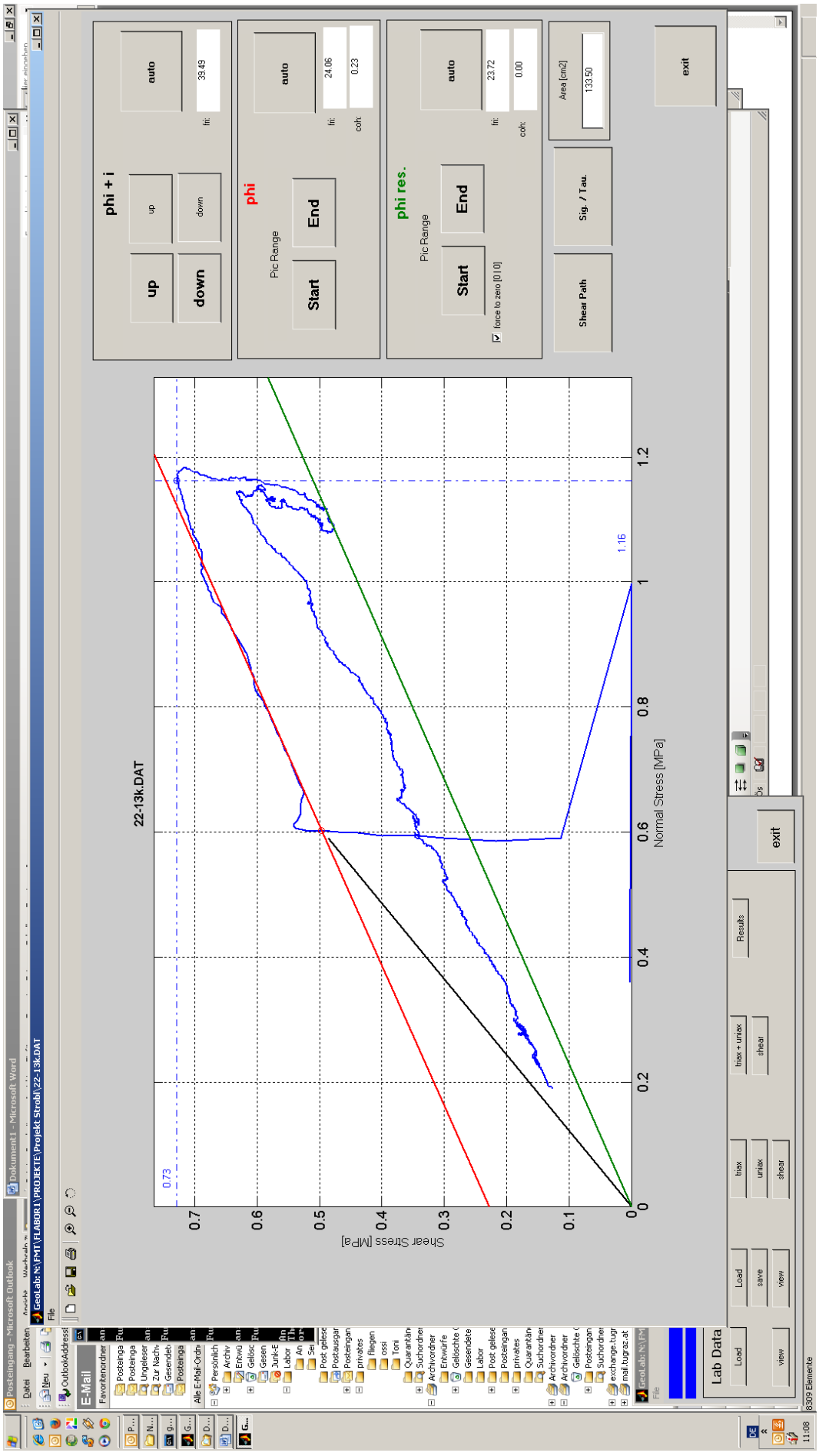
phi + i
up
down
auto
fri:
39.49
phi
Pic Range
Start
End
auto
fri:
24.06
coh:
0.23
phi res.
Pic Range
Start
End
force to zero [0 | 0]
auto
fri:
23.72
coh:
0.00
Shear Path
Sig. / Tau.
Area [cm2]
133.50
exit
22-13k.DAT
0.73
1.16
Shear Stress [MPa]
Normal Stress [MPa]
Lab Data
Load
save
view
triax
uniax
shear
triax + uniax
shear
Results
exit

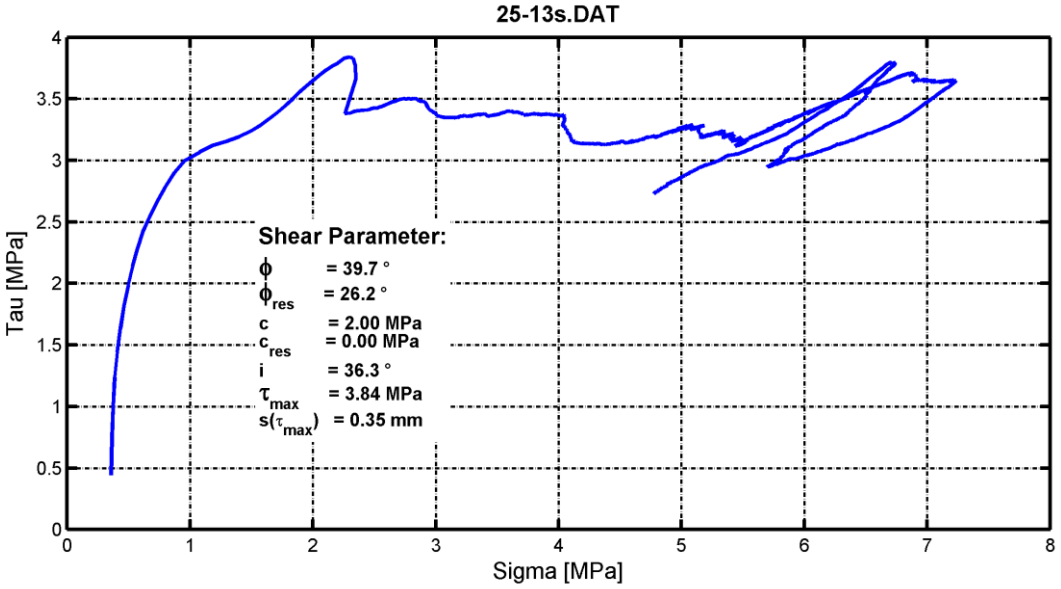
25-13s.DAT
Shear Parameter:
ϕ = 39.7 °
ϕres = 26.2 °
c = 2.00 MPa
cres = 0.00 MPa
i = 36.3 °
τmax = 3.84 MPa
s(τmax) = 0.35 mm
Tau [MPa]
Sigma [MPa]

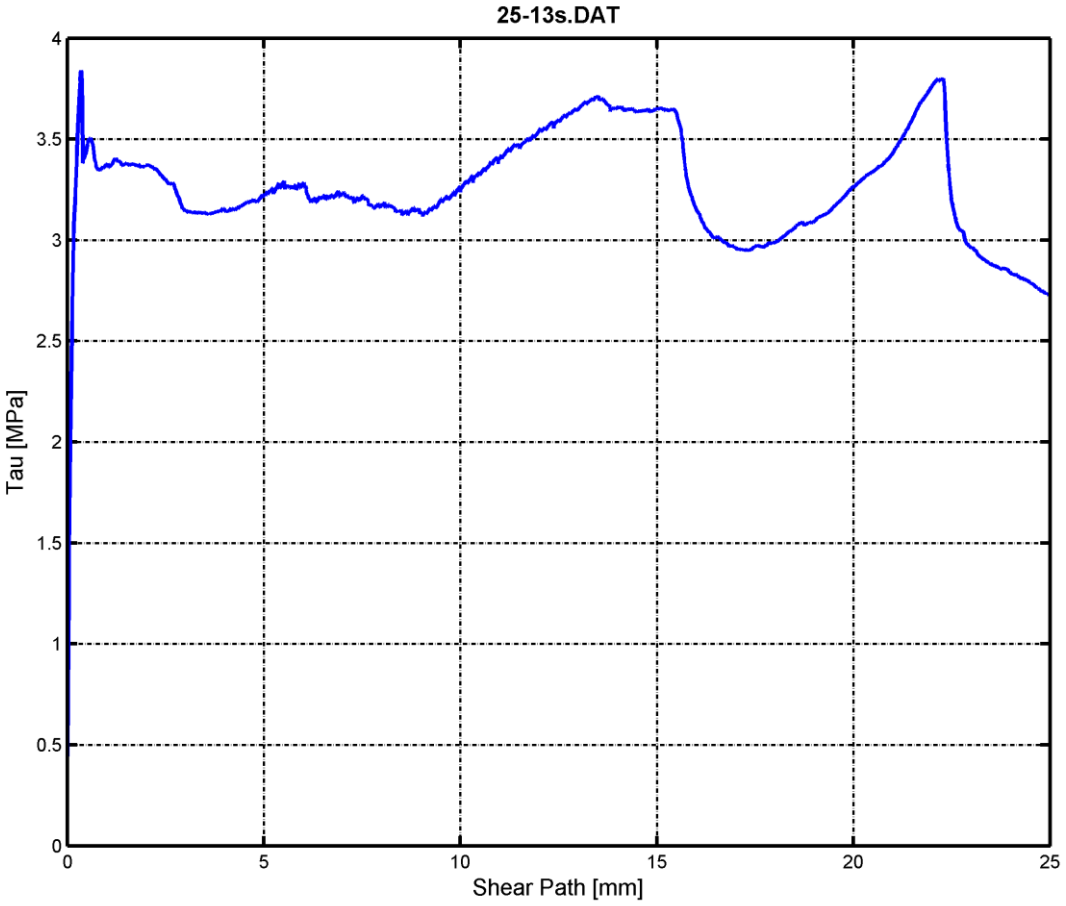
25-13s.DAT
Tau [MPa]
Shear Path [mm]

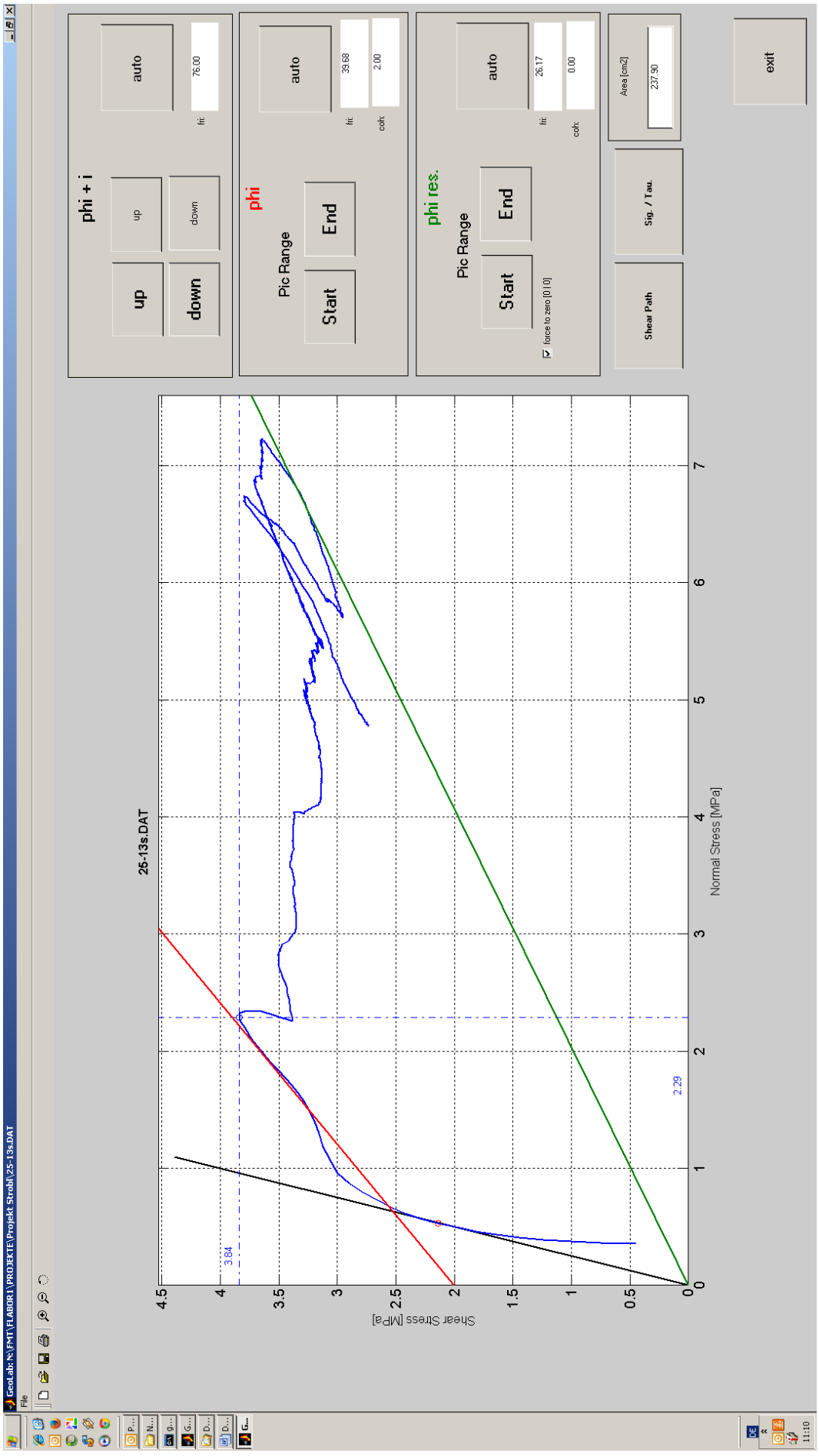
GeoLab: N:\FMT\FLABOR1\PROJEKTE\Projekt Strobl\25-13s.DAT
File
phi + i
up
down
up
down
auto
fi:
76.00
phi
Pic Range
Start
End
auto
fi:
39.68
coh:
2.00
phi res.
Pic Range
Start
End
auto
fi:
26.17
coh:
0.00
force to zero [0 | 0]
Area [cm2]
237.90
Shear Path
Sig. / Tau.
exit
25-13s.DAT
Shear Stress [MPa]
Normal Stress [MPa]
3.64
2.29

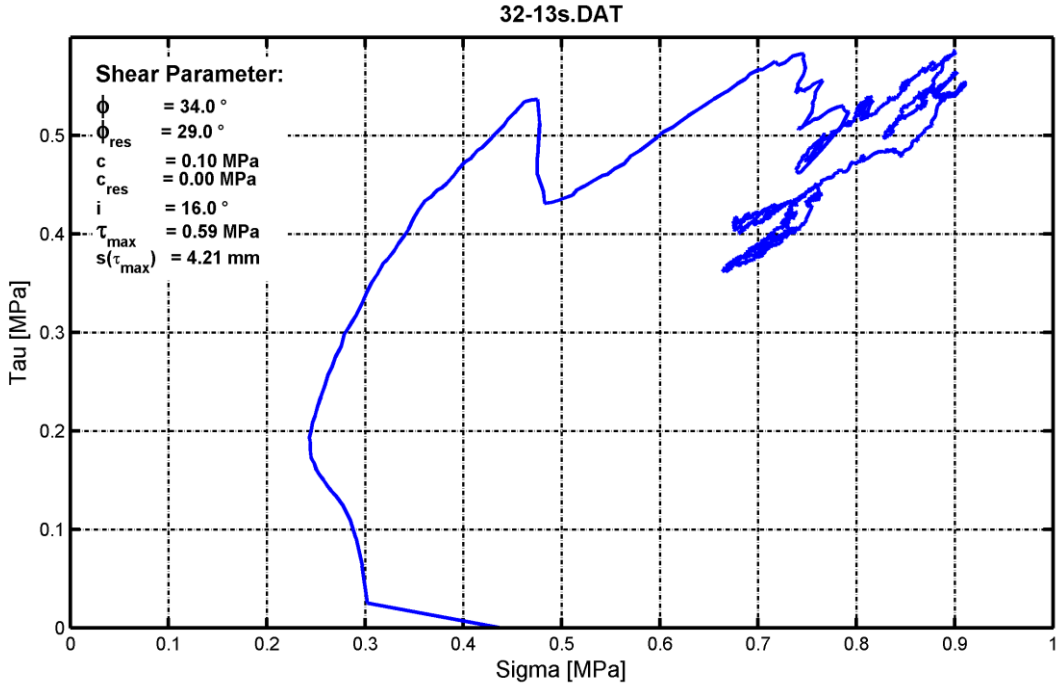
32-13s.DAT
Shear Parameter:
ϕ = 34.0 °
ϕres = 29.0 °
c = 0.10 MPa
cres = 0.00 MPa
i = 16.0 °
τmax = 0.59 MPa
s(τmax) = 4.21 mm
Tau [MPa]
Sigma [MPa]
0
0.1
0.2
0.3
0.4
0.5
0.6
0.7
0.8
0.9
1

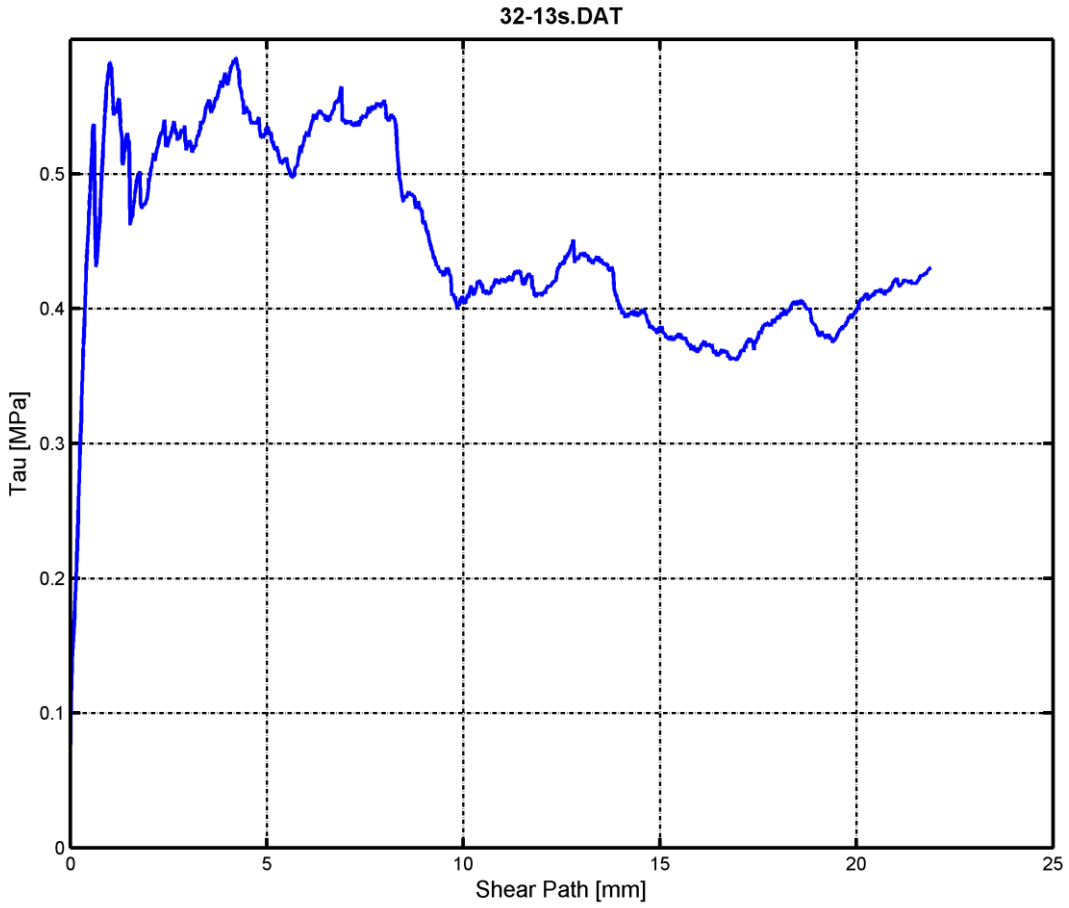
32-13s.DAT
Tau [MPa]
Shear Path [mm]
0
5
10
15
20
25
0.1
0.2
0.3
0.4
0.5

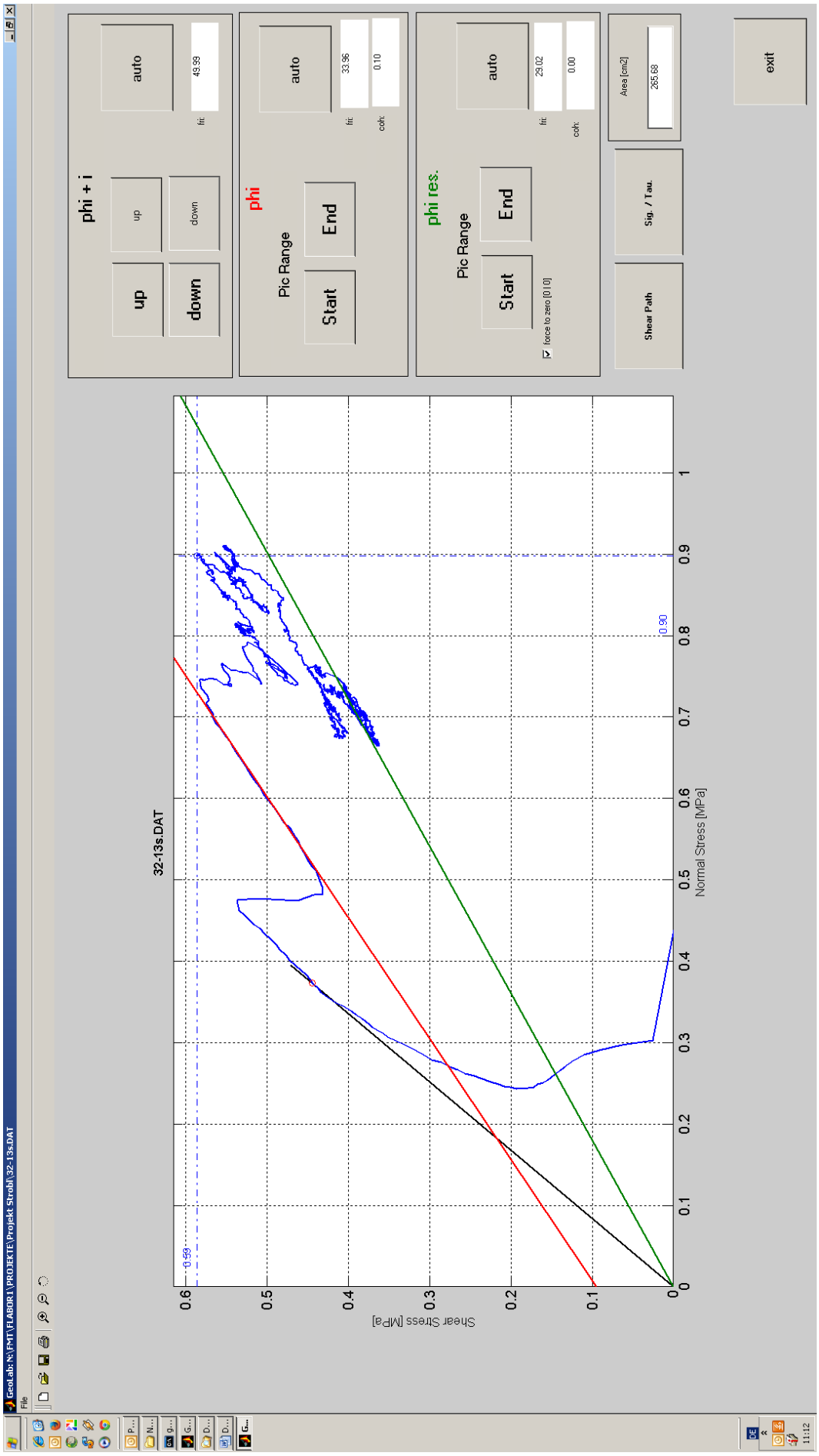
GeoLab: N:\FMT\FLABOR1\PROJEKTE\Projekt Strobl\32-13s.DAT
File
phi + i
up
down
up
down
auto
49.99
fi:
phi
Pic Range
Start
End
auto
33.96
0.10
fi:
coh:
phi res.
Pic Range
Start
End
force to zero [0 10]
auto
29.02
0.00
fi:
coh:
Shear Path
Sig. / Tau.
Area [cm2]
265.68
exit
32-13s.DAT
Shear Stress [MPa]
Normal Stress [MPa]
0.59
0.90
0
0.1
0.2
0.3
0.4
0.5
0.6
0.7
0.8
0.9
1

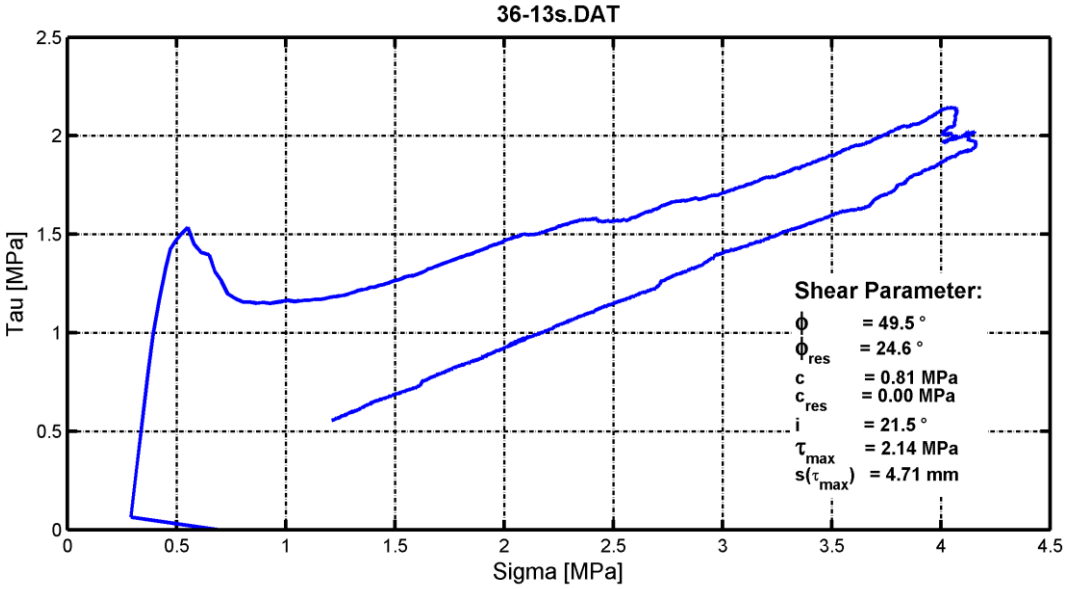
36-13s.DAT
Tau [MPa]
Sigma [MPa]
Shear Parameter:
ϕ = 49.5 °
ϕres = 24.6 °
c = 0.81 MPa
cres = 0.00 MPa
i = 21.5 °
τmax = 2.14 MPa
s(τmax) = 4.71 mm

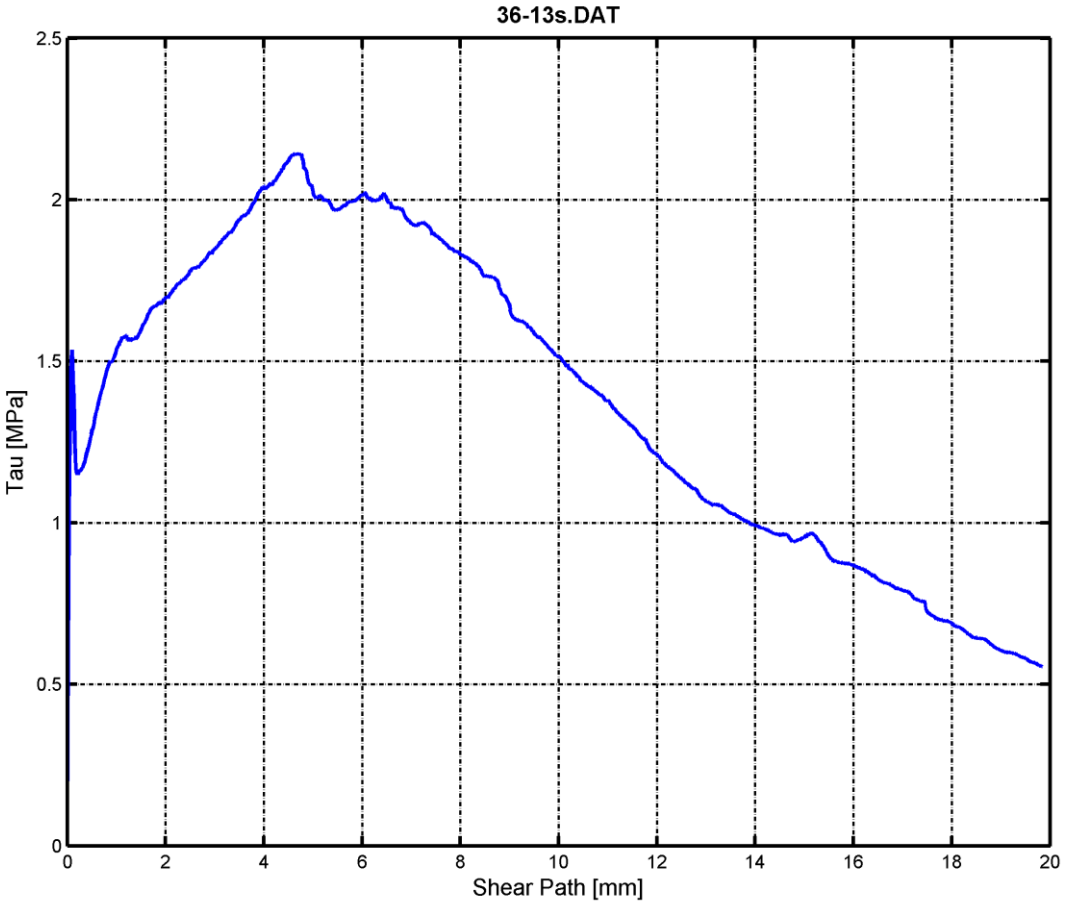
36-13s.DAT
Tau [MPa]
Shear Path [mm]

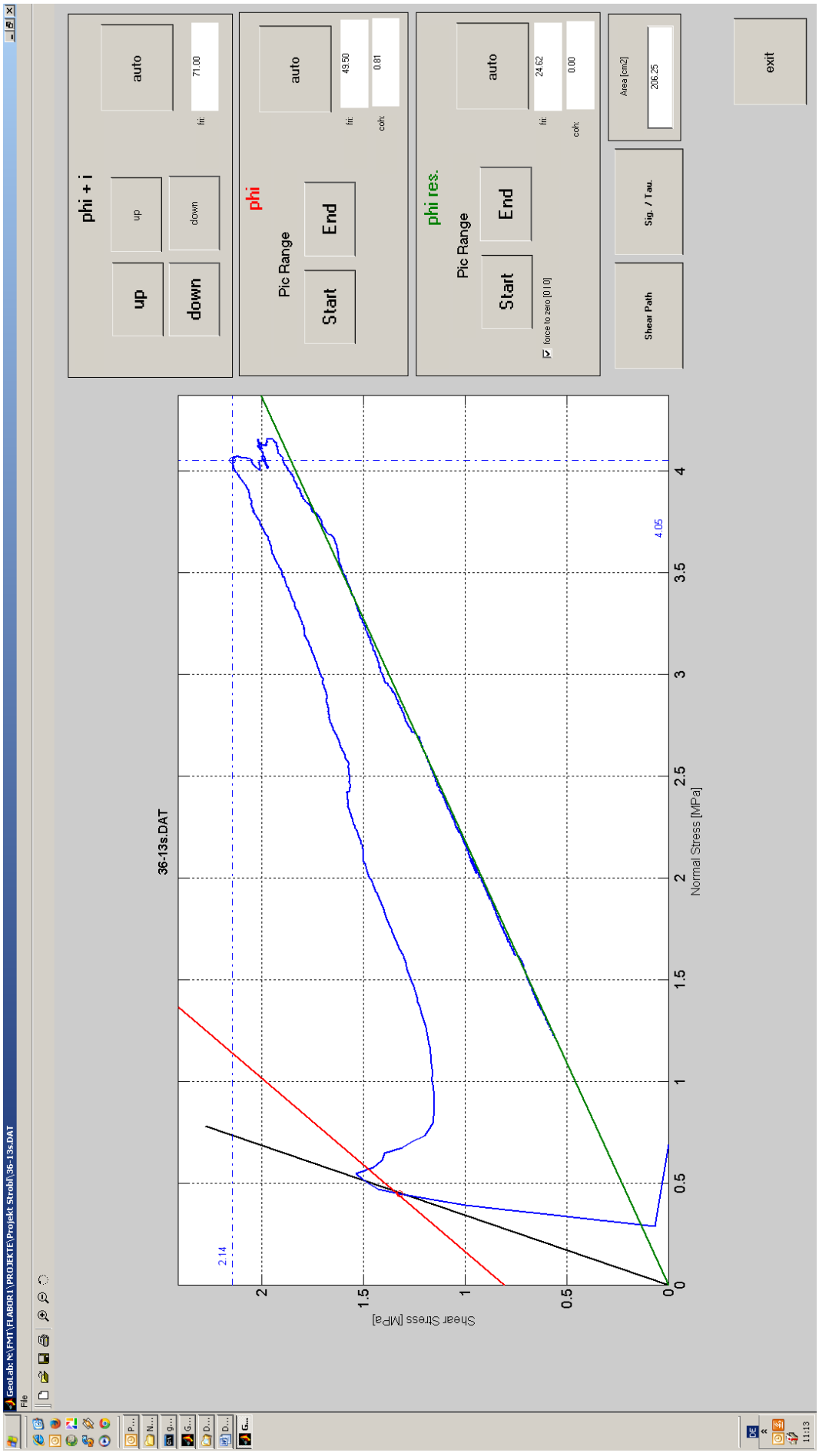
GeoLab: N:\FMT\FLABOR1\PROJEKTE\Projekt Strobl\36-13s.DAT
File
phi + i
up
down
up
down
auto
71.00
fi:
phi
Pic Range
Start
End
auto
49.50
0.81
fi:
coh:
phi res.
Pic Range
Start
End
force to zero [0 10]
auto
24.62
0.00
fi:
coh:
Shear Path
Sig. / Tau.
Area [cm2]
206.25
exit
36-13s.DAT
2.14
4.05
Shear Stress [MPa]
Normal Stress [MPa]
0
0.5
1
1.5
2
2.5
3
3.5
4
11:13

Results from the triaxial compression tests:

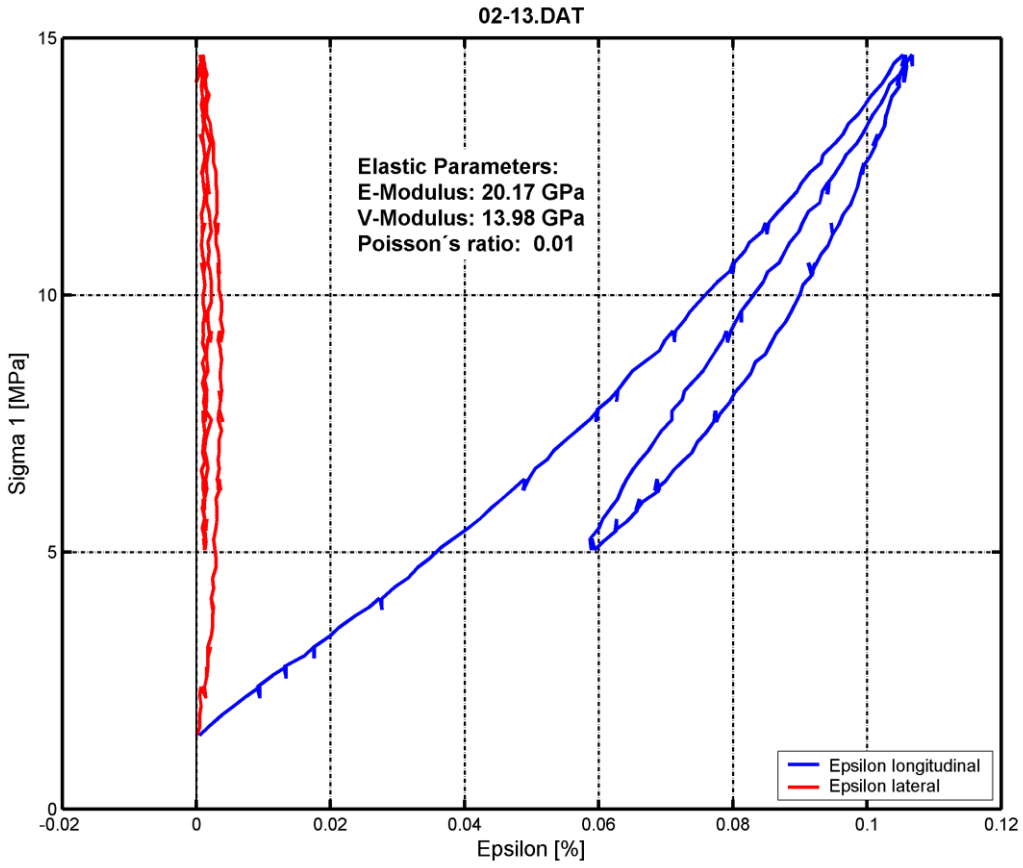

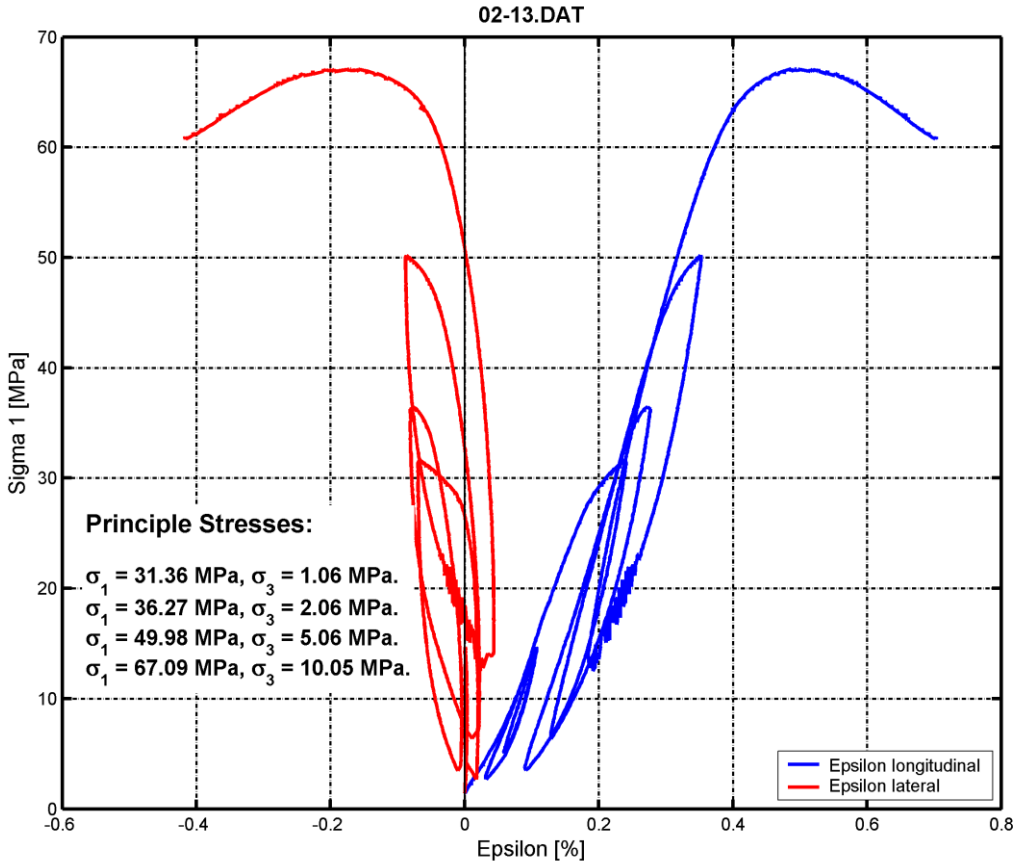

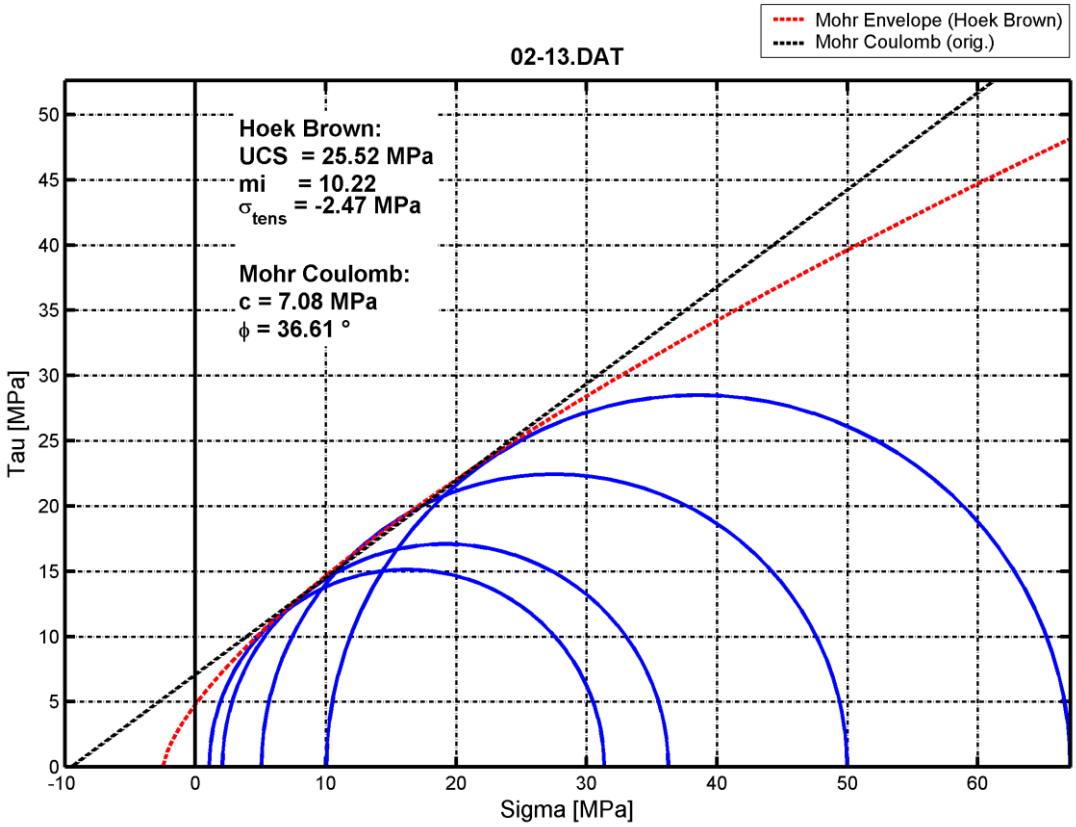
Mohr Envelope (Hoek Brown)
Mohr Coulomb (orig.)
02-13.DAT
Hoek Brown:
UCS = 25.52 MPa
mi = 10.22
σtens = -2.47 MPa
Mohr Coulomb:
c = 7.08 MPa
ϕ = 36.61 °
Tau [MPa]
Sigma [MPa]

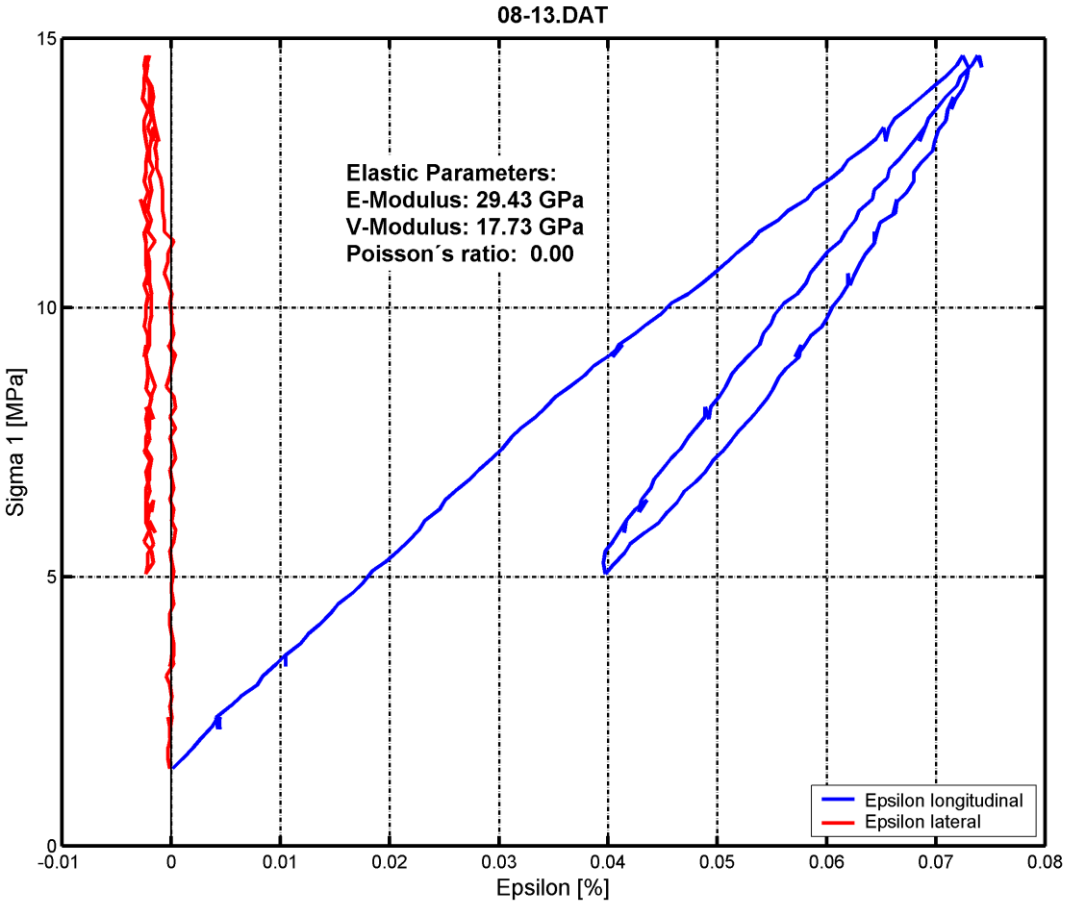
08-13.DAT
Elastic Parameters:
E-Modulus: 29.43 GPa
V-Modulus: 17.73 GPa
Poisson´s ratio: 0.00
Epsilon longitudinal
Epsilon lateral
Sigma 1 [MPa]
Epsilon [%]

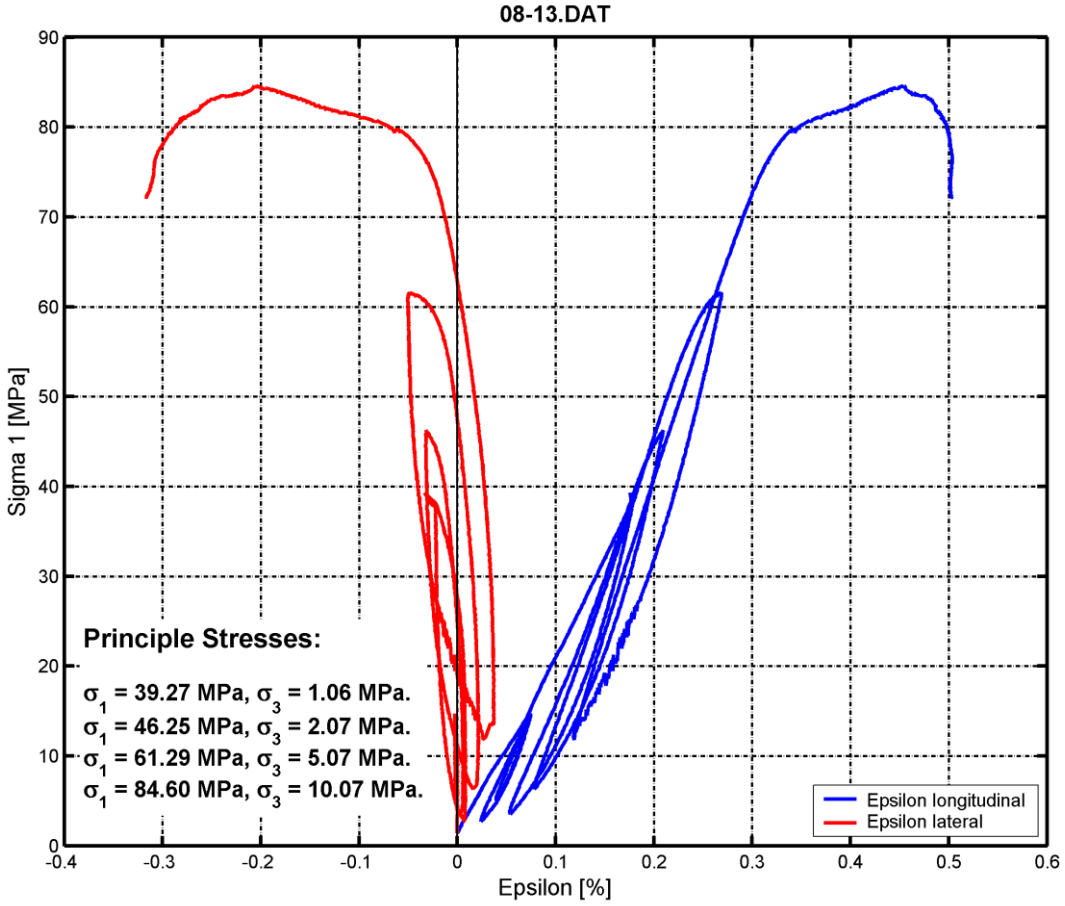
08-13.DAT
Sigma 1 [MPa]
Epsilon [%]
Principle Stresses:
σ1 = 39.27 MPa, σ3 = 1.06 MPa.
σ1 = 46.25 MPa, σ3 = 2.07 MPa.
σ1 = 61.29 MPa, σ3 = 5.07 MPa.
σ1 = 84.60 MPa, σ3 = 10.07 MPa.
Epsilon longitudinal
Epsilon lateral

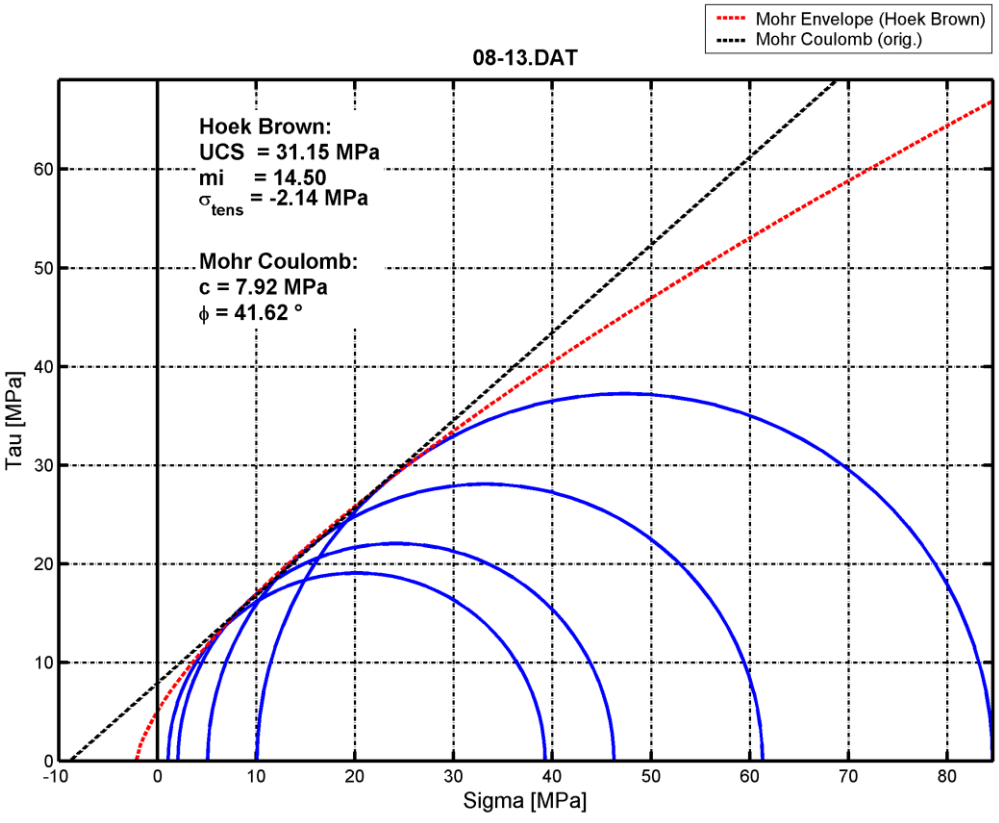
Mohr Envelope (Hoek Brown)
Mohr Coulomb (orig.)
08-13.DAT
Hoek Brown:
UCS = 31.15 MPa
mi = 14.50
σtens = -2.14 MPa
Mohr Coulomb:
c = 7.92 MPa
ϕ = 41.62 °
Tau [MPa]
Sigma [MPa]

Appendix 5: Block Theory Analysis

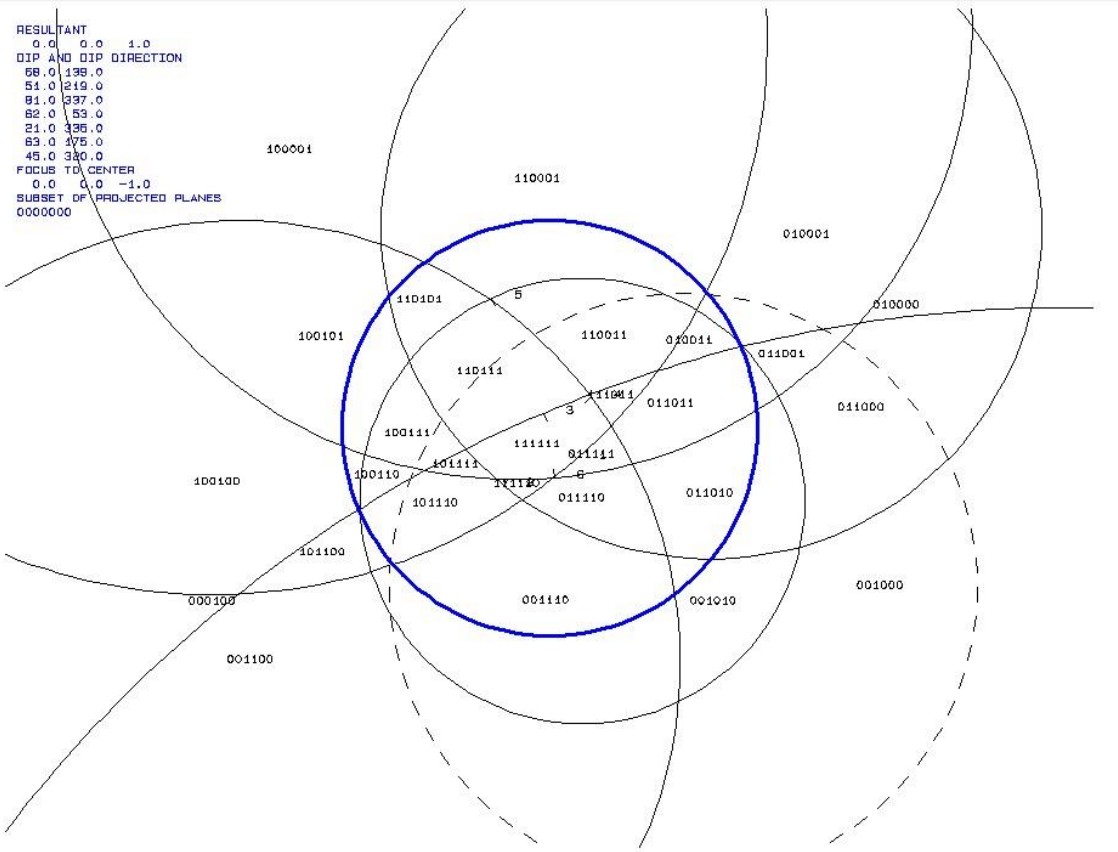

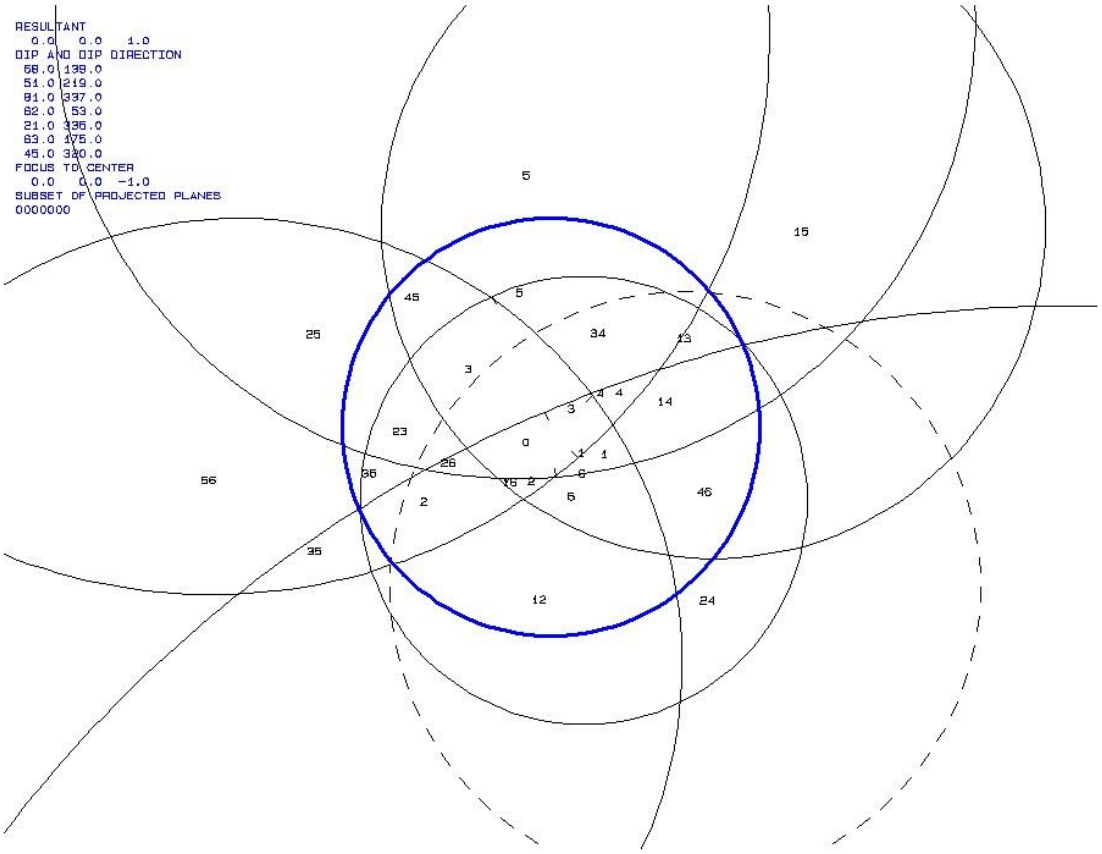

Model of Block 100101:

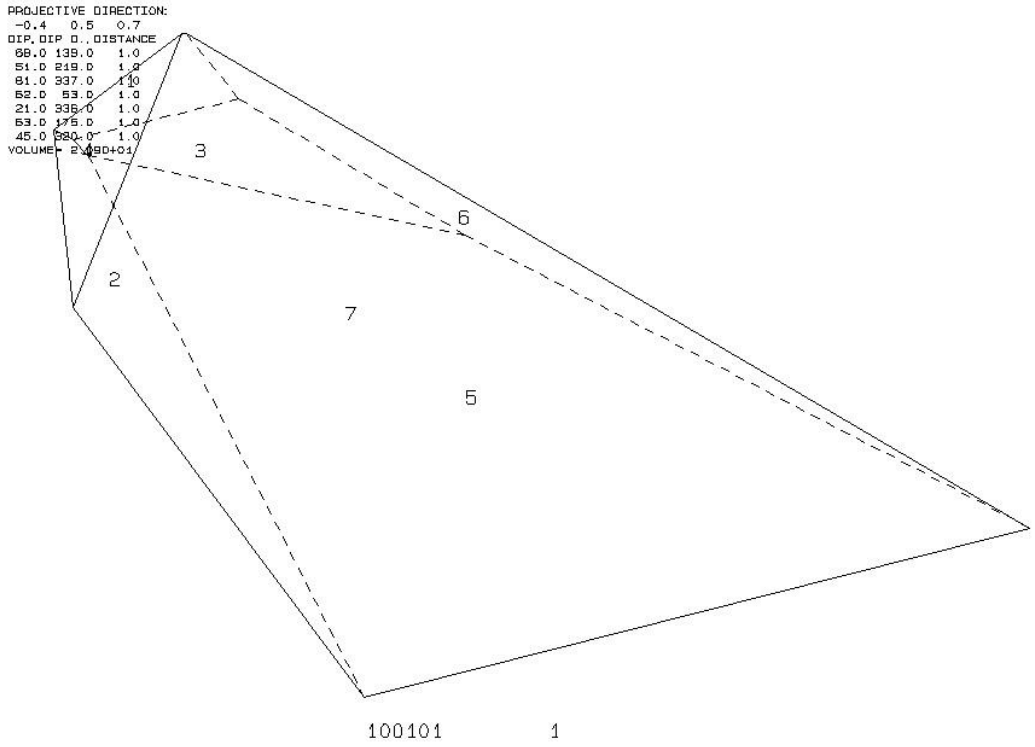

Model of Block 101100:

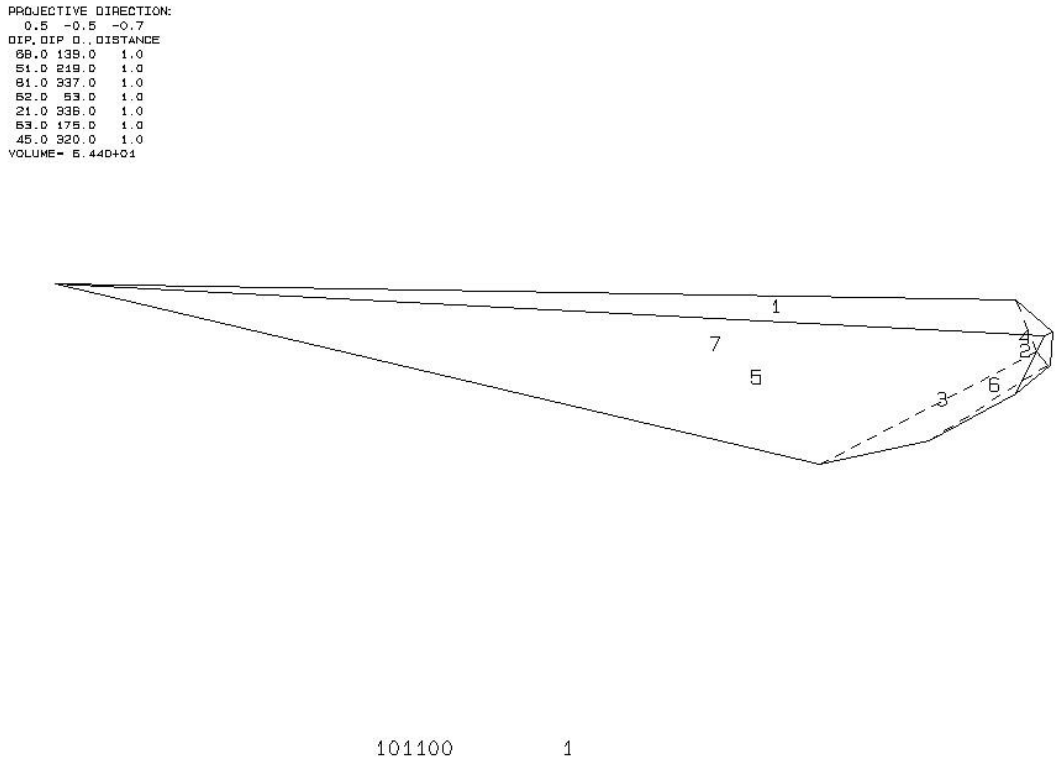

Model of Block 110101:

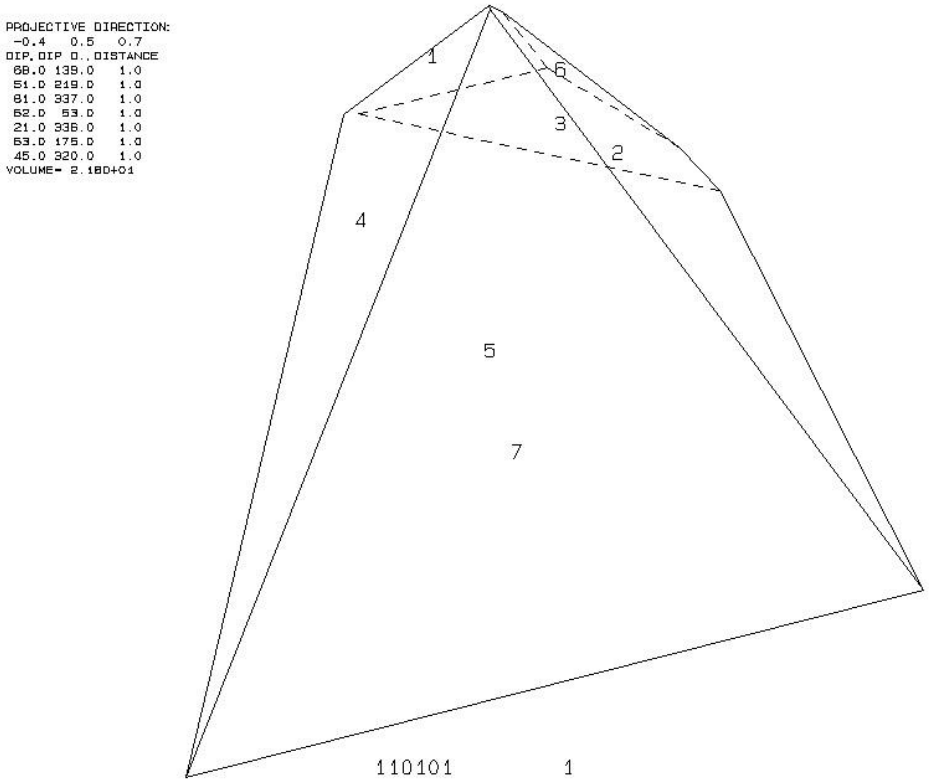
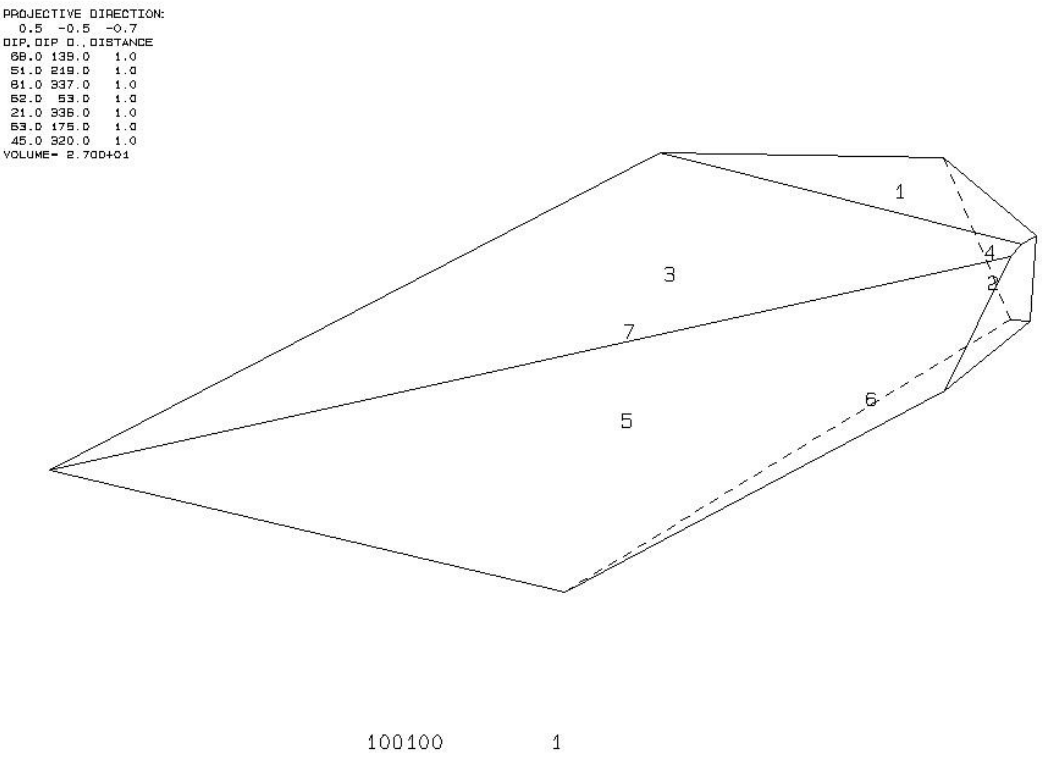
Model of Block 100100: